2008

IN VITRO MODELS FOR INHALED CORTICOSTEROID (ICS) AEROSOLS: A STUDY OF THEIR BIOPHARMACEUTICS AND PHARMACOLOGY

DEEPIKA ARORA
Virginia Commonwealth University

IN VITRO MODELS FOR INHALED CORTICOSTEROID (ICS) AEROSOLS: A STUDY OF THEIR BIOPHARMACEUTICS AND PHARMACOLOGY

A dissertation submitted in partial fulfillment of the requirements for the degree of Doctor of Philosophy at Virginia Commonwealth University

by

DEEPIKA ARORA, B. PHARM.
Delhi Institute of Pharmaceutical Sciences and Research, India
2003

Director: MASAHIRO SAKAGAMI, Ph.D.
Assistant Professor,
Department of Pharmaceutics, School of Pharmacy

Virginia Commonwealth University
Richmond, Virginia
December, 2008

DEDICATIONS

To My Precious Parents,
And
Divya and Reneé

ACKNOWLEDGEMENT

I sincerely express my gratitude to Dr. Masahiro Sakagami for his guidance, constant support, unparalleled enthusiasm and supervision of my doctoral dissertation project. I have great respect towards his dedication to science and his attitude to take everything in stride. He has been very supportive, not only towards my professional aspirations but also to my cultural adjustment in this country. I thank him for being my mentor, in every sense.

I have been very fortunate to have Dr. Peter Byron on my Graduate Advisory Committee and as an advisor for a satellite project that I completed in 2005. He has been a wonderful guide and a source of inspiration. From him I have learnt not only good science, but also entrepreneurial skills, to reason and graceful confidence.

I take this opportunity to thank my Graduate Advisory Committee members; Dr. Drew Jones, Dr. Susanna Wu-Pong, Dr. Suzanne Barbour and Dr. Mario Dance for their constant support throughout the length of this project. I specifically want to thank Dr. Jones for teaching me the basic molecular aspects behind this project and having the answers to all my queries.

I thank the Medical College of Virginia Foundation and School of Pharmacy, VCU for financial support. A special thanks to the International Foundation for Ethical Research for providing a fellowship during my final year of doctoral studies.

I thank Mr. Matthew Halquist for the LC/MS/MS assay development, Kumar for the odd hour support and Judy and Pete at Sanger Hall for catering to “different” requests I made from time to time. Special thanks to Laura, Chris, Mia, Keyetta and Scott at the Department of Pharmaceutics for being so wonderful at all times.

I sincerely express my appreciation to all the current and past ARGers: Dr. Joanne Peart, Dr. Michael Hindle, Reshma, Priya, Joan, Suparna, Bhawana, Swati, Bhawna, Megha and Renish. Many friends that I have made here at VCU will be cherished forever: Soniya, Dave, Satti, Kumar, Prajakta and Abhishek. Thanks to the new family of friends that made my stay in Richmond fly: BS, Kshama, KJ, Parth, Lathika, Leah and so many more; my graduate life has been blissful because of all of you. Special thanks to members of ElderFriends for many beautiful moments.

Finally, I express my gratitude to my family in India: Mom, Dad, my sister Divya and Reneè. You have always believed in me and stood by me. Without your constant love, encouragement and frequent visits, this dream could never become a reality.

TABLE OF CONTENTS

Page

LIST OF TABLES

Page

LIST OF FIGURES

Page

ABBREVIATIONS

%	percentage
=	equal
~	approximately
>	greater than
≥	greater than or equal to
<	less than
≤	less than or equal to
±	plus or minus
Å	angstrom
°C	degrees Celsius
ε	barrier porosity
μ	micro
η	viscosity
Ω	ohm
λ_{ex}	excitation wavelength
λ_{em}	emission wavelength
®	registered trademark
A	area of transwell insert
ACI	Andersen cascade impactor

AIC	air interface culture
ANOVA	analysis of variance
APCI	atmospheric pressure chemical ionization
API	active pharmaceutical ingredient
ATCC	American Type Culture Collection
BCA	bicinchoninic acid
BD	budesonide
BDP	beclomethasone dipropionate
CFC	chlorofluorocarbon
CFC 11	trichlorofluoromethane
CFC 12	dichlorodifluoromethane
CFC 114	dichlorotetrafluoroethane
CH_3CN	acetonitrile
cm	centimeter
COPD	chronic obstructive pulmonary disease
C_{RD}	rhodamine dextran concentration
Da	Dalton
DDW	deionized distilled water
D_i	diffusion coefficient
DMF	dimethylformamide
DMSO	dimethyl sulfoxide

DPCC	dipalmitoyl-L-α-phosphatidylcholine
DPI	dry powder inhaler
e.g.	for example
EDTA	ethylenediaminetetraacetic acid
EGTA	ethylene glycol tetraacetic acid
ELISA	enzyme linked immunosorbent assay
ESI	electrospray ionization
et al	and others
EVOM	EVOM voltohmmeter
FBS	fetal bovine serum
FD	fluorescein isothiocyanate-labeled dextran
FL	flunisolide
FNa	fluorescein sodium
FP	fluticasone propionate
F-PHEA	fluorophore-labeled poly-α,β-[N(2-hydroxyethyl)-D,L-aspartamide
g	gram
GPC	gel permeation chromatography
GPC-F	gel permeation chromatography coupled with fluorescence
h	hour
HEPES	N-[2-hydroxy-ethyl]piperazine-N'-[2-ethanesulfonic acid]
HFA	hydrofluoroalkane

HFA 134a	1,1,1,2-tetrafluoroethane
HPLC	high performance liquid chromatography
HPLC-MS/MS	high performance liquid chromatography coupled with tandem mass spectrometry
i.e.	that is
ICS	inhaled corticosteroid
J	initial rate for mass permeation
k	Boltzmann's constant
k-	kilo-
KRB	Krebs-Ringer buffer
L	liter
L	barrier length
Log P	octanol-water partition coefficient
LOQ	limit of quantitation
M	molarity
m	meter
m-	milli-
min	minute
MW	molecular weight
n	nano
NFκB	nuclear factor kappa B
N.D.	not determined

P_{app}	apparent permeability coefficient
PBS	phosphate-buffered saline
pH	negative log of hydrogen ion concentration or activity
pMDI	pressurized metered dose inhaler
pNFκB-Luc	nuclear factor kappa B-dependent reporter gene of luciferase
PVDF	polyvinylidene difluoride
$R(r_i/r_p)$	Renkin function
r^2	coefficient of determination
RH	relative humidity
r_i	solute radius
RLU	relative light unit
r_p	pore radius
RSD	relative standard deviation
s	second
SD	standard deviation
SE	standard error
SEM	scanning electron microscopy
T	absolute temperature
TA	triamcinolone acetonide
TEER	transepithelial electrical resistance
™	trade mark

TNFα	tumor necrosis factor alpha
USP	United States Pharmacopeia
V	volt
vs.	versus
v/v	volume per volume
V_{LF}	Calu-3 lining fluid volume
w/v	weight per volume
w/w	weight per weight

ABSTRACT

IN VITRO MODELS FOR INHALED CORTICOSTEROID (ICS) AEROSOLS: A STUDY OF THEIR BIOPHARMACEUTICS AND PHARMACOLOGY

By Deepika Arora, B.Pharm.

A dissertation submitted in partial fulfillment of the requirements for the degree of Doctor of Philosophy at Virginia Commonwealth University.

Virginia Commonwealth University, 2008

Major Director: Masahiro Sakagami, Ph.D.
Assistant Professor, Department of Pharmaceutics

Lung cellular disposition and anti-inflammatory pharmacology of inhaled corticosteroids (ICSs) is complex, comprised of a cascade of aerosol deposition and dissolution, followed by cellular uptake for local pharmacological action. This project hypothesized that the kinetics of dissolution for certain ICS aerosols generated from inhaler products were kinetically rate-determined for their cellular uptake and local pharmacological action.

A novel dissolution testing system was developed to determine the dissolution kinetics for the ICS aerosols. A total of 5 ICSs aerosols generated from 6 inhaler products were collected in 2.1-3.3 or 4.7-5.8 μm of aerodynamic diameters at 0.7-19.8

µg on filter membranes by impaction using the Andersen cascade impactor. The filter membrane was then placed on the donor side of the transwell insert, with its face down, and the ICS dissolution in the limited 40 µL of the donor fluid was monitored over time. The dissolution kinetics overall conformed to the rank order of the aqueous solubility, while also being affected by ICS aerosol's mass, size, formulation and dosage forms. For the readily soluble triamcinolone acetonide (TA), the kinetics was first-order, reaching ≥89 % dissolution in 5 h. In contrast, for the least soluble fluticasone propionate (FP), the kinetics was zero-order, reaching only 3 % dissolution in 10 h.

The project then developed an air-interface culture of human bronchial epithelial cell line, Calu-3. Well-differentiated monolayers were formed with sufficiently "tight" barrier for restrictive solute diffusion while their mucosal surface was maintained semi-dry with 39.7±12.1 µL of the mucosal lining fluid in the 4.5 cm^2 transwells. These monolayers were transfected with reporter plasmid of pNFκB-Luc to assess in vitro anti-inflammation via repression of pro-inflammatory NFκB by direct FP or TA aerosol deposition. The FP aerosols at 0.9 µg successfully exhibited significant 35.7±6.3 % repression. Notably, however, an identical ~0.5 µg of FP and TA aerosols caused comparable 15.5±2.2 and 10.4±2.6 % repression, respectively, despite FP's 10-fold greater "intrinsic" anti-inflammatory potency over TA, reported in the literature. This was attributed to FP's slow dissolution resulting in only 4.7 % cellular uptake, compared to 32.6 % for the TA aerosols. Hence, the FP aerosols were shown to be rate-determined by dissolution on the lung cell surface, resulting in reduced anti-inflammatory actions, which was not the case for the readily soluble TA aerosols.

CHAPTER 1

BACKGROUND AND SIGNIFICANCE

Pulmonary drug delivery has been used for more than 50 years as a successful route of administration for delivering drugs for the local treatment of lung diseases like asthma and chronic obstructive pulmonary disease (COPD) [Schleimer *et al*, 2002]. The success of this therapy has primarily been attributed to the enhanced local targeting of the drugs to the airways, thereby reducing the systemic levels that are primarily responsible for their side effects [Hochhaus *et al*, 1997; Hochhaus G, 2004]. Even so, recent evidence has suggested that this route of delivery has not yet been fully optimized to exhibit maximized therapeutic effects, while minimizing the side effects in patients [Leach *et al*, 2002; Usmani *et al*, 2005]. In fact, it becomes clear that determination of the systemic exposure of these drugs following inhalation does not necessarily translate into local or systemic pharmacological actions [Edsbäcker *et al*, 2008]. It is logical therefore to demand accurate determination of the local exposure of these drugs (i.e., in the lung), yet such an attempt has been quite challenging due to the lung's anatomical complexity for delivery and the lung region-specific multiple

mechanisms for disposition [Byron *et al*, 1990, 1994; Patton, 1990; Patton and Byron, 2007].

Generally, pharmaceutical aerosols are administered via inhalation using inhaler products, possibly along with formulation excipients. In most cases, the inhaler products are pressurized metered dose inhalers (pMDIs) or dry powder inhalers (DPIs), while nebulizers are also available for special needs such as hospital or pediatric/geriatric uses [Hickey, 1996; Gonda, 1990; Dhand, 2008]. It is well recognized however that only a certain portion of the formulated drugs can reach the lung from these inhaler products, and this delivery is also dependent upon the patient's inhalation maneuvers [Hickey, 1996; Eiss and Huston, 2003]. Hence, this simply demonstrates a challenge for accurate determination of the local exposure of the drug in experiments. Besides, as illustrated in Figure 1.1, the lung's cellular disposition of deposited aerosol drugs can be made even more complex. Provided both pMDIs and DPIs deliver drugs as solid or semi-solid aerosols, lung disposition includes aerosol particle dissolution in the lung lining fluid, followed by cellular uptake (and/or absorption) and possibly, metabolism, prior to the induction of local pharmacological actions within lung cells. In this context, it has been suggested that the lung lining fluid may serve as a significant barrier for dissolution and/or diffusion due to its limited volume of 10-30 mL and thickness of 0.1-23 μm in humans [Widdicombe, 1997; Patton, 1996]. As a result, it has been recently suggested that estimation of the local exposure of drugs within the lung may also not directly translate into even their local pharmacological actions, especially those occurring within

the lung cells [Esmailpur *et al*, 1997; Edsbäcker *et al*, 2006, 2008; Hogger and Rohdewald, 1994; Derendorf *et al*, 2006].

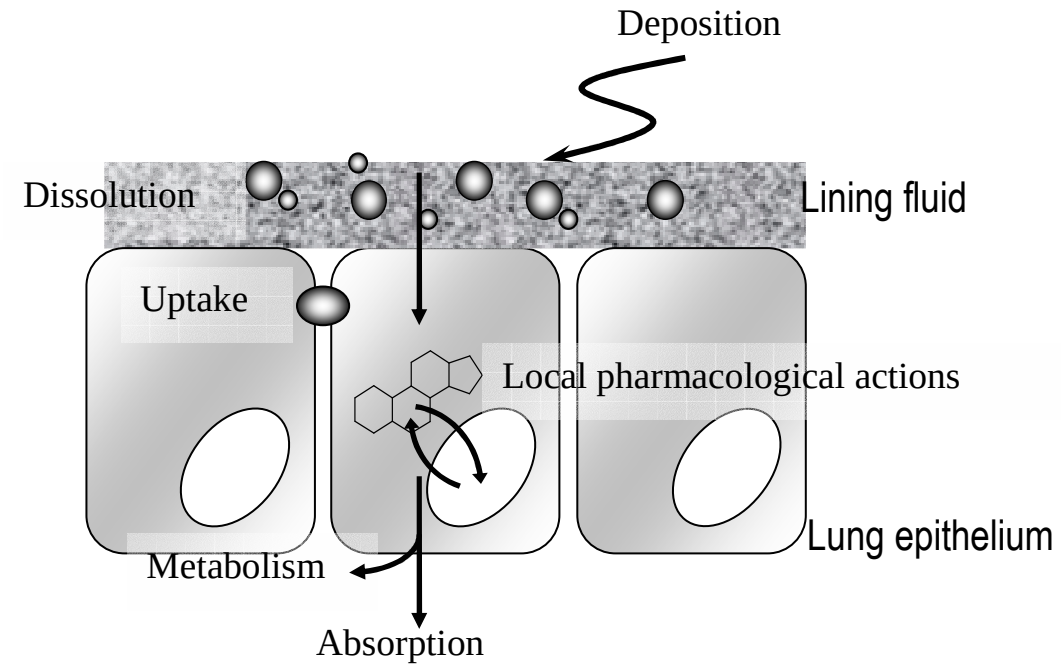

Figure 1.1 Possible lung cellular disposition of an inhaled therapeutic molecule upon aerosol deposition for local pharmacological actions. Inhaled corticosteroid molecules are shown diagrammatically, as an example, interacting with the cellular nuclear materials, alongside a series of alternate disposition processes. The scheme has been adapted from Edsbäcker *et al*, 2006 with slight modifications.

Among a variety of drugs used for inhalation to locally treat lung diseases, inhaled corticosteroids (ICSs) have so far offered one of the most successful and efficacious therapies for asthma and COPD [Schleimer *et al*, 2002; Edsbäcker *et al*, 2006; Hochhaus G, 2004]. As shown in Figure 1.2 (a), in lung diseases like asthma, it has been shown that proinflammatory transcription factors such as nuclear factor kappa B (NFκB) translocates from the cytoplasm into the nucleus where, NFκB binds with its responsive elements to induce the expression of an array of genes for manifestation of inflammatory conditions [Eissa and Huston, 2003; Hogger and Rohdewald, 1993; Hochhaus, 2004]. When ICS molecule is inhaled, as shown in Figure 1.2 (b), they first enter the cells by partition-mediated diffusion and then bind to the glucocorticoid receptors (GRs) that are held in the cytoplasm by heat shock proteins (hsp). This binding causes GR activation and removal from hsp thereby enabling direct interactions of the ICS-GR complex with the proinflammatory transcription factors, e.g., NFκB, within the cytoplasm and/or following translocation into the nucleus. This prevents the induction of gene expression responsible for inflammation and is termed transrepression. In the past decade, it has been increasingly suggested that this action is the primary mechanism of the ICS molecules for anti-inflammatory effects, and a variety of ICSs have been discovered and developed with varying GR binding affinities and thus, varying anti-inflammatory potencies [Roumestan *et al*, 2003; Eissa and Huston, 2003; Winkler *et al*, 2004], as summarized in Table 1.1

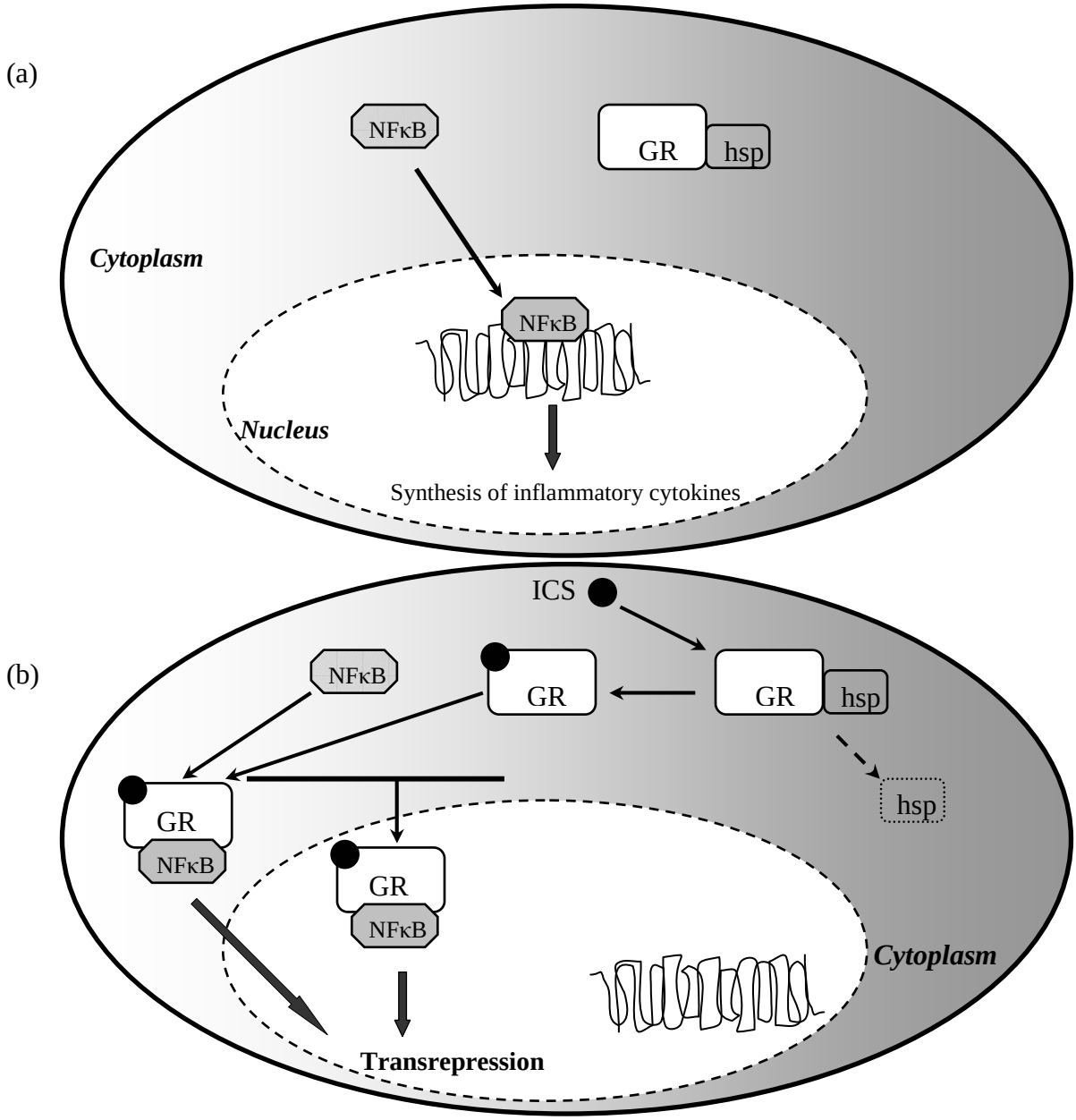

Figure 1.2 Cellular mechanisms of (a) inflammation centered with NFκB and (b) ICS's anti-inflammation via GR binding and its effect on NFκB actions. (a) Glucocorticoid receptor (GR) is held in the cytoplasm chaperoned by heat shock proteins (hsp), while NFκB translocates to the nucleus to cause inflammatory cytokines synthesis. (b) Upon entry into the cell, ICS binds to the GR, which is then activated via hsp removal directly interacting with NFκB. This prevents the synthesis of inflammatory cytokines, i.e., transrepression. Adapted from Hochhaus, 2004.

Table 1.1 Inhaled corticosteroids (ICSs) available in 2008 and their physicochemical properties and intrinsic anti-inflammatory potencies. The data are collectively adapted from Edsbäcker *et al*, 2006 and 2008; Hogger and Rohdewald, 1993; Hochhaus, 2004; Winkler *et al*, 2004; Roumestan *et al*, 2003 and Jafuel *et al*, 2000.

ICS	Molecular Weight [Da]	Log P	Aqueous Solubility [μg/mL]	Relative receptor affinity *	Relative repression potency on NFκB activity**
Flunisolide (FLU)	434	2.28	140.0	190	0.5
Triamcinolone acetonide (TA)	434	2.53	21.0	233	1.0
Budesonide (BUD)	431	3.24	16.0	935	2.2
Beclomethasone dipropionate (BDP)	521	3.63	0.13	1022	0.5
Fluticasone propionate (FP)	501	4.20	0.14	1800	10.0
Mometasone furoate (MF)	427	3.38	<0.1	2300	>10.0

* Relative to a GR affinity of dexamethasone set to 100

** Relative to a half-maximal effective or inhibitory concentration of TA set to 1

As of 2008, a total of 6 ICSs are available in various inhaled dosage forms in the United States [Electronic Orange Book, FDA]. Table 1.1 lists their physicochemical properties, i.e., molecular weight (MW), partition coefficient (Log P) and aqueous solubility, alongside their intrinsic anti-inflammatory potencies, i.e., relative affinity to the GR binding and relative potency of proinflammatory NFκB repression [Edsbäcker *et al*, 2006, Hogger and Rohdewald, 1993, Hochhaus, 2004, Winkler *et al*, 2004, Roumestan *et al*, 2003 and Jafuel *et al*, 2000]. It is clear from Table 1.1 that ICSs differ in physicochemical properties and intrinsic potencies, yet a general notion exists in that

the intrinsic anti-inflammatory potency increases with increasing lipophilicity (i.e., Log P) [Edsbäcker et al, 2006; Hogger and Rohdewald, 1993; Hochhaus, 2004]. This may be logical from the pH-partition hypothesis for drugs exhibiting their pharmacological actions within cells, like the ICSs. However, as the lipophilicity increases, aqueous solubility decreases. In fact, the more widely used ICSs like fluticasone propionate (FP) and beclomethasone dipropionate (BDP) have only 0.14 and 0.13 µg/mL of the aqueous solubility (Table 1.1), respectively. Hence, given their typical single inhaled doses of 40-200 µg and their maximum 20 % of successful delivery to the lung [Byron and Patton, 1994], 8-40 µg of FP or BDP would be expected to land on the lung lining fluid as solid or semi-solid aerosols from their dosage forms of pMDIs and/or DPIs. In an ideal case scenario, where these ICS aerosols uniformly deposit throughout the entire lung mucosal surface with a total lung lining fluid volume of 10-30 mL [Widdicombe, 1997], the ICS concentration would be approximately 0.3-4.0 µg/mL, assuming spontaneous and total dissolution. Obviously, such concentrations far exceed their solubility and therefore, it is likely that substantial portions of the deposited FP and BDP doses remain to be dissolved on the cell surface without being taken up by the cells. In contrast, this would not be the case for a fairly soluble ICS like triamcinolone acetonide (TA). Its single dose from pMDI is 200 µg, and again with 20 % of lung delivery and 10-30 mL of the lining fluid volume, TA concentrations on the lung mucosal surface would reach 1.3-4.0 µg/mL. Such concentrations are much lower than 21 µg/mL corresponding to its aqueous solubility and hence, an ICS, like TA could be dissolved in the lung lining fluid fairly promptly following deposition.

Supportive evidence on this potentially solubility-limited lung disposition for certain aerosol drugs exists in the literature, yet in animals. Carboxylic acid of methyl sulfinyl xanthone was administered to the rat lung as suspension, and its lung disappearance profile was compared with that of its sodium salt given as solution [Chowhan and Amaro, 1976]. The slower and biphasic lung disappearance profile was shown for the suspension administration, compared to the faster and monophasic profile for the solution counterpart. This slower and biphasic profile for the suspension was attributed to a need for xanthone dissolution within the airways prior to lung absorption, suggesting, for the first time, that dissolution could control the kinetics of lung disposition. Likewise, a study with guinea pigs demonstrated that a 6.5-fold increased solubility of the poorly soluble fluorescein (acid; 13.5 µg/mL of aqueous solubility) by amorphous incorporation within the respirable-size microspheres resulted in near 2-fold increased lung absorption following powder aerosol administration to the lung [Sakagami *et al*, 2001]. This rather implied that, a limited 46 % bioavailability for the poorly soluble fluorescein, despite its small molecular weight (i.e., 332 Da), was likely caused by its slower dissolution within the airways of the guinea pigs. However, a counterargument also exists, primarily from a premise that inhaled aerosol particles are so small in size that their dissolution rate should be rapid by virtue of their large surface area per unit weight. A stimulus article recently published by the USP ad hoc Panel [Gray *et al*, 2008] followed this premise, since no compelling evidence for dissolution rate-controlled kinetics of lung disposition have been indicated in the human clinical literature. Accordingly, this debate that addressed our knowledge about this important

biopharmaceutical phenomenon for inhaled therapeutics, i.e., aerosol dissolution on the lung mucosal surface, is still in infancy, even though logically, it relates to the kinetics of lung disposition and possibly, the manifestation of local pharmacological actions.

The USP ad hoc Panel was initially briefed to seek for a need of compendial dissolution testing system, specifically for aerosol drugs from inhaler products [Gray *et al*, 2008]. While the USP currently lacks such an established system to determine the kinetics of dissolution for aerosol particles, a custom-made flow-through system similar to the USP Dissolution Testing Apparatus 4.2 [USP, 2003b] was used for determining the dissolution profiles of selected ICS aerosol particles collected on the membrane filters, generated from their commercial pMDIs and DPIs [Davies and Feddah, 2003]. The aerosol collection on membrane filters was carried out at the exit of the USP induction port coupled with the Andersen cascade impactor (ACI), a compendial apparatus to determine aerodynamic particle size distributions for inhaler products. Such filters carrying ICS particles were subjected to dissolution profile testing in the flow-through system using simulated lung lining fluid at a flow rate of 0.7 mL/min. This approach was surely innovative in that the ICS aerosols generated from the inhaler products were directly tested for dissolution, for the first time. Nevertheless, because the ICS aerosols were collected by filtration at the exit of the USP induction port prior to the entry to the ACI, their sizes remained unknown likely inconsistent between the ICSs products. Moreover, the use of the flow-through system would create rather favorable flow dynamics for dissolution into an unlimited fluid volume, while the real

lung lining fluid is largely stationary and limited in volume. Hence, it would be preferable to develop a dissolution testing method for inhaler products, which enables determination of the dissolution profiles for defined- and respirable-size aerosol particles into a limited volume of stationary fluid; this being more analogous to aerosol particle dissolution on the lung mucosal surface following deposition.

Aerosol particles of ICS deposit and dissolve on the lung's mucosal surfaces prior to drug uptake by the cells. Subsequently, the drugs may exert their anti-inflammatory actions and be absorbed through the cells into the systemic circulation, as described in Figure 1.1; local lung metabolism may also occur for certain ICSs. However, these cellular events have never been successfully studied for ICSs generated from inhaler products other than perhaps, in human clinical trials. Small rodents such as rats, guinea pigs or mice are too small to receive typical aerosol ICS doses by inhalation, especially those directly generated from inhaler products [Sakagami, 2006]. Likewise, cultured lung cell systems have been developed, although these were usually submerged in culture media, precluding direct access of aerosol ICSs generated from the inhaler products to the cell surfaces. In this context, however, evidence has emerged that certain cultured lung cell systems can be prepared as monolayers with their apical mucosal surfaces covered with a limited volume of the cell lining fluid [Forbes 2000; Meaney *et al*, 2002; Sakagami, 2006; Ehrhardt *et al*, 2002; Borchard *et al*, 2002]. Such cultured lung cells are immortalized human bronchial epithelial cell line of cancer-origin, Calu-3, transformed human bronchial epithelial cell line of normal lung-origin,

16HBE14o-, and finally, primary cultured rat alveolar epithelial cells [Sakagami, 2006; Forbes and Ehrhardt, 2004; Ehrhardt *et al*, 2002a and b; Forbes B, 2000; Cheek *et al*, 1989; Dobbs LG, 1990; Fang *et al*, 2004; Elbert *et al*, 1999; Smith, 1977; Wang and Zhang, 2004; Borchard *et al*, 2002; Fiegel *et al*, 2003; Cooney *et al*, 2004; Grainger *et al*, 2006a and b; Mathias *et al*, 2002]. These lung cells have been shown to form monolayers under a culturing condition called "air-interface culture" (AIC) where the cells were fed only with a culture media basolaterally in the transwell system, while the apical mucosal surface was left semi-dry [Fiegel *et al*, 2003; Cooney *et al*, 2004; Grainger *et al*, 2006a and b; Mathias *et al*, 2002]. This culture method appeared to facilitate the development of a well-differentiated barrier, compared to the conventional medium-submerged culture [Adler *et al*, 1990]. The method also enabled direct mucosal access of solutions, suspensions or aerosols by virtue of its semi-dry apical surface on which there is only a limited volume of the lining fluid [Fiegel *et al*, 2003; Cooney *et al*, 2004; Grainger *et al*, 2006b].

The Calu-3 cells available from the American Type Culture Collection (ATCC) have been the most studied in the literature, since their confluent monolayers grown under the "air-interface culture" (AIC) were shown to form a sufficiently tight barrier for diffusive permeation [Borchard *et al*, 2002; Fiegel *et al*, 2003; Cooney *et al*, 2004; Grainger *et al*, 2006a and b; Mathias *et al*, 2002]. These monolayers appeared to be capable of maintaining a semi-dry mucosal surface, thereby offering a unique opportunity for direct deposition of solid or liquid aerosols. The first attempt to do this was made using a multi-stage liquid impinger (MSLI), a compendial apparatus to

determine particle size distribution of inhaler products [Fiegel *et al*, 2003]. The transwell insert of the Calu-3 monolayer grown under the "air-interface culture" (AIC) was placed under the second stage nozzle in the MSLI for aerosol deposition of poly(lactic-co-glycolic)acid microparticles. The Calu-3 monolayers were shown to tolerate this microparticle deposition, as evidenced by their unaltered permeability for a marker solute and unchanged electrophysiological characteristics. Another attempt followed using a viable cascade impactor (VCI) [Cooney *et al*, 2004]. These authors placed transwell inserts just below its Stage 4 for ≤2.1 μm aerosol deposition onto the semi-dry mucosal surface of the Calu-3 monolayers. Unfortunately, in both of those studies, the lining fluid volume of the monolayers was undetermined, thereby precluding determination of solute permeability after aerosol deposition on the mucosal surface. Even so, both attempts proved that the Calu-3 monolayers can be incorporated into a cascade impactor direct aerosol particle deposition in defined sizes on the semi-dry mucosal surface on the monolayer, while maintaining the intact characteristics of the barrier. Such systems would provide a unique opportunity to study cellular lung disposition processes as a cascade, similar to that occurring in human lung after aerosol inhalation.

Meanwhile, cellular pharmacological assessment of anti-inflammatory effects of ICSs has so far largely disregarded the effects of their aerosol deposition onto the lung's mucosal cell barrier in a limited volume of lining fluid. In fact, the anti-inflammatory potencies shown in Table 1.1 were obtained using direct application of ICS solutions to non-confluent medium-submerged lung cells to determine the potency of the anti-

inflammatory response in incubation. The measurement commonly has employed immunoassays with the isolated nuclear fraction of the cells, e.g., enzyme linked immunosorbent assay (ELISA) for the proinflammatory NFκB [Baldwin, 1996]. Alternatively, reporter gene assays with the cells transfected with an inducible NFκB-dependent reporter gene, such as luciferase [Baldwin, 1996; Roumestan *et al*, 2003; Jafuel *et al*, 2000] have been performed. Provided that ICSs exert their actions by repression of the cellular transcription factors like NFκB, these approaches seem reasonable, yet most disregard aerosol deposition and local disposition, because of experimental difficulties. As a result, it has been suggested that their results were an over-simplification of in vivo or clinical events, which may explain certain literature with their puzzling anti-inflammatory potencies [Edsbäcker *et al*, 2006]. It has been well accepted that the local ICS disposition for aerosol drugs should overall define its cellular pharmacodynamic effects following aerosol deposition [Edsbäcker *et al*, 2006; 2008].

It should be clear now that there is a strong desire to develop useful models to address certain important biopharmaceutical processes pertaining to lung disposition preferably without using animals and humans. The examples of important biopharmaceutical processes include dissolution into the mucosal fluids for efficient cellular uptake/absorption as well as manifestation of local pharmacological actions following aerosol drug deposition. Hence, this dissertation project was designed to first determine the kinetics of dissolution for the ICS aerosols generated from inhalers and

then, to assess their importance on lung disposition and local anti-inflammatory effects. Two novel and unique in vitro systems were developed to achieve these objectives: an in vitro dissolution testing system and an in vitro Calu-3 cell monolayer system, both coupled with accurate and precise ICS aerosol deposition from the inhaler products. The project revolved around the central hypothesis that lung cellular disposition and pharmacology of certain aerosol ICSs are kinetically rate-determined by dissolution on the lung surface following aerosol deposition. First, a simple system was developed, capable of assessing the dissolution kinetics for ICS aerosol particles generated from commercial inhaler products. This identified ICSs for which dissolution was most likely rate-determining. Air-interface cultured Calu-3 monolayers with a semi-dry mucosal surface were then developed and validated, thereby, offering an opportunity to directly deposit ICS aerosol particles on their surface in a well-defined and well-characterized deposition system. This system was used to assess anti-inflammatory effects, in relation to dissolution, using the Calu-3 monolayers transfected with a NFκB-dependent reporter gene.

CHAPTER 2

HYPOTHESES

The goal of this dissertation project was to determine the kinetics of dissolution for aerosol particles of inhaled corticosteroids (ICSs) generated from inhaler products and to assess their importance on lung disposition and local anti-inflammatory actions. Overall, it was hypothesized that lung cellular disposition and pharmacology of certain aerosol ICSs were kinetically rate-determined by particle dissolution into a limited volume of lung mucosal lining fluid. Specifically, the project first aimed to develop an in vitro dissolution testing system to determine the kinetics of dissolution for ICSs of a defined-size into a limited volume of fluid upon aerosol deposition from inhaler products. Then, the project proceeded to develop an in vitro lung epithelial cell monolayer system enabling deposition of a defined-size aerosol, followed by assessment of the effects of dissolution on cellular uptake and anti-inflammatory actions. Accordingly, the project was designed to test the following six hypotheses:

a. Aerosol particles of ICSs generated from inhaler products can be accurately and precisely collected on membrane filters in a defined-size in the Andersen cascade

impactor (ACI), such that their kinetics of dissolution in a limited volume of fluid can be determined in a transwell system.

b. The kinetics of dissolution for different aerosol ICSs differ substantially, depending upon not only ICS solubility, but also aerosol mass, particle size and/or formulation and dosage form.

c. A unique lung epithelial cell monolayer of Calu-3 can be formed with its apical mucosal surface left semi-dry with a limited volume of the cell lining fluid that can be successfully as an epithelial barrier for use in pulmonary biopharmaceutics research.

d. Confluent Calu-3 cell monolayers can be transfected with a measurable biomarker for inflammation, nuclear factor kappa B (NFκB) -dependent reporter gene of luciferase (pNFκB-Luc), for use in anti-inflammatory assessment of aerosol ICSs.

e. Aerosol particles of ICSs in defined-size ranges from inhalers can be accurately and precisely deposited on the apical surface of the Calu-3 cell monolayers using the ACI in a modified configuration, in order to determine their mucosal disposition, cellular uptake and anti-inflammatory effects.

f. Cellular uptake of certain aerosol ICSs can be kinetically rate-limited because of mucosal dissolution, thereby, resulting in compromised anti-inflammatory responses; thus signifying that their intrinsic molecular potencies of anti-inflammation in the literature overrate their potencies following aerosol deposition in the lung.

In Chapter 3, a new in vitro dissolution testing system for aerosol ICSs from inhaler products will be described alongside system development and validation. In Chapter 4, lung epithelial cell monolayers of Calu-3 grown under the air-interface culture (AIC) will be described alongside the characterization as an epithelial barrier suitable for direct aerosol deposition. In Chapter 5, aerosol ICS deposition from inhalers onto the semi-dry, transfected Calu-3 monolayers and its anti-inflammatory action assessment via the NFκB activity measured by luciferase will be described. The results are interpreted in the light of knowledge gained on ICS dissolution and cellular uptake from previous chapters. Chapter 6 will summarize the findings of this dissertation project and draw general conclusions.

CHAPTER 3

KINETIC ASSESSMENT OF AEROSOL PARTICLE DISSOLUTION FOR TESTING COMMERCIAL INHALER PRODUCTS

3.1 INTRODUCTION

Inhaled dosage forms deliver their active pharmaceutical ingredients (APIs), along with formulation excipients, onto the lung surface in a solid or semi-solid form, except in case of solution nebulization. Hence, a study of their biopharmaceutics should at least consider API dissolution into a limited volume (e.g., 10-30 mL) of lung lining fluid prior to subsequent cellular uptake or absorption [Hochhaus *et al*, 1997; Edsbäcker *et al*, 2006]. In this context, evidence exists in the literature that aerosol particles generated from inhalers can contain formulation excipients that potentially alter their surface properties and/or form different states of crystallinity due to their formulation and aerosol generation processes [Dalby and Byron, 1993; Thomas *et al*, 2005]. While these may alter the kinetics of dissolution of the APIs themselves, it is also possible that certain APIs and their aerosol particles may suffer from dissolution rate-determined uptake within the lung [Wurster and Taylor, 1965; Sakagami *et al*, 2002].

Given this logical involvement and possible importance of the dissolution kinetics of inhaled therapeutics in lung biopharmaceutics, Davies and Feddah [Davies and Feddah, 2003] developed a unique in vitro method to determine the dissolution profiles of inhaled corticosteroid (ICS) particles generated from commercial pMDIs and DPIs. The aerosol collection on membrane filters was carried out at the exit of the USP induction port using the Andersen cascade impactor (ACI), a compendial apparatus to determine aerodynamic particle size distributions for inhaler products. This was followed by their dissolution profile determination using a custom-designed flow-through system, similar to the USP Dissolution Testing Apparatus 4.2 [United States Pharmacopoeia, 2003b]. This approach was innovative in that the ICS aerosols generated from the inhaler products were directly tested for dissolution, for the first time. Nevertheless, because ICS aerosols were collected by filtration at the exit of the USP induction port prior to the entry to the ACI, their sizes remained unknown and likely inconsistent between the products. In addition, the use of the flow-through system would create rather favorable flow dynamics with an unlimited volume of fluid available for dissolution. In contrast, the lung lining fluid in human is only 10-30 mL in total volume [Widdicombe, 1997], which would limit the dissolution capacity for deposited drugs, while the flow dynamics are relatively stationary. Hence, it would be ideal that a dissolution method for inhaler products enables the kinetic assessment of dissolution for defined- and respirable-size aerosol particles into a limited volume of stationary fluid, analogous to aerosol particle dissolution on the surface of the lung.

Accordingly, this chapter attempted to develop a unique dissolution testing method for aerosol particles generated from commercial inhaler products, focused on collection of defined-size aerosols to be tested for dissolution in a limited volume of stationary fluid. It employed aerosol impaction onto the filter membranes placed on Stage 2 and Stage 4 of the ACI from an airflow rate of 28.3 L/min, so that particles with 4.7-5.8 and 2.1-3.3 µm of aerodynamic diameter, respectively, could be accurately and precisely collected in an amount between 0.6 and 19.8 µg. These filter membranes were then placed in the transwell inserts where sequential events of particle dissolution on the donor side and permeation across the transwell's supporting membrane were monitored following addition of a limited volume (40 µL) of dissolution fluid. A total of 5 ICSs and 7 commercial inhalers that were pMDIs or DPIs were used to collect a variety of drug deposits on the filter membranes. These were tested to pursue the hypothesis that the kinetics of dissolution for aerosol particles may depend on not only the reported aqueous solubility of each API but also the drug deposit mass, aerosol size and formulation and most notably, differ across APIs.

3.2 MATERIALS AND METHODS

3.2.1 COMMERCIAL INHALER PRODUCTS

All commercial inhaler products used in this study were obtained from their vendors through the VCU Health System Pharmacy. Table 3.1 lists 7 ICSs inhaler

products for 5 ICSs along with their physicochemical features. They were packaged in either pMDIs or DPIs. The ICSs differed with respect to their reported aqueous solubilities. Formulations were non-aqueous suspensions and solutions and powder with several different excipients. These products also differed in their metered doses. All products were used prior to their labeled expiry date, except for Vanceril® pMDI that was used as an expired product, as it was withdrawn from the market in 2002. Vanceril® pMDI was used 5 years after the expiry date, yet a negligible degradation of API, BDP, was evidenced by the absence of any chromatographic detection of any peaks other than those of the API from the samples taken from the inhalers (data not shown).

Table 3.1 Inhaled corticosteroids (ICSs) and their commercial inhaler products tested in this study.

Inhaler Product[1]	Drug	Dosage Form[2]	Molecular Weight [Da]	Aqueous Solubility [µg/mL][3]	Formulation[4]	Metered Dose [µg]
AEROBID	Flunisolide (FL)	pMDI	434	140	FL suspended in CFC-11, -12 and -114 with sorbitan trioleate	250
AZMACORT[5]	Triamcinolone Acetonide (TA)	pMDI	434	21	TA suspended in CFC-12 and 1% alcohol	200
PULMICORT TURBUHALER	Budesonide (BD)	DPI	431	16	BD only	200
FLOVENT HFA	Fluticasone Propionate (FP)	pMDI	501	0.14	FP suspended in HFA-134a	44 and 220
FLOVENT DISKUS	FP	DPI	501	0.14	FP and Lactose 200	50
VANCERIL	Beclomethasone Dipropionate (BDP)	pMDI	521	0.13	BDP suspended in CFC-11, and -12 with oleic acid	100
QVAR	BDP	pMDI	521	0.13	BDP dissolved in HFA-134a and ethanol	40

[1] The names of all products are registered trademarks.
[2] pMDI: pressurized metered dose inhaler, DPI: dry powder inhaler
[3] Data were taken from Hogger *et al*, 1993
[4] Prescription information
[5] Used without the built-in spacer.

3.2.2 ICS AEROSOL PARTICLE COLLECTION ON FILTERS BY IMPACTION

Figure 3.1 schematically shows collection of ICS aerosols onto membrane filters by impaction in defined aerodynamic diameter ranges of 4.7-5.8 and 2.1-3.3 µm following generation from each of the inhaler products listed in Table 3.1. An 8-stage, non-viable Andersen cascade impactor (ACI Mark II; Thermo Electron Corporation, Franklin, MA) with stainless steel collection plates was used, coupled with the USP induction port and the mouthpiece adaptor tailored to each inhaler. These were assembled, together with a pump (General Electric Company, Fort Wayne, IN), which was adjusted to operate at 28.3 L/min of airflow rate. During this ACI assembly, however, the stainless steel collection plates on Stage 2 and Stage 4, which are calibrated to collect aerosol particles at 4.7-5.8 and 2.1-3.3 µm in aerodynamic diameters, respectively, at 28.3 L/min [United States Pharmacopoeia], were turned upside down. This allowed 6 polyvinylidene difluoride (PVDF) filter membranes (25 mm in diameter; 0.22 µm Durapore®, Millipore Corporation, Billerica, MA) to be placed at each of these stages, as shown in Figure 3.1; note that the nozzle-to-filter distance was unaltered from those in the conventional, calibrated ACI configuration. Following assembly, ICS aerosols were collected on these PVDF filter membranes following their generation from each of pMDIs and DPIs by using an appropriate number of actuations into the impactor with airflow set to 28.3 L/min. The required number of actuations was chosen to enable collection of the target ICS aerosol deposit on each filter in a range of 0.6-19.8 µg. This was based on preliminary experiments where ICS collections were made over the entire stainless steel plates (80 mm in

diameter; 50.2 cm^2) in order to predict the deposition mass on each membrane filter (25 mm in diameter; 4.9 cm^2) by and its normalization based on its reduced collection area.

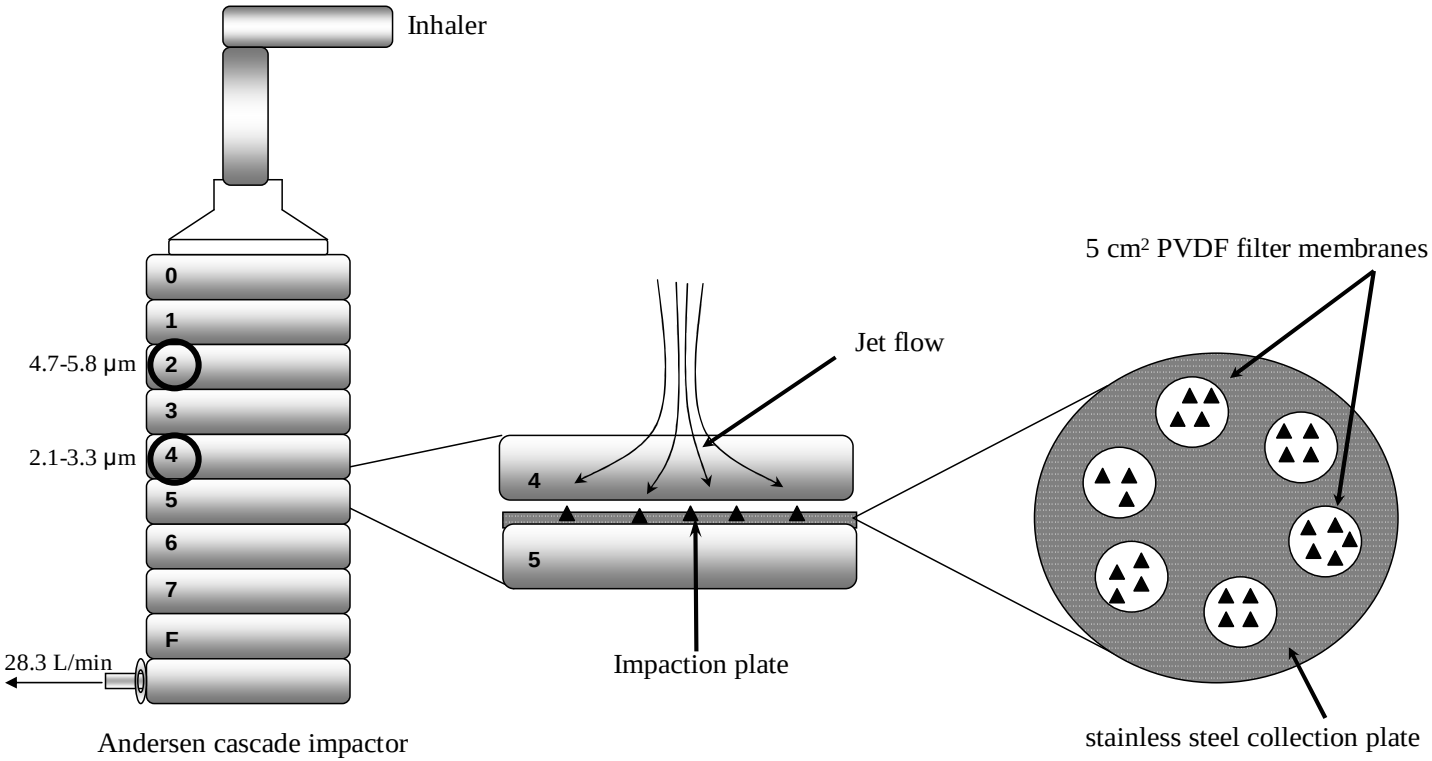

Figure 3.1 A schematic of ICS aerosol particle collection in the defined aerodynamic diameter ranges using the Andersen cascade impactor (ACI). While the ICS aerosols were collected at both Stage 2 and Stage 4, only Stage 4 is shown magnified above for the collection of the 2.1-3.3 µm ICS aerosols on 6 polyvinylidene difluoride (PVDF) filter membranes placed on the reversed stainless steel collection plate. Deposited drug is shown diagrammatically as solid black triangles.

3.2.3 DISSOLUTION AND PERMEATION PROFILES OF ICS AEROSOL PARTICLES

Following ICS aerosol collection, the ACI was disassembled. Each of the filter membranes with 0.6-19.8 µg ICS deposit was placed, with the deposited drug face down, onto the donor compartment of the transwell inserts with semi-permeable polyester membrane (25 mm in diameter; 0.4 µm pore) support (Corning Costar; Cambridge, MA), as shown in Figure 3.2. The insert was then returned to the transwell base containing 1.4 mL of phosphate-buffered saline (PBS; pH 7.4) or distilled, deionized water (DDW; pH 7.0). PBS (pH 7.4) was used for FL, TA and BUD; DDW (pH 7.0) was chosen for FP and BDP as their mass spectrometry analysis disfavored PBS. Immediately, ICS dissolution and transwell membrane (polyester) permeation were initiated by adding 0.04 mL of PBS or DDW onto the donor side and monitored over time (for 5-10 h) at 37 °C and near 100 % relative humidity inside an incubator (Model 5410; NAPCO, Precision Scientific, Inc., Chicago, IL) by taking 0.5 mL samples from the receptor compartment at different time intervals. The receptor compartment was replenished each post-sampling with 0.5 mL fresh and pre-warmed PBS or DDW to maintain its volume at 1.4 mL. At the end of each experiment, the donor compartment was thoroughly washed with 1.0 mL admixture of 60% CH_3CN and 40% DDW to recover the ICS remaining to be dissolved and permeated. All samples were analyzed for ICS quantification by the validated analytical methods described below (Table 3.2), such that the profiles of dissolution and permeation were obtained, as described in 3.2.6.

3.2.4 TRANSWELL MEMBRANE PERMEATION PROFILES OF ICS FOLLOWING SOLUTION APPLICATION

For FL and TA, the permeation profiles across the transwell (polyester) membranes unaffected by dissolution were also determined by direct solution application at 25 and 10 µg/mL, respectively. 0.04 mL of the ICS solution was applied to the donor side of the transwell inserts and their permeation to the receptor side with 1.4 mL of PBS was monitored by sampling 0.5 mL at various times and analyzed, as described below.

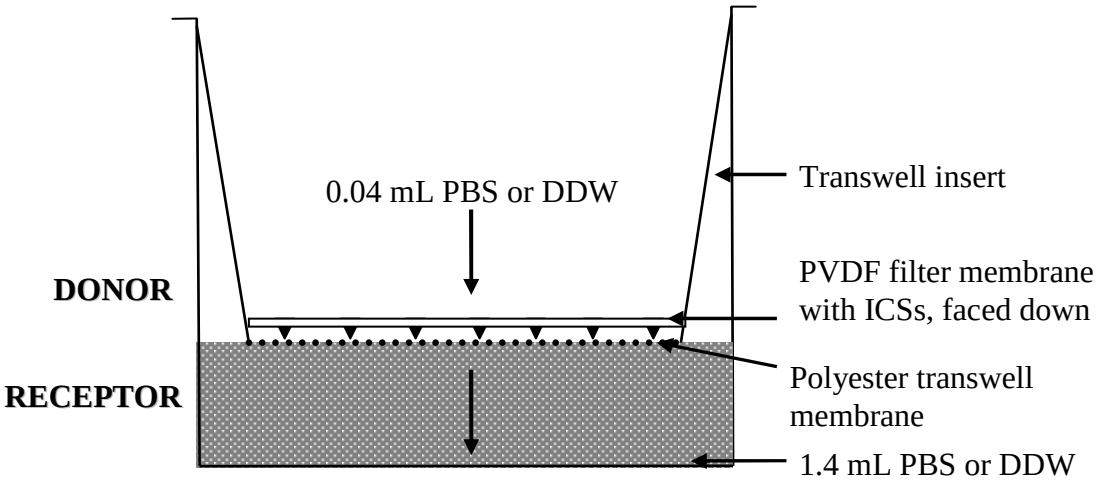

Figure 3.2 A schematic of transwell system to determine dissolution and permeation of the ICS aerosol particles (represented by triangular heaps) collected on the PVDF filter membranes in the ACI. The filter membrane was placed face down on the transwell's supporting membrane. ICS dissolution and permeation was initiated by adding 0.04 mL PBS or DDW on the donor side.

3.2.5 DRUG ANALYSIS

Analytical standards of FL, TA, BD, FP and BDP, HPLC grade CH_3CN and CH_3OH and ammonium formate (NH_4HCO_2) were obtained from Sigma-Aldrich (St. Louis, MO). Each of the ICSs in PBS, DDW or 60% CH_3CN/ 40% DDW samples were analyzed by the methods developed and validated in-house, as summarized in Table 3.2.

FL, TA and BD were analyzed by high performance liquid chromatography (HPLC) coupled with UV detection at 236 nm (Waters Corporation, Milford, MA). The mobile phase comprised of 60 % CH_3CN and 40 % DDW at a flow rate of 1 mL/min. The samples (100 µL) diluted with 60/40 CH_3CN/DDW were injected onto a Spherisorb ODS-2 column (4.6 mm in diameter and 250 mm in length, 5 µm; Alltech Associates Inc., Deerfield, IL), and FL, TA and BD were typically eluted at 3, 5 and 8 min, respectively. Each of the analyses was fully validated with respect to (a) the linearity (r^2>0.999) of the peak area vs. concentration over the range of 0.05 to 5 µg/mL and (b) the limit of quantitation (LOQ) of the assay at 50 ng/mL (Table 3.2).

FP was analyzed by HPLC, coupled with tandem mass spectrometry (MS/MS), modified from Krishnaswamy *et al* [Krishnaswamy *et al,* 2000]. The mobile phase comprised of 50 % CH_3CN and 50 % DDW containing 0.1 % NH_4HCO_2 at a flow rate of 0.3 mL/min. The samples (50 µL) were injected onto a Gemini S_4-C_{18} 110 Å column (4.6 mm x 50 mm, 5 µm) and detected using a triple quadruple mass spectrometer (Quattro-LC, Waters, Milford, MA) with electrospray ionization (ESI) in a positive ion mode. The MS-MS signals were tuned and optimized through a constant infusion of 1.0 µg/mL FP solution in CH_3OH at 1.0 mL/min delivered with an infusion pump (Harvard

Syringe Pump, Harvard Apparatus, Holliston, MA). High-purity nitrogen (National Welders; Richmond, VA) was used as a collision gas. The optimization concluded that the source and the ESI probe temperatures be set at 140 °C and 400 °C, respectively, with the corona and cone voltages at 4.0 kV and 10.0 kV. The assay was used under those conditions and mass resolution was set at unit mass and hence, the m/z transition from 501.44 $(MH)^+$ to 313.21 was monitored. FP was shown to be eluted at 3 min, which was analyzed using MASSLYNX software. The analysis was fully validated with respect to (a) the linearity (r^2>0.999) of the peak area vs. concentration over the range of 3-100 ng/mL and (b) the LOQ at 3.0 ng/mL (Table 3.2).

BDP was analyzed by the HPLC-MS/MS method developed at the VCU Bioanalytical Core Laboratory using the Waters Quattro-Micro (Waters, Milford, MA) mass spectrometer with atmospheric pressure chemical ionization (APCI) in a positive ion mode. The samples (50 µL) were injected onto a Zorbax Eclipse XDB-C8 (4.6 x 50mm, 3.5µm) at a flow rate of 0.6 mL/min. The mobile phase was a gradient of DDW and CH_3OH in the presence of 2 mM NH_4HCO_2 (A and B, respectively). The gradient was set from A to B at 0% B (0.01 min), 50% B (0.4 min), 80% B (6.0 min), 90% B (7.0 min), 50% B (7.1 min) and 0% B (10.0 min), controlled with a Shimadzu 10-AVP (Columbia, MD) system. The probe temperature was set at 350 °C, while the declustering potential, entrance potential, collision energy and collision energy potential were set at 76 V, 10 V, 23 V and 20 V, respectively. The m/z transition from 521.4 $(MH)^+$ to 319.4 was monitored. BDP was eluted in a 10 min run-time. Data analysis was performed using the MASSLYNX software. The analysis was fully validated with

respect to the linearity (r^2>0.999) of the peak area vs. concentration over the range of 1-100 ng/mL along with the LOQ at 1.0 ng/mL (Table 3.2).

3.2.6 PROFILE ANALYSIS

Cumulative ICS mass dissolved and permeated into the receptor compartment at a given sampling time was calculated from the product of the sample concentration and the volume (1.4 mL) of the receptor plus that of the concentrations in previously taken samples and their volumes (0.5 mL). Initial ICS mass deposited on each of the filter membranes were determined from the sum of the ICS masses recovered from the donor and receptor compartments by the end of the experiment. The dissolution and permeation profile of each transwell was described as % ICS mass dissolved and permeated into the receptor compartment over initial ICS mass deposit as a function of time and then, expressed as mean % profiles with sample standard deviation (SD) from triplicate experiments, as shown in Figures 3.3 through 3.8. Apparent half-life ($t_{0.5}$) was calculated from each profile via linear interpolation of the time points that bracketed the 50 % point of ICS mass dissolved and permeated in the mean % profiles, except for FP and BDP, in which the $t_{0.5}$ values were determined by profile extrapolation.

Table 3.2 Inhaled corticosteroids (ICSs) and their analytical methods used in this study.

Drug	Analysis	Separation			Detection	LOQ[1] [ng/mL]
		Column	Mobile Phase	Flow rate [mL/min]		
Flunisolide (FL)	HPLC-UV	Spherisorb ODS, 2-5 µm, Length: 250 mm, ID: 4.6 mm	60% CH_3CN and 40% H_2O	1.0	236 nm	50
Triamcinolone acetonide (TA)	HPLC-UV	Spherisorb ODS, 2-5 µm, Length: 250 mm, ID: 4.6 mm	60% CH_3CN and 40% H_2O	1.0	236 nm	50
Budesonide (BD)	HPLC-UV	Spherisorb ODS, 2-5 µm, Length: 250 mm, ID: 4.6 mm	60% CH_3CN and 40% H_2O	1.0	236 nm	50
Fluticasone propionate (FP)	HPLC-MS/MS[2]	Gemini S_4 C_{18} 110 Å, 5 µm, Length: 50 mm, ID: 2.0 mm	50% CH_3CN and 50% H_2O containing 0.1% NH_4HCO_2	0.3	ESI[3], m/z 501.44 → 313.21	3.0
Beclomethasone dipropionate (BDP)	HPLC-MS/MS	Zorbax Eclipse XDB-C8, 3.5 µm, Length: 50 mm, ID: 4.6 mm	Gradient of 2 mM NH_4HCO_2 in H_2O and 2mM NH_4HCO_2 in CH_3OH (details in text below)	0.6	APCI[4], m/z 521.4 → 319.4	1.0

[1] Limit of quantitation
[2] Krishnaswamy *et al*, 2000
[3] Electrospray ionization
[4] Atmospheric pressure chemical ionization

3.3 RESULTS

3.3.1 ICS AEROSOL PARTICLE COLLECTION ON FILTERS BY IMPACTION

Table 3.3 summarizes the ICS mass deposits collected on the 5.0 cm^2 PVDF filter membranes placed on Stage 2 and Stage 4 of the ACI following various numbers of actuations or doses from each of the pMDIs or DPIs tested in this study (Table 3.1). These various actuations or doses were selected, so that the ICS mass deposits on the filter membranes were best comparable at ~2 (1.6-2.9) µg and otherwise, adequately varied within or across the ICSs and inhaler products. This was aimed to assess the kinetics of dissolution and permeation, in relation to the specific ICS in question, its solubility, dose, formulation and dosage form, as studied and discussed below. Clearly, the required numbers of actuations or doses to achieve the ~2 µg deposit at each stage were different between the ICSs and products, due to the differences in the metered dose (Table 3.1) and aerodynamic particle size distribution. Overall however, the ACI deposition system shown in Figure 3.1 enabled the 4.7-5.8 and 2.1-3.3 µm ICS aerosol deposition on the filter membranes fairly reproducibly with ≤ 23 % of relative standard deviation (%RSD).

Table 3.3 ICS mass deposits collected on the 5.0 cm^2 PVDF filter membranes placed on Stage 2 and Stage 4 of the ACI following various numbers of actuations or doses from each of the pMDIs or DPIs. Data represent mean±SD (n=3).

Inhaler product (Metered dose)	Drug	Number of actuations	Mass deposit on the filter (µg)	
			Stage 2	Stage 4
AEROBID (pMDI) (250 µg)	FL	1	0.7 ± 0.1	2.3 ± 0.1
		5	6.2 ± 1.0	10.9 ± 0.5
		10	9.1 ± 1.7	18.8 ± 1.1
AZMACORT (pMDI) (200 µg)	TA	1	1.1 ± 0.1	0.4 ± 0.03
		5	7.7 ± 1.4	2.5 ± 0.3
		10	14.0 ± 1.0	4.7 ± 0.2
PULMICORT TURBUHALER (DPI) (200 µg)	BD	1	N.A.	0.8 ± 0.04
		5	1.5 ± 0.2	1.7 ± 0.1
		10	1.9 ± 0.1	2.9 ± 0.2
FLOVENT HFA (pMDI) (44 and 220 µg)	FP	5*	1.8 ± 0.1	4.8 ± 0.9
		5**	16.4 ± 3.7	19.8 ± 0.8
FLOVENT DISKUS (DPI) (50 µg)	FP	22	2.2 ± 0.3	2.4 ± 0.4
VANCERIL (pMDI) (100 µg)	BDP	7	1.3 ± 0.1	1.6 ± 0.2
QVAR (pMDI) (40 µg)	BDP	14	0.6 ± 0.1	1.6 ± 0.1

N.A. Not applicable

* 44µg metered dose

** 220µg metered dose

3.3.2 DISSOLUTION AND PERMEATION PROFILES OF ICS AEROSOLS

3.3.2.1 Flunisolide (FL) from AEROBID® pMDI

Figure 3.3-a shows the cumulative % mass of FL dissolved and permeated into the receptor compartment over time for the aerosols collected on Stage 2 of the ACI (4.7-5.8 µm in aerodynamic diameter) from AEROBID® pMDI after 0.7, 6.2 and 9.1 µg of the mass deposit per filter membrane. These profiles reflected the kinetics of FL aerosol dissolution into the 40 µL buffer fluid on the donor side and subsequent permeation through the transwell polyester membrane. Each of the profiles was kinetically apparent first-order, which reached near complete ≥ 91 % dissolution and permeation in 5 h. However, none of the profiles reached a complete 100 % speculating possible adsorption of the drug particles to the hydrophobic PVDF membrane or substantially decreased concentration gradient at ≥3 h, between the donor and receptor compartments. Across 0.7-9.1 µg of the FL deposits under Stage 2 collection, the profiles were shown to be indistinguishable ($p>0.05$, ANOVA) with their apparent half-life ($t_{0.5}$) of 0.88±0.22 h (across mass deposits, mean±SD, n=9). Note however that, in theory, 40 µL of the donor fluid should have exceeded the capacity to dissolve the entire 6.2 and 9.1 µg of the FL deposits, due to the aqueous solubility of 140 µg/ml (Table 3.1). Therefore, compared to its permeation, FL dissolution into the 40 µL donor fluid appeared to be faster and thus, not rate-determined kinetically; otherwise, the excessive mass of the FL particles over the dissolution capacity on the donor side would have slowed down the kinetics at 6.2 and 9.1 µg.

Figure 3.3-b shows the profiles of dissolution and permeation for the FL aerosols collected on Stage 4 of the ACI (2.1-3.3 µm in diameter) at 2.3, 10.9 and 18.8 µg. Despite a difference in size, the profile at 2.3 µg remained effectively consistent with the profiles for the 4.7-5.8 µm aerosols (Figure 3.3-a; $p>0.05$, ANOVA), which resulted in the comparable $t_{0.5}$ value of 0.67±0.06 h. This was presumably because the 40 µL donor buffer fluid could afford dissolving the entire 2.3 µg of the FL deposit, yet the dissolution kinetics were not substantially improved by the smaller aerosol size. In contrast, however, at much higher mass deposits of 10.9 and 18.8 µg, the kinetics of dissolution and permeation became progressively slower (Figure 3.3-b). This could be attributed to the far excessively increased FL particles remaining to be dissolved on the donor side even for this smaller size of the highly soluble FL. Nevertheless, the rather slow kinetics for the smaller 2.1-3.3 µm aerosols at 10.9 µg, compared to those for the 4.7-5.8 µm aerosols at a comparable 9.1 µg, were not certain, leaving a speculation that the profiles were not a reflection of individual particle dissolution, but dissolution from the heaps comprised of the different size particles.

(a)

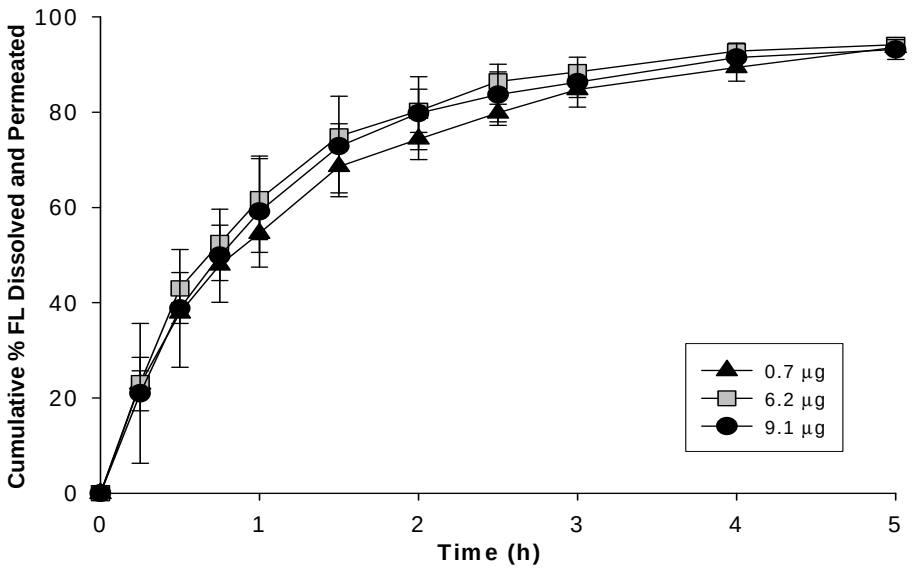

(b)

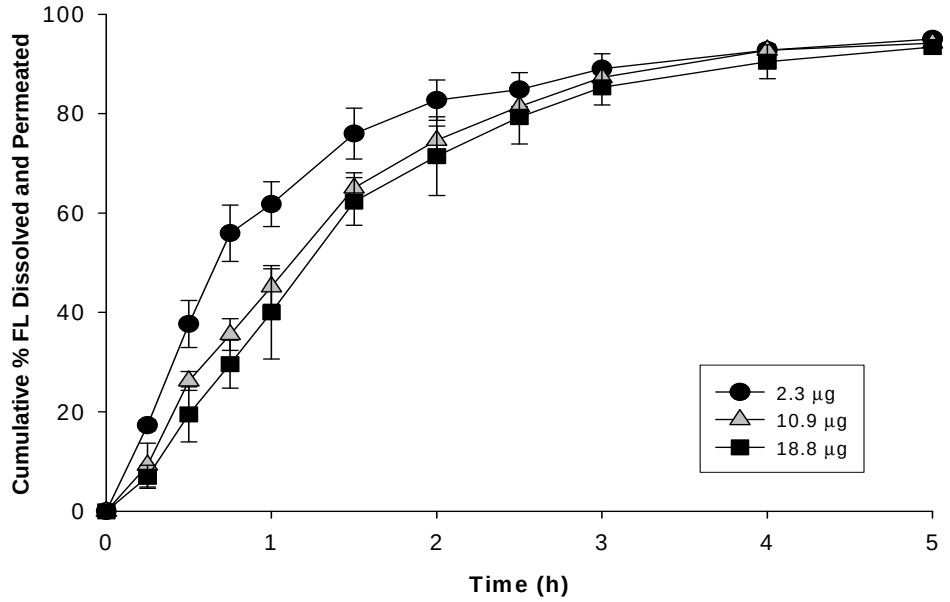

Figure 3.3 Cumulative % mass of FL dissolved and permeated into the receptor compartment as a function of time for the aerosols collected on (a) Stage 2 and (b) Stage 4 of the ACI (4.7-5.8 µm and 2.1-3.3 µm in aerodynamic diameter, respectively) from AEROBID® pMDI at various mass deposits. Data represent mean±SD (n=3). The profiles shown in (a) are statistically indistinguishable ($p>0.05$ by ANOVA) across the FL deposits.

3.3.2.2 Triamcinolone acetonide (TA) from AZMACORT® pMDI

Figure 3.4 shows the profiles of dissolution and permeation for the TA aerosols collected on Stage 2 (4.7-5.8 µm) at 1.1, 7.7 and 14.0 µg and on Stage 4 (2.1-3.3 µm) at 2.5 µg, generated from AZMACORT® pMDI. All the profiles were kinetically apparent first-order like FL, yet approaching different asymptotes between 78-90 % in 5 h, depending on the mass deposit and size. Indeed, in line with the rank of the solubility (Table 3.1), the kinetics of dissolution and permeation for the TA aerosols appeared to be slower than those for the FL aerosols (Figures 3.3 and 3.4, respectively); the $t_{0.5}$ values of 1.03-2.10 h for the TA aerosols, were overall greater than those for the FL aerosols (an averaged $t_{0.5}$ value of 0.88 h). Notably, the kinetics for the 4.7-5.8 µm TA aerosols were shown to slow down with increasing the mass deposits from 1.1 to 14.0 µg. At all of these deposits, TA could not be dissolved entirely in the 40 µL donor fluid for dissolution, in theory, based on its solubility of 21 µg/mL (Table 3.1). It was likely therefore that dissolution of the TA aerosol particles because kinetically significant, relative to the transwell membrane permeation. Meanwhile, the profile for the 2.1-3.3 µm TA aerosols at 2.5 µg was intermediate between the profiles for the 4.7-5.8 µm aerosols at 1.1 and 7.7 µg (Figure 3.4). Hence, like FL, the kinetics of dissolution for this less soluble TA was unlikely to be improved by the smaller size.

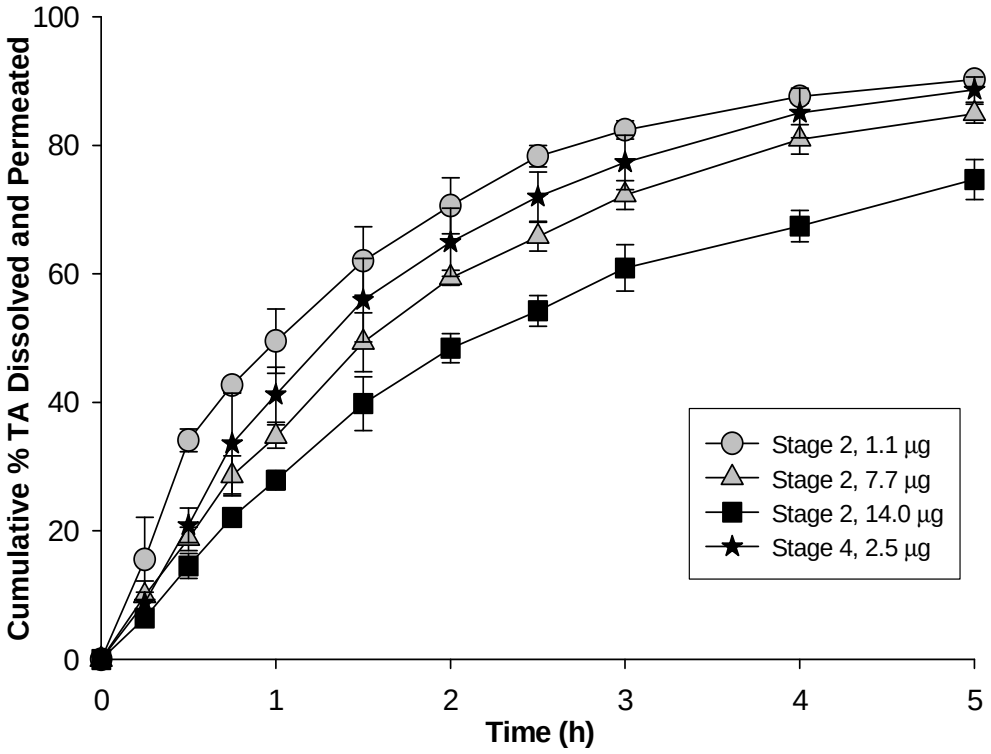

Figure 3.4 Cumulative % mass of TA dissolved and permeated into the receptor compartment as a function of time for the aerosols collected on the Stage 2 at 1.1, 7.7 and 14.0 µg and on the Stage 4 at 2.5 µg in the ACI (4.7-5.8 µm and 2.1-3.3 µm in aerodynamic diameter, respectively) from AZMACORT® pMDI. Data represent mean±SD (n=3).

3.3.2.3 Budesonide (BD) from PULMICORT® TURBUHALER DPI

Figure 3.5 shows the profiles of dissolution and permeation for the BD aerosols collected on Stage 2 (4.7-5.8 µm) at 1.9 µg and on Stage 4 (2.1-3.3 µm) at 0.8 and 1.7 µg, generated from PULMICORT TURBUHALER® DPI. Again, the apparent first-order profiles reached different asymptotes at 56-74 % in 5 h, the values being lowered further than those seen for FL and TA (Figures 3.3 and 3.4). This implied that the kinetics of BD dissolution were slower than those for TA and indeed, the $t_{0.5}$ values at the comparable mass deposits of 1.9 and 1.1 µg on the Stage 2 were 3.90±0.87 and 1.05±0.16 h, respectively. By virtue of their effectively same molecular weights, i.e., 431 and 434 Da (Table 3.1), diffusive permeation across the transwell membranes for BD and TA should be similar. Hence, this profile difference between the BD and TA aerosols was likely caused by differences in their dissolution kinetics, even though their reported aqueous solubilities were almost comparable at 16 and 21 µg/mL, respectively (Table 3.1). This arguably addressed that the kinetic behavior of certain aerosol particle dissolution was not solely in accord with the equilibrium data of the aqueous solubility. Meanwhile, unlike FL or TA, the smaller 2.1-3.3 µm BD aerosols collected on Stage 4 appeared to show faster dissolution and permeation than the larger 4.7-5.8 µm aerosols collected on Stage 2, upon the comparable 1.7 and 1.9 µg mass deposits (Figure 3.5); likewise, the $t_{0.5}$ values were 1.76±0.05 and 3.90±0.87 h, respectively. Once again, given the same rate of the transwell membrane permeation for BD, this could be attributed to a larger surface area per unit weight ratio for the smaller aerosols, finally accelerating their dissolution rates, as have often been the cases for the dissolution of

certain rather larger particles (Martin and Bustamante, 1993a). Nevertheless, the different observation of this aerosol size dependence on the kinetics of dissolution between the BD and TA aerosols, despite their comparable solubility, remained to be substantiated, including the exact controlling mechanism of dissolution for the aerosol particles collected in the form of cone-shaped heaps.

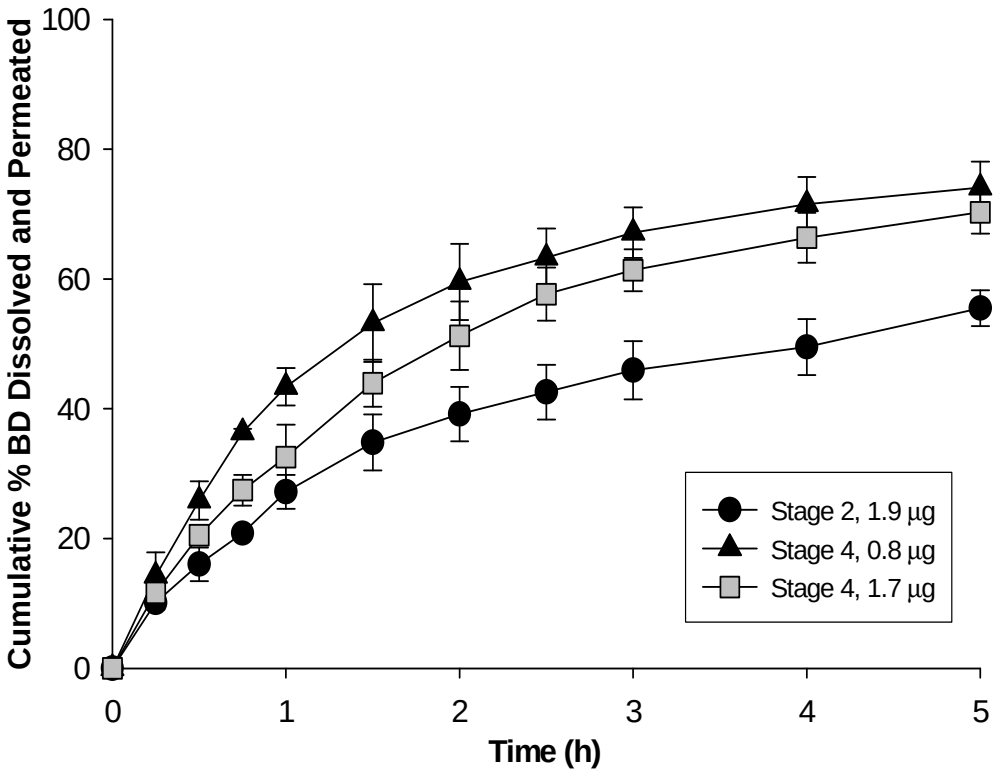

Figure 3.5 Cumulative % mass of BD dissolved and permeated into the receptor compartment as a function of time for the aerosols collected on Stage 2 at 1.9 µg and on the Stage 4 at 0.8 and 1.7 µg (4.7-5.8 µm and 2.1-3.3 µm in aerodynamic diameters, respectively) in the ACI, generated from PULMICORT TURBUHALER® DPI. Data represent mean±SD (n=3).

3.3.2.4 Fluticasone propionate (FP) from FLOVENT HFA® pMDI and DISKUS® DPI

Figure 3.6 shows the profiles of dissolution and permeation for the FP aerosols collected on Stage 2 (4.7-5.8 µm) at 1.8 and 16.4 µg from FLOVENT HFA® pMDI and at 2.2 µg from DISKUS® DPI. The profiles reached only ≤ 6.0 % of dissolution and permeation even by 10 h in an apparently zero-order fashion, demonstrating the slowest kinetics among the ICSs tested in this study including BDP described below. While being consistent with FP's lowest aqueous solubility of 0.14 µg/mL (Table 3.1), this did not allow the $t_{0.5}$ determination except by linear extrapolation, in which case, a $t_{0.5}$ value would be 141.6±60 h. Notably, the profiles of the FP aerosols collected on Stage 2 from FLOVENT® pMDI and DISKUS® DPI at the comparable mass deposits of 1.8 and 2.2 µg, respectively, were not statistically different ($p>0.05$, ANOVA), despite apparent differences after 4 h. This suggested that the dissolution kinetics of the different sized FP aerosols generated from these 2 different inhaler products were equivalent, providing the same rate of the transwell membrane permeation. Nevertheless, like TA and BD, the kinetics of FP dissolution and permeation continued to be dependent upon the deposited masses and slowed down at the higher deposit amounts of 16.4 µg (Figure 3.6).

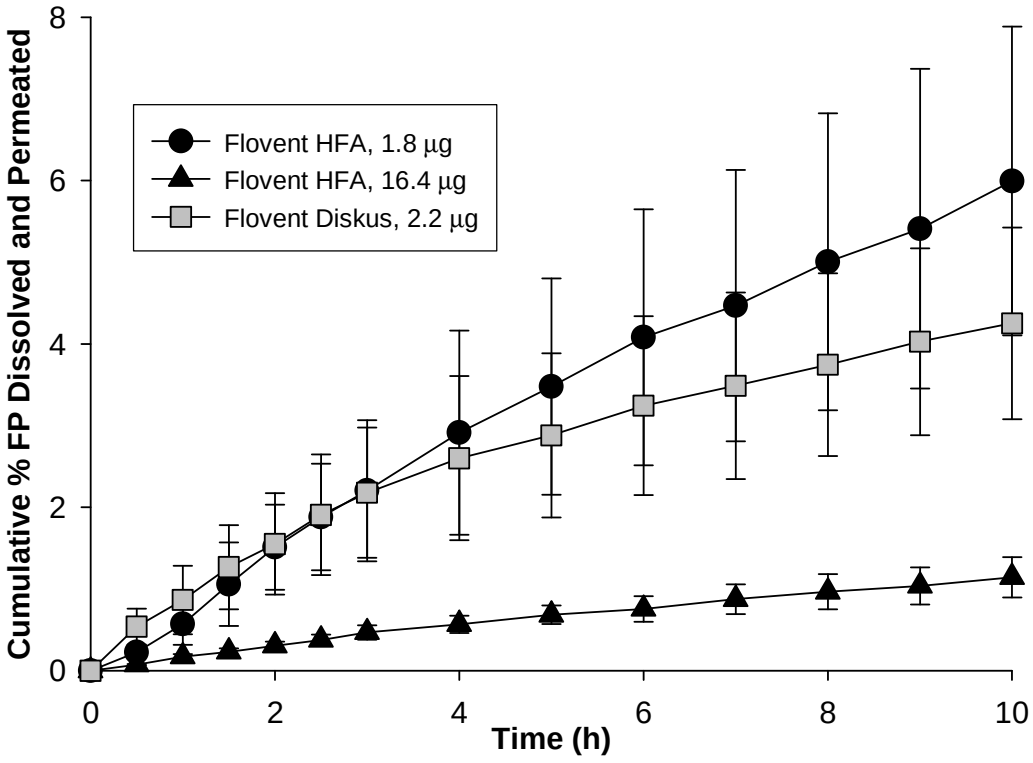

Figure 3.6 Cumulative % mass of FP dissolved and permeated into the receptor compartment as a function of time for the aerosols collected on Stage 2 of the ACI (4.7-5.8 µm in aerodynamic diameter) at 1.8 and 16.4 µg from FLOVENT HFA® pMDI and at 2.2 µg from DISKUS® DPI. Data represent mean±SD (n=3).

3.3.2.5 Beclomethasone dipropionate (BDP) from VANCERIL® and QVAR® pMDIs

Figure 3.7 shows the profiles of dissolution and permeation for the BDP aerosols collected on Stage 4 (2.1-3.3 µm) at 1.6 µg from VANCERIL® and QVAR® pMDIs. Like FP, the profiles appeared to be zero-order, yet reaching a much higher 12 % and 16 % of dissolution and permeation in 10 h, despite the identical reported aqueous solubility of 0.13 µg/ml (Table 3.1). Given the comparable rate of diffusive permeation across the transwell membrane by virtue of their similar molecular weights (i.e., 521 and 445 Da, respectively), this implied that either or both of the BDP and FP profiles resulted from changes in the dissolution kinetics induced by formulation effects when compared to those for the pure crystalline materials with 0.13 and 0.14 µg/mL of solubility, respectively. In this context, it was intriguing that the BDP aerosols from QVAR® showed significantly faster dissolution and permeation than those from VANCERIL® ($p=0.013$, ANOVA). Indeed, this faster kinetics for the QVAR® aerosols appeared to result from the rapid dissolution in the first 1 h where the rate was 5.0±0.8 %/h as compared to 2.3±0.0 %/h for the VANCERIL® aerosols. Then, the profiles in the subsequent periods (i.e., ≥1h) appeared to parallel those for VANCERIL®; their linear slopes, 1.1±0.03 and 1.1±0.04 %/h, respectively, were insignificantly different ($p>0.05$, unpaired Student's t-test). While remaining speculative, as discussed below, these different kinetics between the QVAR® and VANCERIL® aerosols were most likely caused by differences in their formulations (Table 3.1) and the resultant solid aerosol particles following propellant evaporation.

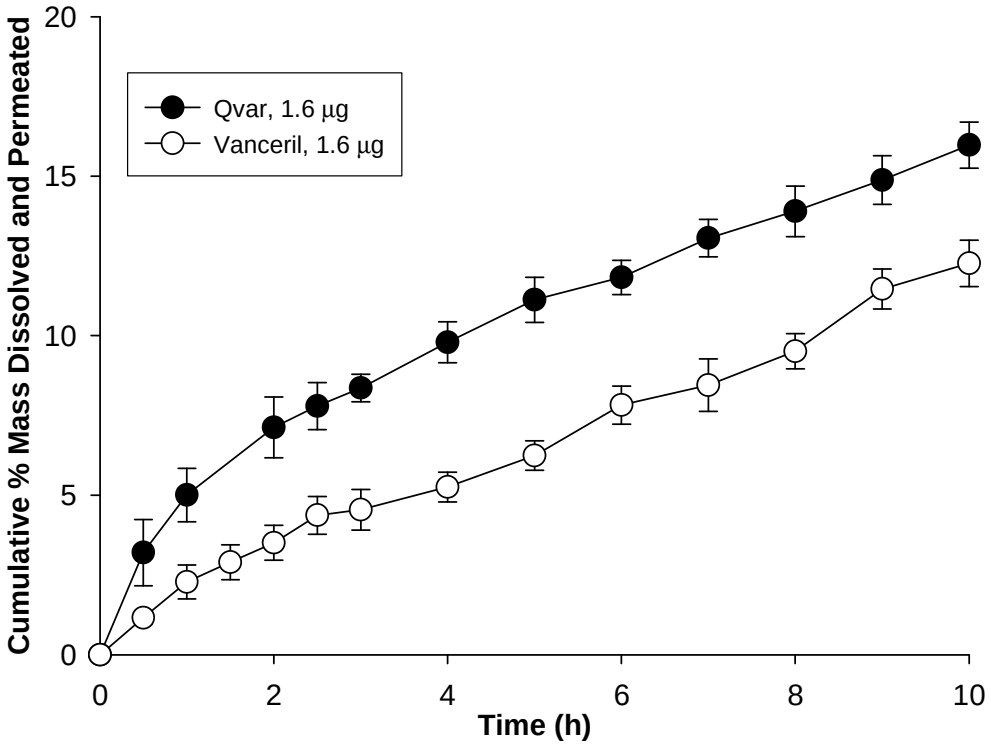

Figure 3.7 Cumulative % mass of BDP dissolved and permeated into the receptor compartment as a function of time for the aerosols collected on Stage 4 of the ACI (2.1-3.3 µm in aerodynamic diameter) at 1.6 µg from VANCERIL® and QVAR® pMDIs. Data represent mean±SD (n=3). The dissolution and permeation profile of QVAR® is significantly faster than that of VANCERIL® (p=0.013, ANOVA).

3.4 DISCUSSION

The assessment of dissolution of aerosol particles generated from commercial inhalers was possible in this simple system. The uniqueness of this method was primarily the experimental conditions employed to study the dissolution kinetics. The most important aspect was the use of a stationary fluid environment in which the dissolution of aerosol particles in the limited volume of the fluid (40 µL) was studied. This condition was designed to be semi-quantitatively analogous to humans, where the total lung fluid volume has been predicted to be 10-30 mL over $100m^2$ of the lung surface [Widdicombe, 1997]. Moreover, the use of stationary conditions was also analogous to that in the respiratory tract. Hence, this new system was more relevant, with respect to the flow dynamics for aerosol particle dynamics than the prior attempt [Davies and Feddah, 2003], in which a flow-through apparatus was used. This present method also enabled the collection of aerosols in a specific range, generated from the inhalers. This allowed the determination of the influence of particle size on the rate of dissolution, as attempted for the FL, TA and BD particles generated from respective inhaler products. In this sense, the previous attempt [Davies and Feddah, 2003] collected the aerosol particles that escaped the USP inlet port, such that their particle sizes were largely unknown. In contrast, a possible limitation exists in this system developed in this chapter by the use of PBS and DDW as its dissolution media. Such solvent may not be the best mimics for the lung fluids. Indeed, surfactants present in the lung like dipalmitoyl-L-α-phosphatidylcholine (DPCC) have been shown to hasten the kinetics of dissolution of some ICSs, especially the more lipophilic FP by the previous

attempt [Davies and Feddah, 2003]. However, the present study did not attempt the influence of such a surfactant on the dissolution of lipophilic ICSs due to analytical limitations.

Figure 3.8 summarizes the profiles of dissolution and permeation for 5 ICS aerosol particles in the size-range 2.1-3.3 µm in size (Stage 4 collection) following collection of comparable ~2 (1.6-2.9) µg deposits generated from 5 inhaler products. Because their molecular weights are similar (431-521 Da; Table 3.1), the kinetics of diffusive permeation should be consistent. This was indeed supported in part by apparently same profiles for FL and TA upon their 40 µL solution applications (data not shown); in fact, when 40 µL aqueous solutions of FL and TA were applied to the donor compartment of the transwell system at a concentration of 25 and 10 µg/mL respectively, their $t_{0.5}$ values 0.17±0.06 and 0.16±0.04h were consistent, both of which were much shorter than those for their aerosols shown in Figures 3.3 and 3.4. Therefore, it was likely that the profile differences for these 5 ICSs aerosols in Figure 3.8 were primarily caused by the differences in their kinetics of dissolution into 40 µL of the donor fluid in the transwell. Overall, the kinetics of dissolution for the 2.1-3.3 µm aerosol particles was shown to differ substantially between the ICSs, but conform to the rank order of their aqueous solubilities. However, such reported solubility values were not the only factor defining the kinetic profiles. Pairs of ICSs with similar solubilities still produced different profiles such as TA and BD or FP and BDP (Figure 3.8). This was presumably because some of the ICS aerosol particles generated from the respective inhaler products resulting from certain changes caused by, for example,

formulation excipients, particle wettability and/or ICS crystallinity. In this context, our satellite experiments showed that 1 % ethanol addition into the 40 µL donor fluid did not accelerate the profile for BD, compared to the use of the 40 µL fluid (data not shown). Hence, the faster kinetics for TA over BD in Figure 3.8 were apparently not due to co-solvent effects by ethanol [Kibbe, 2000], a formulation excipient in Azmacort® (TA; Table 3.1). However, it was reasonably possible to speculate that TA and BD possess different wettabilities and/or the TA particles generated from the MDI containing 1 % ethanol were altered, fully or in part, in their crystallinity, which may have contributed to these different profiles; in contrast, it was highly unlikely that BD formulated as the pure drug and generated from the DPI had altered crystallinity induced by formulation. A similar observation was seen for the BDP aerosol particles that exhibited faster dissolution than FP (Figure 3.8), despite their reported similar solubilities (~0.14 µg/mL, Table 3.1). In this case, it has been reported that BDP forms solvate crystals in the presence of both CFC and HFA propellants like Vanceril® and Qvar®, respectively (Dalby *et al*, 1993), while FP particles generated from the DPI were most likely crystalline. Thus, it appeared that the BDP aerosols were more prone to have crystallinity changes than the FP aerosols. Between the BDP aerosols, an inter-product difference was observed. The aerosols generated from Qvar®, a solution of BDP in HFA propellant with ethanol, showed faster dissolution kinetics than the aerosols from Vanceril®, a suspension of probably crystalline BDP in CFC propellants suspended with the aid of dissolved oleic acid (Figure 3.7). Such a difference could partly be attributed to the clathrate crystal formation of BDP (Dalby *et al*, 1993) upon

interaction with both CFC and HFA propellants, which could alter the apparent solubility to varying extents. Incidentally, Freiwald *et al*, 2005 observed different pulmonary absorption of BDP delivered by two different HFA-propelled aerosols (Sanasthmax®/Becloforte™ and Ventolair®/Qvar). They confirmed that the BDP particles delivered by Ventolair®/Qvar™ were significantly smaller and displayed faster dissolution in human bronchial fluid, compared to the particles delivered by Sanasthmax®/Becloforte™. Their work also illustrated certain crystallinity changes for the BDP particles, resulting in the different dissolution kinetics. While these issues should be further clarified, it is clear that the ICS aerosol particles generated from the inhaler products should be the subject matter for this dissolution testing rather than the pure ICS drugs themselves.

Currently, the USP standards for product performance of inhaled dosage forms require the testing for delivered dose and aerodynamic particle size distribution yet have not included the testing of dissolution. [United States Pharmacopoeia, Chapter <601>] This is primarily because drug delivery to, and regional deposition within, the lung are considered to far outweigh aerosol particle dissolution in controlling the effective dose and its therapeutic effect. Indeed, their literature review failed to locate substantial concerns about the issue of dissolution for inhaled therapeutics with respect to their pharmacokinetics or clinical performance among the currently approved products [Gray *et al*, 2008]. In contrast, such data were available in the literature for animal testing. Chowhan and Amaro, 1976, demonstrated a substantially delayed disappearance of methyl sulfinyl xanthone, from the rat lung, when the molecule was administered as its

carboxylic acid suspension, compared to its sodium salt given as a solution. This was attributed to dissolution effects, when the acid was employed in suspension. Likewise, sustained dissolution or release from the respirable-size microspheres led to prolonged durations in pharmacokinetics and/or pharmacodynamics following aerosol administration to the lung in several studies using dogs, rats and guinea pigs [Sakagami e*t al*, 2002 and 2005]. However, no such modified dissolution or release products have been so far clinically marketed for inhalation use in humans. The performance tests for the currently marketed oral inhaled dosage forms have thus, concerned only the lung delivery and regional deposition. e.g., delivered dose and aerodynamic particle size distribution [FDA, Guidance for industry; metered dose inhaler and dry powder inhaler, 1998], and their dissolution testing is not considered critical. However, this in vitro dissolution testing of aerosol particles suggested that this process may be rate determined for some highly lipophilic ICSs like FP.

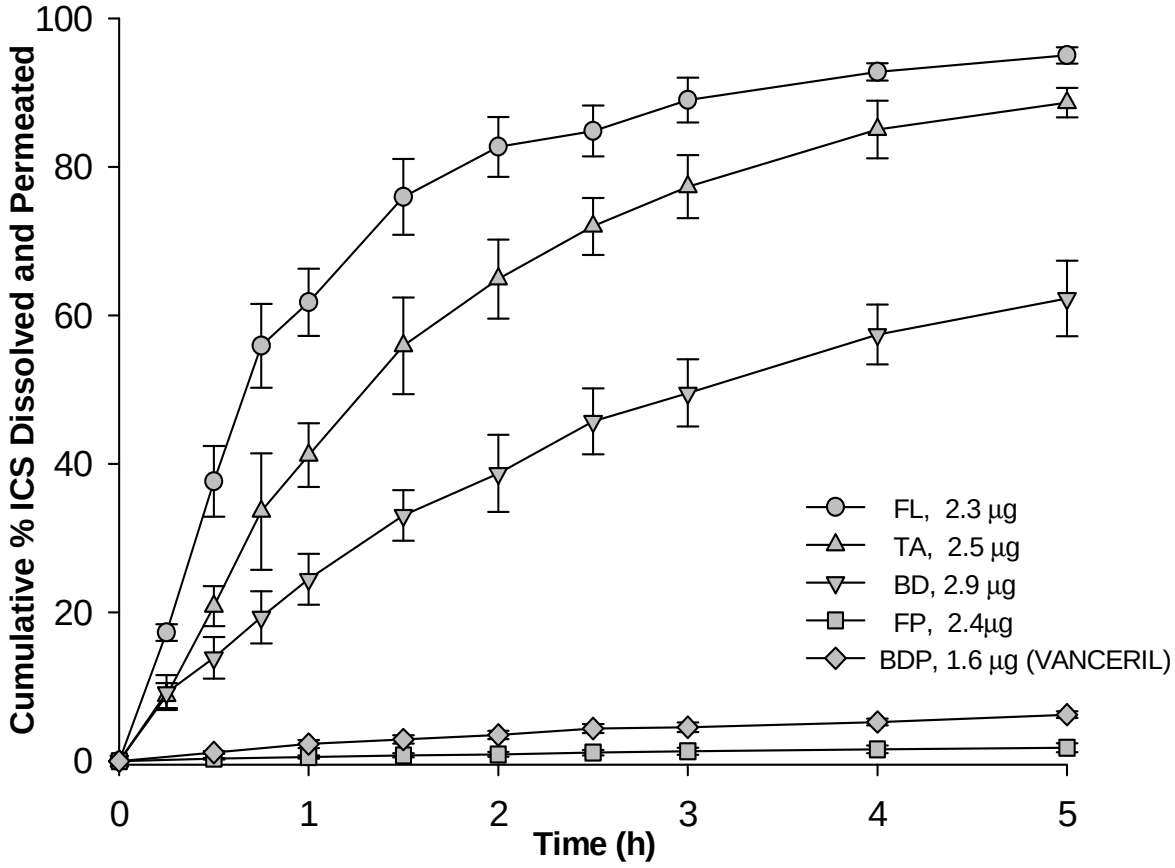

Figure 3.8 Cumulative % mass of 5 ICSs dissolved and permeated into the receptor compartment as a function of time for the aerosols collected on the Stage 4 (2.1-3.3 µm in aerodynamic diameter) of the ACI from their inhaler products at the best comparable ~2 (1.6-2.9) µg mass deposits. Data represent mean±SD.

3.5 SUMMARY & CONCLUSIONS

A unique dissolution testing method was developed for defined-size aerosol particles generated from commercial inhaler products of various ICSs with different physicochemical properties. Upon defined size aerosol particle collection in the ACI, dissolution took place in a limited volume (40 µL) of stationary fluid, followed by membrane permeation to determine their transfer kinetic profiles. This was an attempt to determine the rate of dissolution in the limited volume of the fluid like aerosols in the lung mucosal surface, while also controlling the aerosol size and mass deposit, in order to identify their effects on the kinetics of aerosol dissolution and permeation. Overall, the kinetics of dissolution differed substantially between the ICSs but conformed to the rank order of their reported aqueous solubilities. However, solubility values alone were not the only factor that influenced dissolution kinetics, as the profiles for ICSs with similar solubility were sometimes different, such as TA and BD or FP and BDP. Moreover, certain ICSs, especially those with a low solubility, showed substantially slower profiles with an increase in the aerosol size and mass deposit. While the exact causes of these differences and changes remained speculative, it became clear that ICS aerosol particles delivered by inhaler products should be tested for dissolution rather than the pure drugs.

Specifically, it was of interest that this non-biological system of dissolution and permeation identified exceptionally slow dissolution kinetics for the least soluble ICS, fluticasone propionate (FP). Only 3 % of the 2.4 µg deposited mass was shown to be dissolved in 10 h, which was quite a contrast to the 89 % in 5 h for the readily soluble

ICS, triamcinolone acetonide (TA), as shown in Figure 3.8. This raised a question concerning whether the cellular anti-inflammatory activity of FP could be dissolution rate-determined and thus, compromised by this slow event though the “intrinsic” molecular anti-inflammatory activity of FP has been shown to be the most potent among these drugs.

CHAPTER 4

DEVELOPMENT AND CHARACTERIZATION OF THE AIR-INTERFACE CULTURED CALU-3 CELL MONOLAYERS

4.1 INTRODUCTION

Lung cellular disposition of inhaled therapeutics is a complex cascade of their aerosol deposition onto, and dissolution into, the lining fluid, followed by their cellular uptake and/or absorption, as described in Figure 1.1 [Edsbäcker *et al*, 2006]. In this context, none of the available in vitro lung cell culture models have been applicable due to their culture being necessary in media-submerged conditions and hence, resulting in an inability of aerosol deposition on their surface. While this has demanded the use of less favorable and more complex models with animals or humans in this research arena, evidence has recently emerged in the cell culture techniques suggesting that certain lung epithelial cells can be grown without apical culture media [Sakagami, 2006]. A continuous cell line of human bronchial epithelial carcinoma, Calu-3, is one of such unique cells that grow to form the monolayers under the culture leaving their apical surface semi-dry [Borchard *et al*, 2002; Fiegel *et al*, 2003; Cooney *et al*, 2004; Grainger *et al*, 2006a and b; Mathias *et al*, 2006]. In fact, these monolayers appeared to be more

differentiated, with cilia and a thicker mucosa, compared to those grown under the conventional submerged culture [Grainger *et al* 2006a]. Nevertheless, their characterization in the literature has been confounded, as also discussed in this chapter, due to a lack of universal validation to ensure the consistent formation of the sufficiently restrictive monolayers. This culturing technique is termed as an air interface culture (AIC) where the culture medium has access to the Calu-3 cells only from the basolateral side.

In this chapter, Calu-3 monolayers grown under the AIC were assessed if they indeed formed sufficiently "tight" diffusive barrier for their use in pulmonary biopharmaceutics, while maintaining their semi-dry mucosal surface with a limited volume of the lining fluid. Various culturing conditions were tested with respect to the restrictive barrier formation for the selection of the most suitable monolayers. Then, they were further characterized by scanning electron microscopy (SEM), transepithelial resistance (TEER) and permeability of various model solutes. The lining fluid volume on the apical (mucosal) surface of the monolayers was also determined using a tracer dilution technique. This enabled the development of sufficiently restrictive lung epithelial cell monolayers enabling direct aerosol deposition to study a cascade of aerosol dissolution and cellular uptake and/or absorption in the in vitro system.

4.2 MATERIALS AND METHODS

4.2.1 CALU-3 CELL CULTURE AND MONOLAYER FORMATION

Calu-3 cells were obtained at passage 19 from the American Type Culture Collection (ATCC; Rockville, MD) and propagated in the 25 or 75 cm^2 culture flasks (Corning Costar; Cambridge, MA), prior to use according to the supplier's protocol [Product Information Sheet, ATCC]. For propagation, the cells were seeded at 0.1 $x10^6$ cells/cm^2 in the flasks and cultured in 8 or 20 mL of the Eagles Minimum Essential Medium (EMEM; ATCC, Rockville, MD; Table A.1) supplemented with 10% (v/v) fetal bovine serum (Invitrogen, Carlsbad, CA) and 1% (v/v) penicillin-streptomycin (Sigma-Aldrich; St. Louis, MO). They were maintained under the humidified 95% (v/v) air and 5% (v/v) CO_2 at 37 °C in the incubator (Model 5410, NAPCO; Milliville, NJ) connected to a CO_2 gas cylinder (National Welders; Richmond, VA). The culture media was changed every other day, during which the cell growth was monitored under the microscope (Nikon-TMS phase contrast microscope, Image Systems Inc.; Columbia, MD). Typically, the cells reached the confluence by 5-7 days, such that they were passaged in a new flask or frozen for the cell bank storage following trypsin-EDTA (Sigma-Aldrich) treatment. The standard operating procedures for cell propagation, passage and banking are described in detail in Appendix A.

For experimentation, the Calu-3 cells between passage 21 and 42 were used. They were seeded onto 1.13 or 4.5 cm^2 clear polyester transwell filter inserts (Corning Costar) at a density of 0.1 or 0.5 $x10^6$ cells/cm^2 and cultured for 24 h with the media

filled in both apical and basolateral compartments of the transwells at 0.5 and 1.5 mL for the 1.13 cm^2 transwells and 1.5 and 2.6 mL for the 4.5 cm^2 transwells, respectively. At 24 h after the seeding, the apical medium was removed, commencing the air-interface culture (AIC) where the cells were fed only with 0.5 and 1.4 mL of the basolateral medium, respectively, in the 1.13 and 4.5 cm^2 transwells, as shown in Figure 4.1. The medium was replaced everyday, during which the cell growth was monitored under the microscope. In some experiments, transepithelial electrical resistance (TEER) was measured everyday using an Epithelial Voltohmmeter (EVOM) and STX or Endohm electrodes (World Precision Instruments, Sarasota, FL), as described below. Typically, the cells reached the confluent monolayers by 7-10 days, irrespective of different seeding densities (0.1 or $0.5x10^6$ cells/cm^2) or transwell areas (1.13 or 4.5 cm^2).

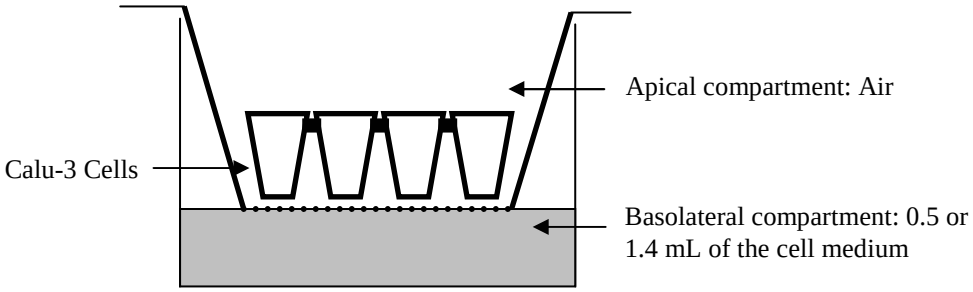

Figure 4.1 Air-interface culture (AIC) of the Calu-3 cells in the transwell. The basolateral volumes of the culture medium were 0.5 and 1.4 mL for the 1.13 and 4.5 cm^2 transwells, respectively. The Calu-3 cells are shown as the confluent monolayer, typically observed by 7-10 days in culture.

4.2.2 BARRIER ASSESSMENT FOR THE CALU-3 CELL MONOLAYERS

4.2.2.1 SCANNING ELECTRON MICROSCOPY (SEM)

On day 7-10, upon confirmation of the monolayer confluence under the microscope, the surface morphology was assessed under the scanning electron microscope (SEM; JSM-820, JEOL, Peabody, MA). This was carried out at the electron microscopy facility of the VCU Department of Anatomy. The monolayers grown on the transwell inserts were fixed in 2.5% glutaraldehyde (Sigma-Aldrich) in 0.1 M cacodylate buffer (Invitrogen) overnight, followed by repeated rinse with 0.1 M cacodylate buffer. The monolayers were then fixed with 2 mL of 1% osmium tetroxide (Invitrogen), applied apically, on ice for 1 h and then, rinsed several times with the cacodylate buffer. The monolayers and supporting membranes were carefully removed

from the transwell insert and subjected to a series of graded ethanol bathes (70 %, 80 % and 90 % for 5-10 min each and 3 times of 100 % for 10 min each) for dehydration. They were placed in hexamethyldisilazane reagent (Electron Microscopy Sciences, Hatfield, MA) and finally mounted on the stubs using double sticky tape. Following gold coating using a sputter coater (EMS-550 Sputter Coater, EMS, Harfield, MA) with a thickness of 10 Å, the sections were observed under the SEM (JSM-820 JOEL, USA Inc., Peabody, MA).

4.2.2.2 TEER MEASUREMENT

TEER was measured with an EVOM and STX or Endohm electrodes during the culture to assess the monolayer confluence and tightness. For each measurement, the cells were first equilibrated with appropriate volumes of the culture media for 15 min; the volumes were 0.5 and 1.5 mL for the 1.13 cm^2 transwells and 1.5 and 2.6 mL for the 4.5 cm^2 transwells, respectively, on the apical and basolateral compartments. Then, TEER was measured using chopstick STX electrodes for the 1.13 cm^2 transwells and Endohm electrodes for the 4.5 cm^2 transwells, according to the supplier's protocol. The observed resistance values were corrected by subtracting the resistance of the transwell's membrane, obtained from the cell-free transwells and then, converted to the TEER values with the area-normalization via multiplication, i.e., 1.13 and 4.5 cm^2; these were then expressed as $\Omega \cdot cm^2$.

4.2.2.3 PERMEABILITY DETERMINATION

On day 7-10 upon the visual confluence and sufficiently high TEER development, the permeability of the Calu-3 monolayers was determined for various solutes to assess their barrier nature. Table 4.1 lists 7 model solutes tested in this assessment along with their molecular weights and analytical methods validated in-house previously. These solutes were all hydrophilic, yet different in molecular weights ranging from 376 to 150k Da. For the permeability determination, the Calu-3 monolayers were first equilibrated for 90 min in the incubator with 1.5 and 2.6 mL for 4.5 cm^2 and 0.5 and 1.5 mL for 1.13 cm^2 transwells, respectively, of the Krebs-Ringer buffer (KRB, pH 7.4) in the apical and basolateral compartments. The KRB solution consisted of 15.0 mM HEPES (N-[2-hydroxy-ethyl]piperazine-N'-[2-ethanesulfonic acid]), 116.4 mM NaCl, 5.4 mM KCl, 0.78 mM NaH_2PO_4, 25.0 mM $NaHCO_3$, 1.8 mM $CaCl_2$, 0.81 mM $MgSO_4$ and 5.55 mM glucose, and freshly prepared before each study. Then, the apical media was replaced with the KRB solution containing certain known concentrations (C_o) of each solute listed in Table 4.1, except for insulin. For insulin, the Krebs–Henseleit buffer (pH 7.4) containing 4 % (w/v) bovine serum albumin was used to avoid insulin's adsorptive loss to the plastics, as described previously [Pang *et al*, 2005]. The concentrations were chosen to monitor the permeation profiles and therefore, 10 μg/mL for FNa, 1.0 mg/mL for 4.3 kDa F-PHEA, 1.0 IU/mL for insulin, 2.0 mg/mL for 8.4 kDa F-PHEA, 0.5 mg/mL for FD-10, 1.0 mg/mL for FD-70 and 5.0 mg/mL for FD-150. At various time intervals (10, 30, 60, 90, 120, 150 and 180 min), 200 μL aliquots were withdrawn from the basolateral compartment; 200 μL of the fresh

media was added each post-sampling. These samples were analyzed by the method shown in Table 4.1 to determine their concentrations. The concentration at each time point was converted to the solute mass permeated into the basolateral compartment by its product with the basolateral volume, i.e., 2.6 mL or 1.5 mL. The cumulative solute mass permeated into the basolateral compartment plus the product of the concentrations in previously taken samples and their volumes (i.e., 0.2 mL) was plotted as a function of time so that the apparent permeability coefficient (P_{app}) was calculated from their initial linear portions using Eq 4.1:

$$P_{app} = J / (A.C_o) \qquad \text{(Eq. 4.1)}$$

where J is the initial solute mass for permeation obtained from the linear slope of the cumulative mass permeated *vs.* time profiles, A is the area of the transwell inserts, 1.13 or 4.5 cm^2, and C_o is the initial concentration of each solute applied to the apical compartment. The linear portions of the profiles were ensured with their regression coefficients >0.95 under <5% permeation of the sink condition. The supporting membrane (polyester) of the transwell was shown to be a negligible barrier for all tested solutes, as evidenced by >100-fold higher P_{app} values, justifying the lack of necessity of the correction.

Table 4.1 Model solutes used to determine the apparent permeability coefficients (P_{app}) across the Calu-3 monolayers and their molecular weights and analytical methods.

Solute	MW (Da)	Analytical Method	LOQ (ng/mL)	Accuracy [5]	Precision	Reference
FNa	376	Fluorimetry[2]	1	3%	9%	[1]
F-PHEA	4,300 [1]	GPC-F [3]	100	10%	5%	[1]
Insulin	5,800	ELISA[4]	100	11%	15%	[2]
F-PHEA	8,400 [1]	GPC-F [3]	100	10%	5%	[1]
FD-10	4,500 [1]	GPC-F [3]	100	10%	5%	[1]
FD-70	9,500 [1]	GPC-F [3]	100	10%	5%	[1]
FD-150	150,000 [1]	GPC-F [3]	100	10%	5%	[1]

FNa: sodium fluorescein; F-PHEA: fluorophore-labeled poly-α,β-[N(2-hydroxyethyl)-D,L-aspartamide; FD: FITC-labeled dextran

[1] Averaged weight-based molecular weight

[2] Fluorescence spectrometer (Model LS 50; Perkin Elmer Ltd., Norwalk, CT) with excitation and emission wavelengths (λ_{ex} and λ_{em}) of 490 and 520 nm, respectively

[3] Gel permeation chromatography coupled with fluorescence detection (Model RF-535; Shimadzu Corporation, Kyoto Japan) with λ_{ex} and λ_{em} of 486 and 516 nm, respectively

[4] Enzyme linked immunosorbent assay, ALPCO, Windham, NH

[5] Accuracy and precision defined by difference from nominal concentration (DFN) and %RSD, respectively.

[1] Sakagami, 2000; [2] Pang, 2004

4.2.2.4 THE RENKIN FUNCTION'S APPROACH FOR THE MONOLAYER'S DIFFUSIVE PORE SIZE ESTIMATION

The P_{app} values for the 7 model solutes across the Calu-3 monolayers were used to estimate the diffusive pore size using the Renkin function approach [Renkin, 1954]. The Renkin function, $R\left(\frac{r_i}{r_p}\right)$ is the dimensionless molecular sieving function for the cylindrical pore channels and described with Eq. 4.2:

$$R\left(\frac{r_i}{r_p}\right) = \left[1-\left(\frac{r_i}{r_p}\right)\right]^2 \left[1 - 2.104\left(\frac{r_i}{r_p}\right) + 2.09\left(\frac{r_i}{r_p}\right)^3 - 0.95\left(\frac{r_i}{r_p}\right)^5\right] \quad \text{(Eq. 4.2)}$$

where r_i is the solute radius and r_p is the pore radius of the barrier, i.e. Calu-3 monolayers. Meanwhile, the P_{app} values were considered as a result from restricted diffusion and/or steric hindrance and frictional resistance of the solutes and therefore, described with this Renkin function, as shown in Eq. 4.3:

$$P_{app} = D_i \left(\frac{\varepsilon}{L}\right) R\left(\frac{r_i}{r_p}\right) \quad \text{(Eq. 4.3)}$$

where D_i is the diffusion coefficients of the solutes, ε is the barrier porosity and L is the barrier length. For each solute listed in Table 4.1, the diffusion coefficient (D_i) was estimated from its molecular weight (MW) using Eq. 4.4, empirically derived by Seki *et al*, 2003.

$$\log D_i = -0.434 \log MW_i - 4.059 \quad \text{(Eq. 4.4)}$$

This further enabled the determination of the solute radius (r_i) using the Stokes-Einstein equation, Eq. 4.5:

$$D_i = \frac{kT}{6\eta\Pi r_i} \qquad \text{(Eq. 4.5)}$$

where k is the Boltzmann constant, T is the absolute temperature and η is the viscosity of the barrier (assumed to be equivalent to that of water, 1 cP.

Accordingly, the values for $\left(\frac{\varepsilon}{L}\right)$ and r_p became floating unknown values for each solute in Eqs. 4.2 and 4.3, which were estimated using the mean P_{app} values for the 7 solutes and their molecular weights using the Microsoft Excel and its built-in Solver. The spreadsheet was prepared, tabulating the values for P_{app}, D_i and r_i for each solute. They were subjected to Solver's optimization to derive the best estimates for $\left(\frac{\varepsilon}{L}\right)$ and r_p, based upon the simplex, generalized reduced gradient algorithms [Fylstra *et al*, 1998]. In this algorithm, the estimates for $\left(\frac{\varepsilon}{L}\right)$ and r_p should yield the minimum sum of squared differences between the predicted and experimental P_{app} values.

4.2.3 CELL LINING FLUID VOLUME DETERMINATION

On Day 7-10 upon the visual confluence and sufficiently high TEER development, the Calu-3 monolayers were subjected to the determination of the cell lining fluid volume using tracer dilution method. Rhodamine B isothiocyanate-labeled, 7.0 kDa dextran (RD-7; Sigma-Aldrich) was used as a tracer. Its 1.0 mL KRB solution at 0.1 mg/mL was applied to the apical compartment and thoroughly yet gently washed by repeat pipetting action. Then, the apical solution was recovered and analyzed by GPC coupled with fluorescence detection (Model RF-535; Shimadzu Corporation) with

λ_{ex}=540 nm and λ_{em}=573 nm. The GPC column was a Separon^{TM} HEMA-Bio 40 column (8 x 250 mm, 10 µm particle size; Tessek Ltd., Prague, Czech Republic) and the mobile phase was 0.05 M PBS (pH 7.4) at 1.0 mL/min. The analysis was validated with the linear range over 50-120 µg/mL (r^2>0.999), and ≤5.0 % of the precision (RSD: relative standard deviation; n=3).

RD-7 concentration (C_{RD}) of the recovery samples from the monolayers was decreased due to the additionally recovered volume of the Calu-3 cell lining fluid (V_{LF}). Hence, the V_{LF} values were calculated from Eq. 4.6, assuming mass balance:

$$V_{LF} = \frac{100\ \mu g/mL \times 1.0\ mL}{C_{RD}} - 1.0\ mL \qquad \text{(Eq. 4.6)}$$

4.3 RESULTS AND DISCUSSION

4.3.1 THE CULTURING CONDITIONS FOR THE HIGHLY RESTRICTIVE CALU-3 MONOLAYERS

Irrespective of 0.1 or 0.5 x 10^6 cells/cm^2 of the seeding density or the use of 1.13 or 4.5 cm^2 transwells, the Calu-3 cells grown under AIC formed confluent monolayers by day 7-10 visually confirmed under the microscope. However, as shown in Table 4.2, the values of the steady state TEER and P_{app} for FNa were shown to differ in different culturing conditions. In the smaller transwells (i.e., 1.13 cm^2), the higher seeding density of 0.5 x10^6 cells/cm^2 resulted in the higher TEER and a lower FNa P_{app}, which indicated relatively restrictive monolayer formation. Even so, these values were somewhat more variable, suggesting the formation of rather inconsistent monolayers between the transwells, possibly associated with the formation of cell multilayers and stacking [Mathias *et al*, 2002; Sambuy *et al*, 2005]. In contrast, in the 4.5 cm^2, the highly restrictive "tight" monolayers were reproducibly formed at a seeding density of 0.1 x 10^6 cells/cm^2, yielding 1486±42 $\Omega \cdot cm^2$ of TEER and 1.35±0.09 x 10^{-7} cm/s of P_{app} for FNa.

Table 4.2 Values of the steady state TEER and P_{app} for FNa obtained from the Calu-3 monolayers grown under AIC at various culturing conditions.

Transwell area (cm^2)	**Seeding density ($x10^6$ cells/cm^2)**	**TEER* ($\Omega \cdot cm^2$)**	**P_{app} for FNa * ($x10^{-7}$ cm/s)**
1.13	0.1	324 ± 27	4.03 ± 0.29
1.13	0.5	888 ± 96	0.90 ± 0.30
4.5	0.1	1486 ± 42	1.35 ± 0.09

* Data represent mean±SD from n≥3.

Table 4.3 summarizes the culturing conditions, TEER and FNa P_{app} obtained from the study, compared to those reported in the literature, for the Calu-3 monolayers grown under the AIC. It was evident that the literature employed different transwell area, seeding density, coating, and day of use, which resulted in substantially variable TEER ranging from 306 to 1486 $\Omega \cdot cm^2$ and P_{app} for FNa from 1.0 to 2.2 x 10^{-7} cm/s. Moreover, the observation was inconsistent across the literature, thereby requiring the condition optimization for each laboratory to yield sufficiently "tight" monolayers in a reproducible fashion, like the present study. It was notable that the Calu-3 monolayers formed in the present study resulted in the highest TEER at ~1500 $\Omega \cdot cm^2$ in the 4.5 cm^2 transwells without a use of coating upon a seeding density of 0.1 $x10^6$ cells/cm^2. However, as shown in Figure 4.2, the TEER development towards the steady state value appeared to be dependent upon the passage. It was shown that the TEER development took longer for the cells with a higher passage. This was probably also the case for the literature shown in Table 4.3 where the Calu-3 cells with the higher passages, e.g. 38-56 and 36-41, resulted in a lower TEER by day 8 (750 $\Omega \cdot cm^2$) or a longer time period (17-

19 days) to reach the steady state TEER [Fiegel *et al*, 2003; Trehin *et al*, 2004, respectively]. Similarly, the use of lower passages, e.g. 20-40, resulted in higher TEER of 1056-1126 $\Omega \cdot cm^2$ [Mathias *et al*, 2004]. Such passage effects have also been reported for the human intestinal Caco-2 cell line [Yu *et al*, 1997].

Table 4.3 The Calu-3 monolayers grown under the AIC and their culturing conditions reported in the literature.

Transwell area [cm^2]	Seeding density [$\times 10^6/cm^2$]	Transwell coating	Day of use	TEER [$\Omega \cdot cm^2$]	P_{app} for FNa [$\times 10^{-7}$/cm/s]	Reference *
4.5	0.1	None	8-10	1486±42	1.4±0.1	Table 4.2
4.5	0.1	None	8	750	2.2	Fiegel, 2003
4.2	1.0	Collagen	17-19	362	N.D	Trehin, 2004
1.13	0.1	None	16	500	1.1	Ehrhardt, 2002
1.13	2.5	Collagen	8-16	800-1200	N.D	Li, 2006
1.13	2.5	Collagen	14-21	550	1.0	Cooney, 2004
1.13	5.0	Collagen	8-16	1056-1126	1.5	Mathias, 2002
1.0	1.0	Vitrogen™	16-18	350-400	N.D	Meaney, 2002
1.0	5.0	Collagen	10-14	~ 400	N.D	Yang, 2004
0.33	5.0	None	11-13	306	1.5	Grainger, 2006

N.D. Not determined
* First authors are only shown.

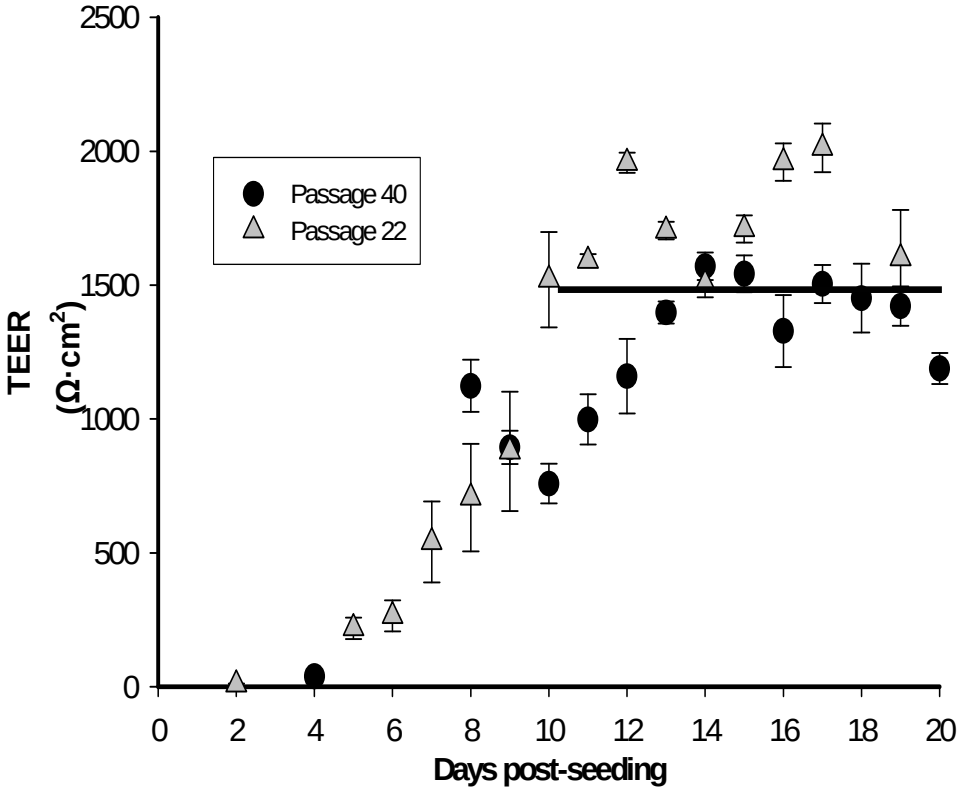

Figure 4.2 TEER development of the Calu-3 cells during 20 days of the air-interface culture (AIC) in the 4.5 cm^2 transwell upon a seeding density of 0.1 x 10^6 cells/cm^2 with the passages 22 and 40.
Data represent mean±SD from n=6.
The solid line indicates the steady state TEER observed as an average of the TEER values for day 10-20 across the cells with passages 22 and 40.

4.3.2 BARRIER ASSESSMENT OF THE CALU-3 MONOLAYERS GROWN UNDER THE AIC

Figure 4.3 shows a scanning electron micrograph of the Calu-3 monolayers grown under AIC in the 4.5 cm^2 transwell upon a seeding density of 0.1 x 10^6 cells/cm^2 and taken on day 10 following visual confluence. This condition was selected by virtue of the highest TEER value for the monolayers reaching steady state reaching ~1.5 k $\Omega \cdot cm^2$. The Calu-3 cell bodies are shown in its typical size of 5-10 µm with cilia on their mucosal cell surface. The intercellular junctions are also shown surrounding the cells. These were consistent with those reported in the literature [Mathias *et al*, 2002; Grainger *et al*, 2006], despite substantial differences in the TEER and P_{app} values as described in Table 4.3.

In the literature, the submerged condition with both the apical and basolateral sides receiving culture media was also shown to be suitable for the growth of Calu-3 monolayers [Grainer *et al*, 2006]. However, their epithelial morphology was reported to be different from the monolayers grown under the AIC, as no ciliated structures or mucus was observed [Grainger *et al*, 2006]. The AIC culture has shown an enhanced transport of Na^+ across the epithelium because of the greater availability of oxygen for the cells [Johnson *et al*, 1993]. Such factors can indirectly contribute to the differences in morphology observed under these conditions.

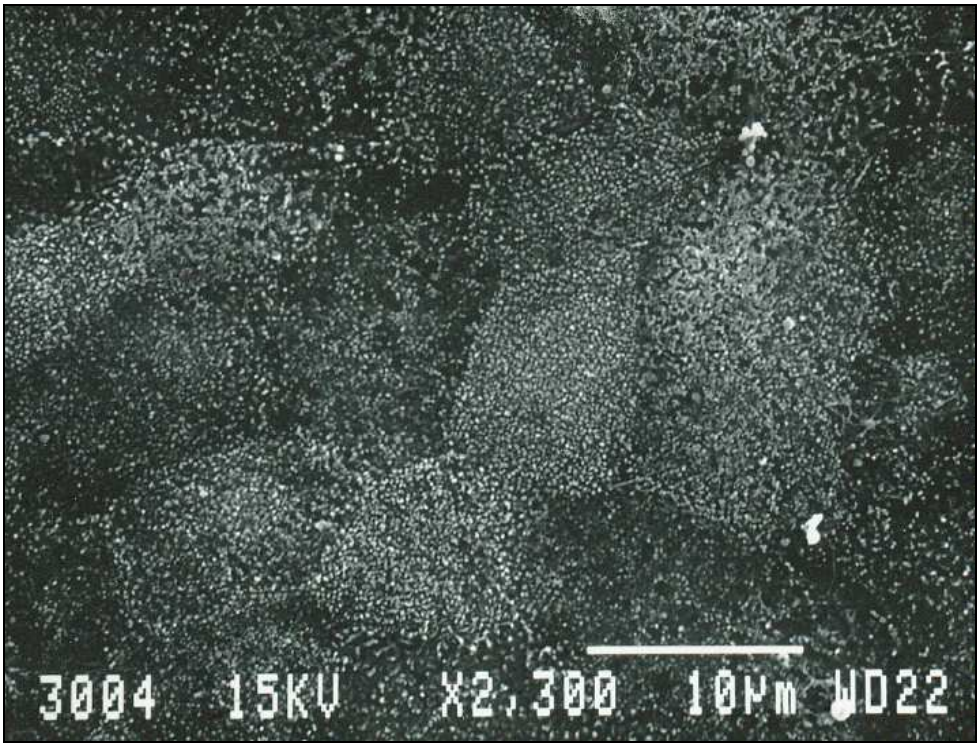

Figure 4.3 A representative scanning electron micrograph of the Calu-3 cell monolayer grown under the air-interface culture on day 10 (Passage-35) in the 4.5 cm^2 transwell, upon a seeding density of 0.1 $x10^6$ cells/cm^2. The bar indicates a 10 µm scale.

Figure 4.4 shows the cumulative % mass permeated into the basolateral compartment vs. time profiles for 7 solutes tested in this study across the air-interface cultured Calu-3 cell monolayers. The maximum cumulative % mass permeated by 180 min was 0.4 %, which justified the assumption of the sink conditions across these solutes. With increasing the molecular weights of the solutes (Table 4.4), the cumulative % mass permeated was decreased, which was in line with their diffusive permeation and the Fick's theory [Martin and Bustamante, 1993b]. Correspondingly, the lag times of the profiles became more evident for the macromolecules (e.g. FDs), which required the linear steady slope calculation from the data excluding those in the lag phase. Table 4.4 summarizes the P_{app} values for the 7 solutes across the Calu-3 monolayers derived from the profiles shown in Figure 4.4. The P_{app} values decreased with increasing the molecular weights, as deduced from the profiles shown in Figure 4.4. When these P_{app} values were plotted as a function of MW in a logarithmic format, an excellent linear correlation was observed for 6 solutes excluding FD-150, as shown in Figure 4.5. This suggested that diffusive permeation of these 6 solutes was equally restricted, while a further size exclusive steric hindrance and frictional resistance became effective for the largest molecule, FD-150 [Martin and Bustamante, 1993b; Renkin, 1954]. Indeed, the linear slope for the 6 solutes in Figure 4.5 was -0.36±0.13 (r^2=0.92), which was effectively consistent with -0.33, the theoretical slope value based on the Stokes-Einstein assumption of diffusion for the spherical molecules [Byron *et al*, 1994a]. Accordingly, all of the P_{app} data shown in Table 4.4 were possible to estimate the diffusive pore radius (r_p) by the Renkin function approach. The diffusive pore radius

of the Calu-3 monolayers (r_p) was derived to be 13.2 nm, while the ratio, ε/L (the ratio of the barrier porosity to barrier length) was 0.03 nm^{-1}, as described in Table 4.5. This derived r_p of 13.2 nm was close to the solute diameter for FD-150, ~11.0 nm [Hastings *et al*, 1992], which well explained the deviation from linearity for the Figure 4.5.

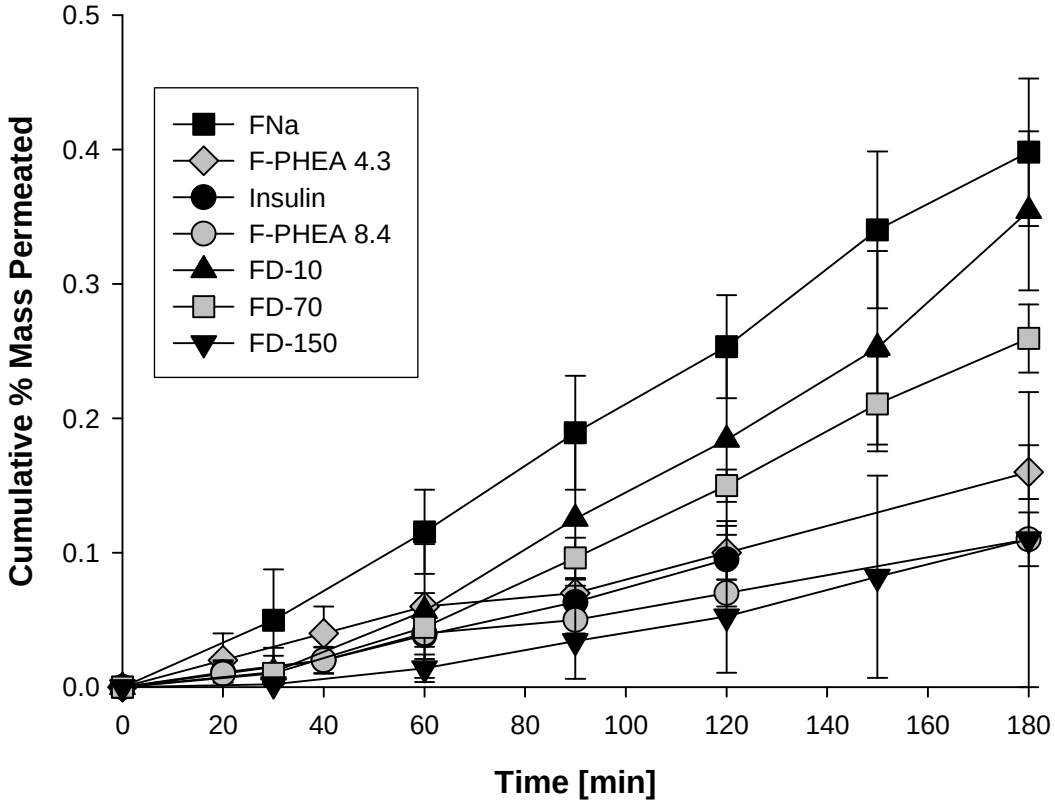

Figure 4.4 Cumulative % mass permeated into the basolateral compartment for 7 solutes across the Calu-3 monolayers as a function of time. The monolayers were grown under the air-interface for 8-10 days in the 4.5 cm^2 transwells upon a seeding density of $0.1x10^6$ cells/cm^2. Data represent mean±SD from n=4-6.

Table 4.4 P_{app} values for 7 model solutes across the Calu-3 monolayer grown under AIC (4.5 cm^2 transwell; 0.1 x 10^6 cells/cm^2 of seeding density).

Solute	**MW (Da)**	**P_{app}* (x10^{-7} cm/s)**
FNa	376	1.35 ± 0.10
F-PHEA	4,300	0.53 ± 0.11
Insulin	5,808	0.56 ± 0.15
F-PHEA	8,400	0.35 ± 0.06
FD-10	9,500	0.55 ± 0.01
FD-70	50,700	0.20 ± 0.04
FD-150	150,000	0.02 ± 0.01

*Data represent mean±SD from n=4-6
MW: molecular weight

Figure 4.5 also plotted the P_{app} values vs. the molecular weights of several solutes tested with the Calu-3 monolayers in the literature. In line with a much lower TEER of 306 Ω·cm^2, the P_{app} values by Grainger *et al*, 2006 appeared to be higher overall, while a deviation from the linearity became evident at 70 kDa in molecular weight. On the other hand, Mathias *et al*, 2002 reported quite a different slope of the linearity from the Calu-3 monolayers with fairly high TEER of ~1100 Ω·cm^2. Table 4.5 summarizes the linear slopes obtained from Figure 4.5 alongside the r_p values of the Calu-3 monolayers across 3 institutions. The slope of the present study agreed with the Stokes-Einstein relationship, while the remaining two slopes resulted in different estimates. The pore radius (r_p) of the Calu-3 monolayers for the present study was close to that reported by Grainger *et al*, 11.0 nm, despite the differences in TEER and slopes. This could also be attributed to the differences in porosity of the cell membranes (ε; also calculated by Renkin function analysis) between the work of Grainger *et al* and the

present study. Such inconsistencies also addressed the inability of the data comparison across the institutions, in Figure 4.5, for the standardization of the Calu-3 monolayers, emphasizing a need for this study for own laboratory establishment and validation.

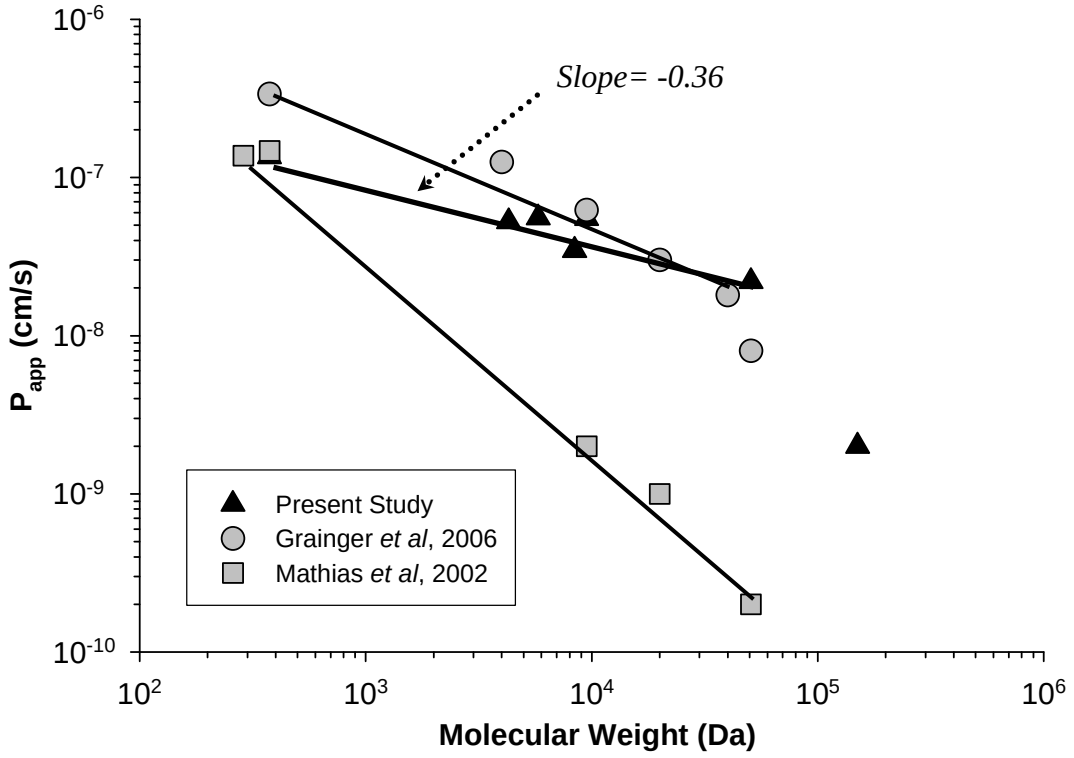

Figure 4.5 P_{app} values across the air-interface cultured Calu-3 monolayers *vs.* molecular weights of various hydrophilic solutes obtained at three different institutions.

Table 4.5 The linear slopes derived from the plots in Figure 4.5 and pore radius (r_p) of the Calu-3 monolayers estimated using the Renkin function approach.

	Slope	r_p (nm)
Present Study	-0.36±0.13	13.2
Grainger *et al*, 2006	-1.22±0.06	11.0
Mathias *et al*, 2002	-0.63±0.07	5.7

4.3.3 CELL LINING FLUID VOLUME OF THE CALU-3 MONOLAYERS

The tracer-dilution technique with RD-7 yielded 39.7±12.1 µL (mean±SD, n=3) of the cell lining fluid for the apical surface of the Calu-3 monolayers grown under AIC on day 8-10 in the 4.5 cm^2 transwells upon a seeding density of $0.1x10^6$ cells/cm^2. The high % CV of ~30 % on the fluid volume estimation could be because of biological or analytical variability which may require further repeated determination to use this volume with confidence. Nevertheless, this estimate was useful in approximation of the lining fluid thickness, yielding 88.2±26.7 µm. A similar value of 90.9 µm has been recently reported with the similarly grown Calu-3 monolayers yet in the 0.33 cm^2 transwells under the AIC [Grainger *et al*, 2006b]. Therefore, this consistency between institutions gave a strong support on the accuracy on the V_{LF} value, though with a high variability. Even so, the ~90 µm thickness of the lining fluid was much greater than 10-23 µm of the lining fluid thickness measured in the tracheo-bronchial regions in humans [Widdicombe, 1997]. Hence, the Calu-3 monolayers grown under the AIC still favored the fluid capacity per unit surface area for dissolution of deposited aerosols on the lung

surface by a factor of 4-9. Hence, the semi-dry apical surface of the Calu-3 monolayers with sufficiently "tight" restriction to this diffusion would enable a valid argument for aerosol dissolution, if some ICSs showed this process to be rate-determined.

4.4 SUMMARY AND CONCLUSIONS

The air-interface culture of the human bronchial epithelial cell line, Calu-3, formed well-differentiated monolayers with a sufficiently "tight" barrier for restrictive diffusion with a high TEER of ~1.5 k $\Omega \cdot cm^2$. The monolayers resembled the airway luminal surface with respect to the presence of cilia and intercellular junctions and a limited volume of the lining fluid. The intercellular junctions were shown to serve as the restrictive diffusive barrier, which was capable of differentiating permeation of various model solutes with varying MW. Nevertheless, the cell passage and culturing conditions were shown to affect such tight junction formation and thus, it became essential to ensure the consistent formation of the "tight" monolayers at each laboratory. The present study concluded that the Calu-3 monolayers grown under the AIC in 4.5 cm^2 transwells upon a seeding density of $0.1x10^6$ cells/cm^2 was the most suitable model by virtue of their restrictive barrier formation for diffusion while maintaining the semi-dry mucosal cell surface with ~40 µL of the lining fluid. This would provide the unique opportunity to study aerosol particle deposition, dissolution and uptake or absorption in the in vitro system, the cascade of events that have only been studied with animals or humans.

CHAPTER 5

IN VITRO CELL MONOLAYER-BASED ANTI-INFLAMMATION ASSESSMENT OF INHALED CORTICOSTEROIDS UPON AEROSOL DEPOSITION

5.1 INTRODUCTION

In vitro cellular assessment of anti-inflammatory potencies and activities for inhaled corticosteroids (ICSs) has conventionally employed application of ICS solution to non-confluent lung cells in culture [Jafuel *et al*, 2000; Roumestan *et al*, 2003]. While such a method has enabled the assessment of their "intrinsic" molecular anti-inflammatory potencies, it has been criticized that lung organ-related issues such as deposition, dissolution and cellular uptake, when administered as ICS aerosols, are not taken into account [Edsbäcker *et al*, 2006; 2008]. As a result, these potencies have been suggested to overrate their in vivo or clinical anti-inflammatory potencies and activities upon inhalation [Edsbäcker *et al*, 2008]. In this context, in chapter 3, only 3 % of 2.4 µg of the deposited mass of the least soluble ICS, fluticasone propionate (FP), was shown

to be dissolved in 10 h in the presence of the limited 40 µL fluid (Figure 3.8). This logically implied that 97 % of FP would be left undissolved and thus unavailable for its anti-inflammatory action, when deposited on the lung's mucosal surface with an equally limited volume of the lining fluid. In contrast, 2.4 µg of the deposited mass of the readily soluble triamcinolone acetonide (TA) showed near complete 89 % dissolution in the 40 µL fluid by 5 h (Figure 3.8). It was likely therefore that, compared to FP, dissolution for TA aerosols, would not be problematic for cellular uptake and thus, anti-inflammatory action. Even so, the conventional assessment has rated that FP is 10-fold potent than TA in the "intrinsic" anti-inflammatory potency (Table 1.1).

The Calu-3 cell monolayers developed and characterized in chapter 4 possess a unique feature that their confluent mucosal surfaces are left semi-dry with the limited volume of the lining fluid. This would enable direct deposition of ICS aerosols on their mucosal surfaces like the airways, provided that their accurate and precise deposition system can be established. In contrast, the assessment of the cellular anti-inflammatory activity via certain proinflammatory transcription factor markers faces an experimental challenge. It has been well recognized that confluent monolayers like Calu-3 are quite formidable for gene construct to be sufficiently transfected, and otherwise, the cellular anti-inflammatory activity would not be measurable [Uduehi *et al*, 1999; Florea *et al*, 2002; Düchler *et al*, 2001]. Hence, it became quite essential to develop the effective transfection method, specifically for the confluent Calu-3 monolayers, so that their anti-inflammatory activity in response to the ICS aerosol deposition could be determined via repression of the measurable proinflammatory transcription factor marker.

Accordingly, in this chapter, FP and TA were chosen as the least and fairly soluble ICSs, respectively, to determine their cellular anti-inflammatory activities upon aerosol deposition on the confluent Calu-3 monolayer system. Accurate and precise ICS aerosol deposition system from the inhaler products was developed and validated using the modified assembly of the Andersen cascade impactor (ACI). Then, the Calu-3 cell monolayers were optimally transfected with a nuclear factor kappa B (pNFκB; a proinflammatory transcription factor) -dependent reporter plasmid of luciferase (pNFκB-Luc) to determine its response following aerosol deposition of FP and TA on the monolayer surface. By so doing, the FP aerosols were identified to be kinetically rate-limited by their mucosal dissolution, which resulted in rather inefficient manifestation of the anti-inflammatory action, compared to the TA aerosols, despite the 10-fold potency in the "intrinsic" molecular activity in the literature.

5.2 THEORY: TRANSFECTION AND REPORTER GENE ASSAY

Generally, most cells including Calu-3 do not express basal levels of inflammatory markers that are measurable. Therefore, it becomes necessary that such measurable inflammatory markers be sufficiently introduced into the cells, so that the cellular anti-inflammatory potencies or activities of aerosol ICSs can be determined. Reporter genes serve as such measurable markers, when attached to another gene of interest in the same plasmid construct, for its insertion into the cells. This molecular biology technique called transfection has been increasingly employed to study the

mechanisms by which transcription factors act to control eukaryotic gene expression. NFκB is one of the proinflammatory transcription factors directly involved and activated through the cascade of cellular inflammation [Jafuel *et al*, 2000; Roumestan *et al*, 2003]. However, preliminary attempts using specific enzyme-linked immunosorbent assay (ELISA) resulted in undetectable cellular NFκB levels in the Calu-3 cells, thereby requiring the transfection of a plasmid construct of NFκB-dependent reporter gene of luciferase enzyme (pNFκB-Luc). In this chapter, this plasmid was transfected into the Calu-3 cell monolayers using a commercially available kit, Effectene® transfection kit (Qiagen, Valencia, CA). While its details remain proprietary, it has been described that the plasmid is condensed by interaction with the Enhancer in the EC buffer system, both of which are supplied in the kit to form a complex with the Effectene® reagent. The technique appears to employ the negative-positive charge attraction for successful insertion (i.e., transfection) of the plasmid-Effectene® complex into the cells, rather than liposome lipid formulation. A typical incubation is 24 h in culture and then, the cells are lysed to measure the luciferase (Luc) activity generated from the Luc reporter genes by luminescence assay. In this assay, Luc catalyses a bioluminescent reaction of its substrate, luciferin, in the presence of ATP, Mg^{2+} and O_2, emitting a flash of light signals proportional to the NFκB activity. These light signals can be measured using a luminometer [Kumar *et al*, 2003; Roumestan *et al*, 2003; Effectene® Transfection Reagent Handbook 2002; Baldwin, 1996].

5.3 MATERIALS AND METHODS

5.3.1 CALU-3 CELL CULTURE AND MONOLAYER FORMATION

The Calu-3 cells (ATCC) were propagated, as described in Chapter 4 (as well as Appendix A) and used between passages 27 and 36. Their monolayers were formed, as also described in Chapter 4 (as well as Appendix A). Briefly, the cells were seeded at a density of 0.1 $x10^6$ cells/cm^2 in the 4.5 cm^2 transwells (Corning Costar) and cultured overnight under the medium-submerged condition with 1.5 and 2.6 mL of the apical and basolateral media, respectively. On day 2, the culture was changed to the air-interface culture (AIC) where the cells were fed and grown only with 1.4 mL of the basolateral media, while their apical surface was left semi-dry. The basolateral media was changed everyday, during which the cell growth was monitored under the microscope until the confluent monolayers were formed. The culture was maintained under the humidified 95% (v/v) air and 5% (v/v) CO_2 at 37 °C in the incubator (NAPCO) throughout. Whereas the monolayers were generally formed by day 8-11, most of the experiments described below (e.g., aerosol deposition assessment and/or plasmid transfection) were carried out on day 11-12 after their TEER values were ensured to exceed 700 $\Omega \cdot cm^2$.

5.3.2 ICS AEROSOL DEPOSITION ON THE CALU-3 MONOLAYERS

Figure 5.1 schematically describes ICS aerosol deposition collection onto the Calu-3 monolayers in a defined aerodynamic diameter of $\leq$3.3 µm, generated from commercially available inhaler products. The 8-stage Andersen cascade impactor (ACI

Mark II; Thermo Electron Corporation) was used for the aerosol collection, yet under a slightly different airtight assembly configuration, in order to accommodate the transwell inserts under Stage 4. That is, the ACI was assembled in a descending order of the Stages 0, 1, 2, 3, 4 and the filter stage, followed by Stages 5, 6 and 7, as shown in Figure 5.1. For the ≤3.3 µm aerosol collection, the 4.5 cm^2 transwell insert of the confluent Calu-3 monolayer was placed on the filter stage under Stage 4, using a plastic cup custom-made by the VCU Custom Design and Fabrication. The cup held 0.2 mL of pre-warmed culture media, so that the basolateral compartment remained submerged, while protecting the basolateral plastics from ICS contamination. The impactor was coupled with the USP induction port and the mouthpiece adaptor, and operable with the pump (General Electric Company) adjusted at 28.3 L/min of airflow rate. In some experiments, the ACI was assembled in a descending order of the Stages 0, 1, 2 and the filter stage, followed by the Stages 3, 4, 5, 6 and 7, in order to collect the ≤5.8 µm aerosols under the Stage 2.

Fluticasone propionate (FP) aerosols were generated from Flovent HFA® 220 µg MDI (GlaxoSmithKline, Research Triangle Park, NC), while triamcinolone acetonide (TA) aerosols were from Azmacort® 200 µg MDI (Abbott, Abbott Park, Illinois); their product details are shown in Table 3.1 in Chapter 3. They were actuated at various times (e.g., 1, 3, 10 or 20 times for Flovent HFA® and 25 times for Azmacort®) within a period of 30 s under the airflow at 28.3 L/min to deposit the target masses of each ICS. For determination of ICS aerosol mass deposit, the ACI was immediately disassembled, and the Calu-3 monolayer surface was thoroughly washed with 1.0 mL admixture of

CH_3CN and H_2O (60/40). The recovery solution was centrifuged at 12,000 *g* for 1 min to remove the dislodged cells, and the supernatant was analyzed by the HPLC-UV method developed and validated in-house. The analysis employed Spherisorb ODS-2 column (4.6 mm x 250 mm, 5 μm; Alltech Associates Inc.) for separation at 1.0 mL/min of the mobile phase, CH_3CN/H_2O (60/40), followed by detection at 236 nm (Waters Corporation). It was fully validated for both FP and TA with respect to their calibration linearity (r^2>0.999) over the range of 0.05 to 5 μg/mL and 0.05 μg/mL as the limit of quantification (LOQ). Meanwhile, for determination of NFκB repression by the ICS aerosols, this ICS aerosol deposition was carried out to the Calu-3 monolayers transfected with pNFκB-Luc, as described below.

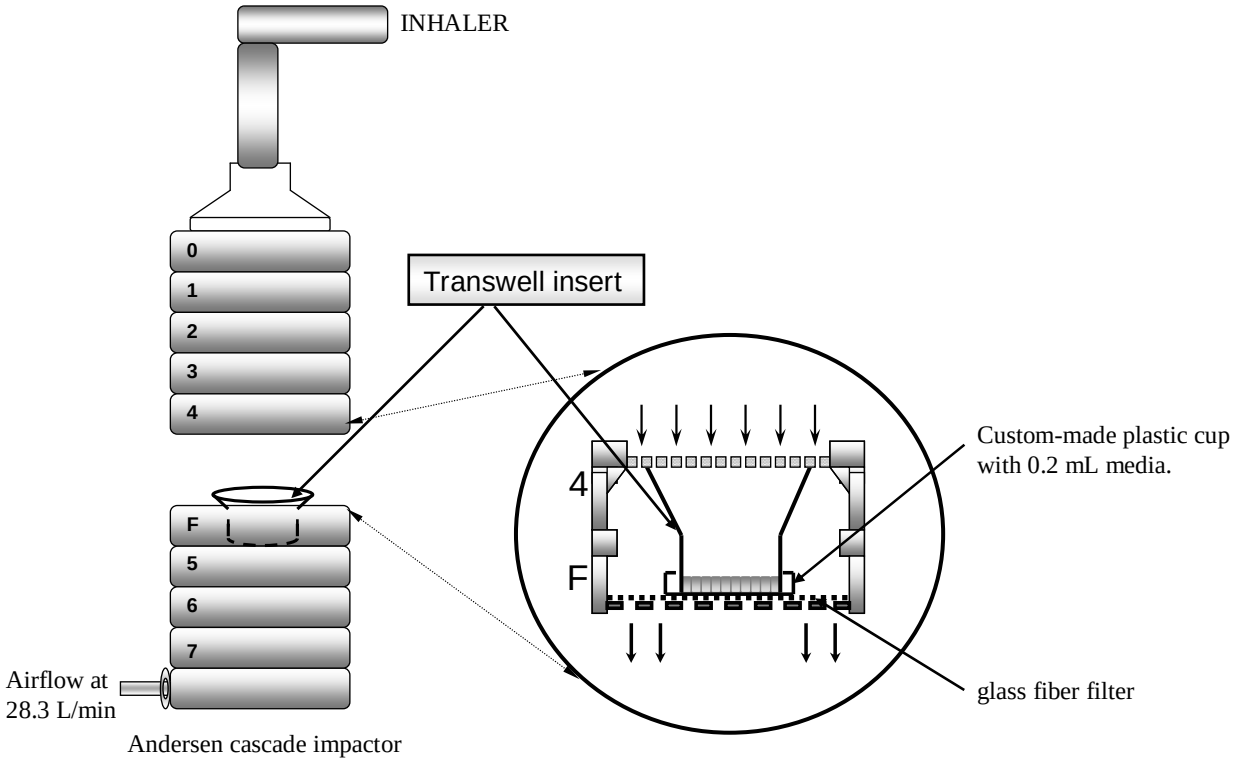

Figure 5.1 Defined-size aerosol deposition and collection on the Calu-3 monolayers using the Andersen cascade impactor (ACI). The Stage 4 and filter stage are magnified to describe the placement of the transwell insert of the Calu-3 monolayer with a custom-made plastic cup containing 0.2 mL of the culture media. The transwell insert shown is placed under the Stage 4 to collect the ≤3.3 µm aerosols, while some experiments placed the inserts under the Stage 2 for the ≤5.8 µm aerosol deposition.

5.3.3 pNFκB-Luc TRANSFECTION OF THE CALU-3 MONOLAYERS

Transfection of the Calu-3 monolayers required exhaustive optimization attempts of the protocol, referenced to the transfection kit [Effectene® Transfection Reagent Handbook, Qiagen, Valencia, CA 2002] in order to maximize the retention of the NFκB-dependent plasmid construct of the luciferase (pNFκB-Luc) in the monolayers. The pNFκB-Luc contains the reporter gene of luciferase enzyme with 5 tandem repeats of the binding sites for the proinflammatory transcription factor, NFκB, which was obtained from Stratagene (La Jolla, CA) and later, custom-made at the VCU Molecular Biology Core Facility. The transfection was carried out using the Effectene® transfection kit (Qiagen) with the best quantity combination of pNFκB-Luc and the kit's reagents (Effectene, Enhancer and Buffer EC), optimized in the preliminary attempts. The optimization studies concluded that, for the 4.5 cm^2 transwells, the best retention and expression of pNFκB-Luc was obtained by the use of 0.8 µg pNFκB-Luc incubated for 10 min with 100 µL Buffer EC and 6.4 µL Enhancer, followed by another 10 min incubation with 8 µL Effectene. This master-mix solution was finally diluted to 1.5 mL with the culture media and added to the apical surface of the transwells and incubated for 24 h with 2.6 mL of the basolateral media (i.e. under the medium-submerged condition), yet following 15 min apical pretreatment with 2.5 mM ethyleneglycotetraacetic acid (EGTA, Sigma-Aldrich) in phosphate-buffered saline (pH 7.2; PBS, Gibco Invitrogen, Carlsbad, CA). For the Luc activity measurement, the Calu-3 cell monolayer surface was rinsed thoroughly with PBS, followed by cell harvest with 200 µL of the lysis reagent (Promega, Madison, WI). The lysed cell samples were

centrifuged at 12,000 *g* for 30 min, and their 20 µL supernatants were measured for luminescence using the 20/20 luminometer (Turner Biosystems, Sunnyvale, VA). The NFκB activity was obtained as the Luc activity in the relative light unit (RLU), which was then normalized by unit mg protein determined via the bicinchoninic assay (BCA protein assay kit, Thermo Fisher Scientific, Rockford, IL) of the lysed samples.

5.3.4 TNFα-INDUCED NFκB ACTIVITY REPRESSION IN THE CALU-3 MONOLAYERS UPON ICS AEROSOL DEPOSITION

On day 11-12 post-seeding, pNFκB-Luc transfection of the confluent Calu-3 monolayers with TEERs ≥ 700 $\Omega \cdot cm^2$ was carried out for 24 h, as described above. This was followed by 4 h incubation under the air-interface culture by removing the apical solution, in order to restore the semi-dry apical mucosal surface temporarily disturbed by the transfection. Then, the transfected Calu-3 monolayers in the transwell inserts were placed within the ACI where FP or TA aerosols were deposited from Flovent HFA® and Azmacort®, respectively, as described above. The transwell inserts were returned to their base plate, and the monolayers were stimulated with 60 ng/mL of human tumor necrosis factor-α (TNFα; BD Bioscience, San Jose, CA) for 6 h in the incubator. Before each experiment, the TNFα solution was prepared freshly from 10 µg/mL stock solution of serum-free Eagles Minimum Essential Medium (EMEM; ATCC, Rockville, MD), and its 0.04 and 1.4 mL prepared in the culture media were applied to both the apical and basolateral compartments, respectively. In addition, the basolateral media contained 0.14 µg/mL FP and 21 µg/mL TA (saturated solubility of

FP and TA) in the Flovent® HFA and Azmacort® studies, respectively, in order to avoid ICS permeation into the basolateral compartment. It should be noted however that neither of this 0.14 µg/mL FP nor 21 µg/mL TA in the basolateral compartment exerted any repression of this TNFα-induced NFκB activity by itself. At 6 h of this aerosol ICS and TNFα incubation, the monolayers were harvested with 200 µL of the lysis reagent (Promega), and the lysed samples were subjected to the luminescence and protein determinations, as described above. In some experiments, the monolayer surfaces were washed with 1.0 mL admixture of CH_3CN and H_2O (60/40), at 6 h to determine the FP and TA masses remaining for dissolution and uptake by the analytical method described above.

5.3.5 TNFα-INDUCED NFκB ACTIVITY REPRESSION IN THE CALU-3 MONOLAYERS UPON ICS SOLUTION OR SUSPENSION APPLICATION

On day 11-12 post-seeding, the 24 h pNFκB-Luc transfection was carried out to the confluent Calu-3 monolayers, followed by the 4 h incubation under the air-interface culture to restore the semi-dry apical mucosal surface, as described above. FP (Sigma-Aldrich; St. Louis, MO) solution was prepared at 15 µg/ml (30 µM) from serial dilution of 1 mg/mL stock solution in N, N-dimethylformamide (DMF, Acros Organics, NJ, New Jersey) with the culture media. This appeared to maintain the formulation of FP solution, by virtue of the presence of <1% v/v DMF. Meanwhile, FP suspension was also prepared at 15 µg/ml, yet from FP powder directly added into, and diluted with, the culture media; its visual observation confirmed the suspension. For determination of

true concentration with respect to dissolved FP, these solution and suspension were filtered using a syringe filter (0.45 µm, Fisher Scientific, Pittsburg, PA) and the filtrate was analyzed by the validated HPLC-UV method described above. The pNFκB-Luc transfected Calu-3 monolayers in the transwell inserts were apically incubated for 6 h with 1.5 mL of the FP solution or suspension, during which the monolayers were also stimulated by the apical and basolateral media with 60 ng/mL of TNFα; the volume of the basolateral media was 2.6 mL. At 6 h of this ICS and TNFα incubation, both the apical and basolateral surfaces of the monolayers were thoroughly washed with PBS and then, harvested with 200 µL of the lysis reagent (Promega). The lysed samples were subjected to the luminescence and protein determinations, as described above. In some experiments, the apical solution (1.5 mL) was recovered and the monolayer surfaces were washed with 1.0 mL admixture of CH_3CN and H_2O (60/40). This ~2.5 mL recovery samples was further mixed with 10 mL of the admixture to dissolve all suspended FP. This enabled the determination of FP mass remaining for dissolution and uptake at 6 h by the analytical method described above.

5.4 RESULTS

5.4.1 ICS AEROSOL DEPOSITION ON THE CALU-3 MONOLAYERS

The Calu-3 monolayers were well tolerated to 30 s of the airflow at 28.3 L/min in the ACI, evidenced by insignificant < 5% changes in the TEER values post-airflow exposure. The microscopic observation of the monolayer surfaces also confirmed no appreciable morphological changes. Accordingly, Table 5.2 shows the FP and TA aerosol masses collected on the Calu-3 cell monolayers on the 4.5 cm^2 transwells placed under Stage 4 and Stage 2 of the ACI, generated from various actuations of the Flovent® HFA and Azmacort® MDIs. For both FP and TA, the aerosol mass deposits were shown to be reproducible, suggesting that the system described in Figure 5.1 enabled accurate and precise collection of the ICS aerosols on the Calu-3 monolayers. With increasing the number of actuations, the aerosol deposits were also increased for FP, somewhat proportionally. They were ranged from 0.06 to 0.90 µg under the Stage 4 and thus, ≤ 3.3 µm in the aerodynamic diameter. Provided that these Calu-3 cell monolayers grown under the air-interface culture were shown to maintain their lining fluid volume at 39.7 µL, as determined in Chapter 4, these FP mass deposits would result in 1.5-22.7 µg/mL (3.0-45.3 µM) of the theoretical concentrations upon complete dissolution. Obviously, such concentrations were not possible, since FP's aqueous solubility was reported to be only 0.14 µg/mL (0.28 µM; Table 3.1 in Chapter 3). It was most likely therefore that the majority of the deposited FP masses remained to be dissolved on the Calu-3 monolayer surface without efficient intracellular uptake. Meanwhile, even with 25 actuations, only

0.10 µg of the TA aerosols was deposited on the Calu-3 monolayers from the Azmacort® MDI, when the transwell inserts were placed under the Stage 4 of the ACI (Table 5.1). This deposit was much smaller than that from the Flovent® HFA, given that the latter MDI enabled much greater 0.90 µg deposits with the fewer 20 actuations (Table 5.1). Because both MDIs metered almost equivalent ICS masses (220 and 200 µg, respectively; Table 3.1), this lower TA deposit upon Stage 4 collection suggested that a smaller fraction of the ≤ 3.3 µm aerosols was generated from the Azmacort®, compared to the Flovent® HFA. Instead, when collected under Stage 2 (≤ 5.8 µm), a much greater 0.52 µg of the TA aerosols was deposited on the Calu-3 cell monolayers upon identical 25 actuations (Table 5.2). Hence, the Azmacort® appeared to generate relatively larger size ICS aerosols, compared to the Flovent® HFA. Because of this difference in their generated aerosol size distribution, an equivalent ICS mass of 0.10 µg was deposited under the Stage 4 following 3 actuations of the Flovent HFA® and 25 actuations of the Azmacort®. Likewise, an equivalent mass of ~0.5 µg was deposited following 10 actuations of the Flovent® HFA and 25 actuations of the Azmacort®, even though their aerosol sizes were different, ≤ 3.3 and ≤ 5.8 µm, respectively, due to the need for using different collection stages. It was lastly calculated that 0.10 and 0.52 µg of the TA aerosols deposited on the Calu-3 monolayers would result in 2.5 and 13.1 µg/mL (5.0 and 26.2 µM) of the theoretical concentrations upon complete dissolution in the 39.7 µL of the lining fluid, respectively. These were clearly possible, given 21 µg/mL of the TA's aqueous solubility. Hence, all of the TA aerosol deposits in these

experiments were likely to undergo fairly fast and complete dissolution on the Calu-3 monolayer surface.

Table 5.1 Fluticasone propionate (FP) and triamcinolone acetonide (TA) aerosol masses collected on the 4.5 cm^2 transwell inserts with the Calu-3 monolayers placed under Stage 4 or 2 of ACI, generated from various actuations of the Flovent® HFA 220 µg and Azmacort® 200 µg MDIs.

ICS	Number of actuations	Stage for collection	Mass (µg) (mean±SD, n=3)
FP	1	4	0.06 ± 0.02
FP	3	4	0.10 ± 0.02
FP	10	4	0.55 ± 0.02
FP	20	4	0.90 ± 0.03
TA	25	4	0.10 ± 0.03
TA	25	2	0.52 ± 0.03

5.4.2 pNFκB-Luc TRANSFECTION AND TNFα INDUCTION IN CALU-3 MONOLAYERS

Figure 5.2 shows the luciferase (Luc) activity measured as the RLU per mg protein, for the Calu-3 monolayers transfected with pNFB-Luc with or without 6 h stimulation of 60 ng/mL TNFα in 2 representative experiments carried out on 2 different days. By virtue of successful transfection, the Luc activity was shown to be measurable in both experiments, yielding 2.4±0.6 $x10^5$ and 1.6±0.3 $x10^5$ RLU/mg protein. Moreover, these values were significantly increased to 9.5±0.3 $x10^5$ and 5.1±0.9 $x10^5$ RLU/mg protein by the TNFα stimulation ($p<0.05$; unpaired t-test), respectively, which demonstrated successful induction of the proinflammatory

transcriptional response in these confluent Calu-3 monolayers. However, the RLU/mg protein values in the same treatments were different in different experiments, presumably due to variable nature of the transfection efficiency. Accordingly, these values were unable to be compiled directly across the experiments and this necessitated taking these transfection efficiency differences in each experiment into account. In this context, Table 5.2 shows the fold-induction of the RLU/mg protein values by the TNFα stimulation, relative to the transfection control, i.e., the transfected Calu-3 cell monolayers without TNFα stimulation, obtained in each of 4 experiments. These fold induction values were shown to be more consistent across the experiments and therefore, used for the data analysis from multiple experiments. As a result the TNFα stimulation was shown to cause 3.97±1.07-fold increase in the Luc activity, compared to the transfection control.

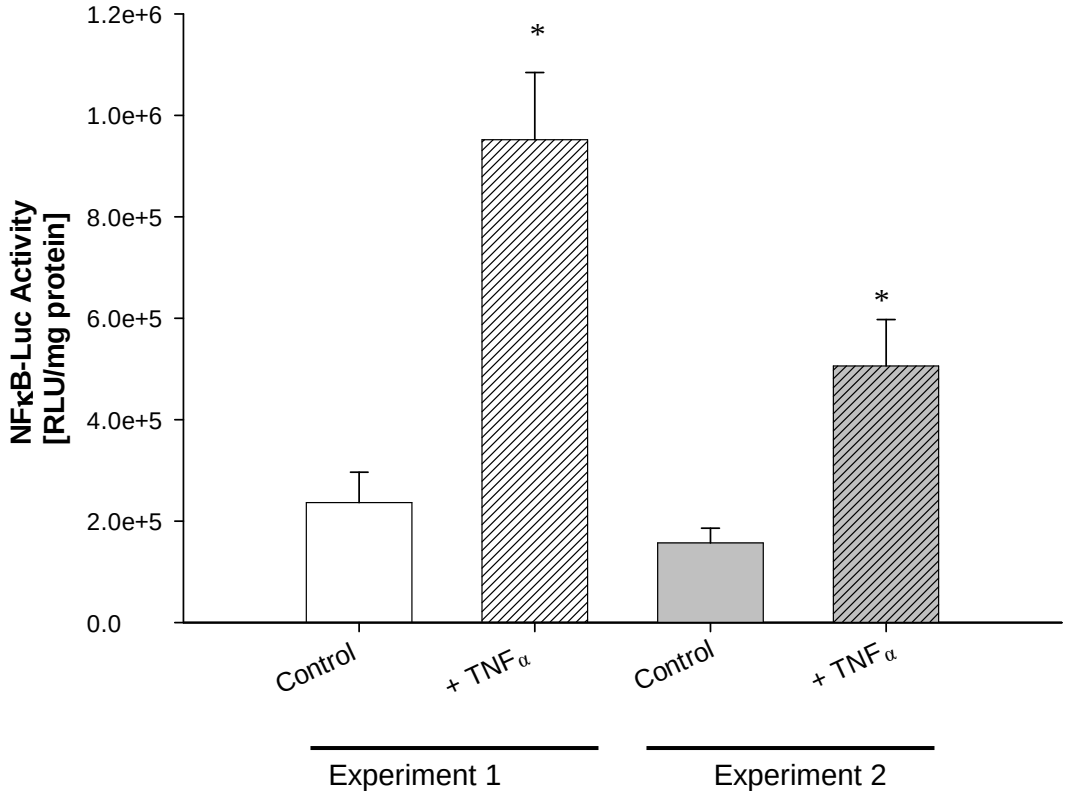

Figure 5.2 Luciferace (Luc) activity expressed as RLU/mg protein with or without 6 h stimulation of 60 ng/mL TNFα in the pNFκB-Luc transfected Calu-3 monolayers from 2 independent experiments. Data represent mean±SD from n=3. * indicates the significant increase of the Luc activity compared to the transfection control ($p<0.05$; t-test).

Table 5.2 Fold-induction of the RLU/mg protein values by the TNFα stimulation, relative to the transfection control, i.e., the transfected Calu-3 cells without the TNFα stimulation, in each transwell carried out on different days.

Fold-Induction							
Expt# 1	4.55	Expt# 2	3.02	Expt# 3	4.84	Expt# 4	3.92
	4.10		2.76		3.29		3.32
	3.44		3.88		6.59		
Mean±SD (n=11): 3.97±1.07							

5.4.3 TNFα-INDUCED NFκB ACTIVITY REPRESSION IN THE CALU-3 MONOLAYERS UPON ICS AEROSOL DEPOSITION

Figure 5.3 shows the fold-induction of the Luc activity representing the NFκB activity in the Calu-3 monolayers in response to various mass deposits of the ICS aerosols upon TNFα stimulation. As concluded above, the TNFα stimulation resulted in 3.97±1.07-fold increase in the NFκB activity, compared to the transfection control, demonstrating significant inflammatory response in the Calu-3 monolayers. This 3.97-fold induction of the NFκB activity was shown to be repressed by the ≤3.3 µm aerosol deposition of FP generated from the Flovent® HFA in an apparently dose-related manner. Indeed, 35.7±6.3 % repression observed at 0.90 µg of the FP aerosols was statistically significant ($p<0.05$, ANOVA), while such a mass deposition required 20 actuations of the Flovent® HFA; a lower 15.5±2.2 % repression for the 0.55 µg FP did not reach statistical significance. Unfortunately, a further increased mass deposition was not attempted, since the maximum 30 s of the airflow in the ACI would not allow over

25 actuations. Meanwhile, as shown in Figure 5.3, an insignificant 10.4±2.6 % repression was observed at 0.52 µg of the TA aerosols generated and deposited from 25 actuations of the Azmacort®. Though insignificant, this was quite of interest that the equivalent mass deposits of FP and TA (i.e., ~0.5 µg) resulted in comparable % repression in the NFκB activity of the Calu-3 monolayers (i.e., 15.3 and 10.4 %, respectively), despite a 10-fold higher "intrinsic" molecular anti-inflammatory potency for FP over TA, based on their cellular NFκB activity repression upon solution application [Jafuel *et al*, 2000].

Table 5.3 shows the FP and TA mass and % taken by the Calu-3 cells in 6 h following aerosol deposition and incubation alongside % NFκB repression obtained above. The ICS masses were calculated from the differences between the aerosol mass deposit and the mass recovered from the Calu-3 apical surface at 6 h. Notably, even following 6 h incubation, only 42.2±24.7 ng and 29.1±22.2 ng of the FP were taken by the Calu-3 monolayers upon 0.90 and 0.55 µg of aerosol deposition. This represented 4.7 and 5.6 % of the mass deposits, and therefore, near 95 % of the FP deposit remained on the cell surface and was uninvolved in the NFκB repression in these transfected Calu-3 monolayers (Figure 5.3). This was presumably due to FP's least aqueous solubility of 0.14 µg/mL, in line with ~4-5 % of dissolution and permeation for FP in 6 h in the dissolution testing system described in chapter 3 (Figure 3.6). In contrast, the TA aerosols appeared to undergo much greater intracellular uptake for 6 h, and demonstrated that 170.7±40.6 ng or 32.6±7.8 % of the 0.52 µg deposit was taken by the Calu-3 cell monolayers (Table 5.3). It was likely therefore that the higher aqueous

solubility of TA (21 µg/mL; Table 5.3) enabled faster and greater ICS aerosol dissolution on the Calu-3 cell monolayers and hence, greater cellular uptake upon aerosol deposition. In this sense, comparable 15.5 and 10.4 % repression in the NFκB activity of the Calu-3 monolayers for the FP and TA aerosols were still reasonable attributed to the greater TA mass taken by the cells, which compensated its 10-fold lower intrinsic potency of the NFκB activity, compared to the FP aerosols.

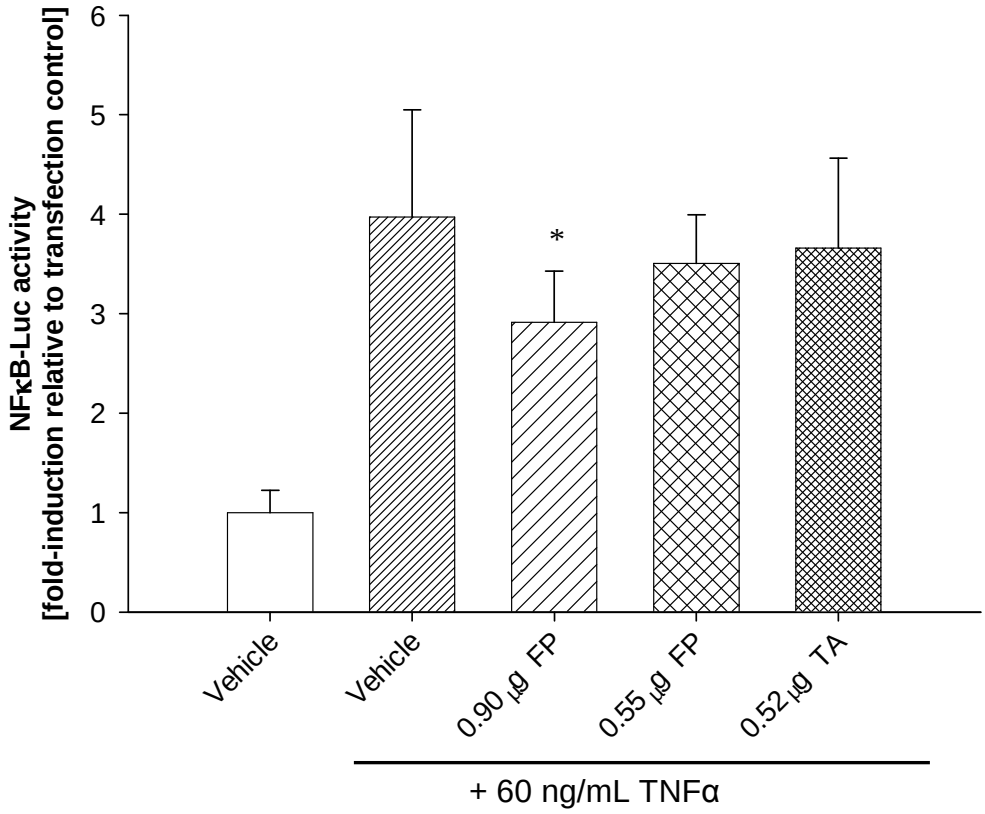

Figure 5.3 Fold-induction of the Luc activity representing the NFκB activity of the transfected Calu-3 monolayers in response to various FP and TA aerosol deposition from Flovent® HFA and Azmacort® MDIs, respectively, with or without 6 h stimulation of 60 ng/mL TNFα. Data represent mean±SD from n=10 for the control, n=11 for the TNFα stimulated group and n=6 for the FP and TA tested groups. * indicates the significant decrease in the NFκB-Luc activity by the FP aerosols, compared to the TNFα stimulated group ($p<0.05$; t-test).

Table 5.3 FP and TA mass and % taken by the Calu-3 monolayers following aerosol deposition at various masses from the Flovent® HFA 220 µg and Azmacort® 200 µg MDIs after 6 h incubation, alongside % NFκB activity repression.

ICS	Aerosol Deposit [1] [µg]	Cellular ICS Mass at 6 h [2] [ng]	% Mass taken by the cells [3]	% Repression [4] of NFκB activity
FP	0.90	42.2 ± 24.7	5.6 ± 4.2	35.7 ± 6.3
	0.55	9.1 ± 22.2	4.7 ± 2.7	15.5 ± 2.2
TA	0.52	170.7 ± 40.6	32.6 ± 7.8	10.4 ± 2.6

[1] Data: mean: derived from Table 5.1

[2] (Cellular ICS mass) = (Aerosol deposit) – (ICS mass recovered from the Calu-3 cell surface at 6 h). Data: mean ± SD (n=3).

[3] (Cellular ICS mass)/ (Aerosol deposit) x 100. Data: mean ± SD (n=3).

[4] Data: mean±SD

5.4.4 TNFα-INDUCED NFκB ACTIVITY REPRESSION IN THE CALU-3 MONOLAYERS UPON ICS SOLUTION OR SUSPENSION APPLICATION

Figure 5.4 shows the fold-induction of the Luc activity representing the NFκB activity in the Calu-3 monolayers in response to 15 µg/mL FP solution and suspension application upon TNFα stimulation. Despite their preparation at the theoretical 15 µg/mL, these solution and suspension were shown to contain 11.2 and 0.4 µg/mL of dissolved FP from the filtrate analysis, respectively, and thus, considered to be 74.7 % solution and 97.3 % suspension. The 3.97-fold induction of the NFκB activity by TNFα was shown to be clearly repressed by these solution and suspension, yielding only 1.18±0.22 and 1.75±0.18 (n=4) of the fold-induction, respectively. These represented significant 94.0±17.8 % and 74.6±7.5 % repression ($p<0.05$, ANOVA) of the TNFα-induced NFκB activity and suggested that the solution application caused a greater

repression than the suspension counterpart, even though both were applied at the identical total FP concentration, 15 µg/mL.

Table 5.4 shows the FP mass and % taken by the Calu-3 cells in 6 h following 15 µg/mL solution and suspension application and incubation alongside % NFκB repression obtained above. The masses were calculated from the differences between the mass applied at the beginning of the experiment, and the mass recovered from the Calu-3 apical surface at 6 h. It was evident that for this 6 h incubation, much greater 8.0±0.7 and 0.7±0.2 µg of FP in the solution and suspension, respectively, were taken by the Calu-3 monolayers which represented 39.3 and 3.4 % of the total FP mass applied at the beginning of the study. It was clear that when suspension was applied, ~4 % was taken by the cells at 6 h, which was comparable to the uptake by cells following aerosol deposition (Table 5.3). Hence, FP appeared to suffer from extremely poor dissolution kinetics resulting in an inefficient repression of the NFκB activity. Nevertheless, 74.6 % repression of the NFκB activity was seen following suspension application, much greater than 35.7 % following aerosol deposition (Table 5.3), simply because of the larger FP uptake by the cells during the 6 h incubation (0.7 µg vs. 0.04 µg). In contrast, the solution application of FP was not affected by these protracted dissolution kinetics and resulted in a much higher % cellular uptake (39.3 %, Table 5.4) and a near complete (94 %) repression of the NFκB activity. Again, this was purely based on 8.0 µg taken by the cells for the 6 h incubation.

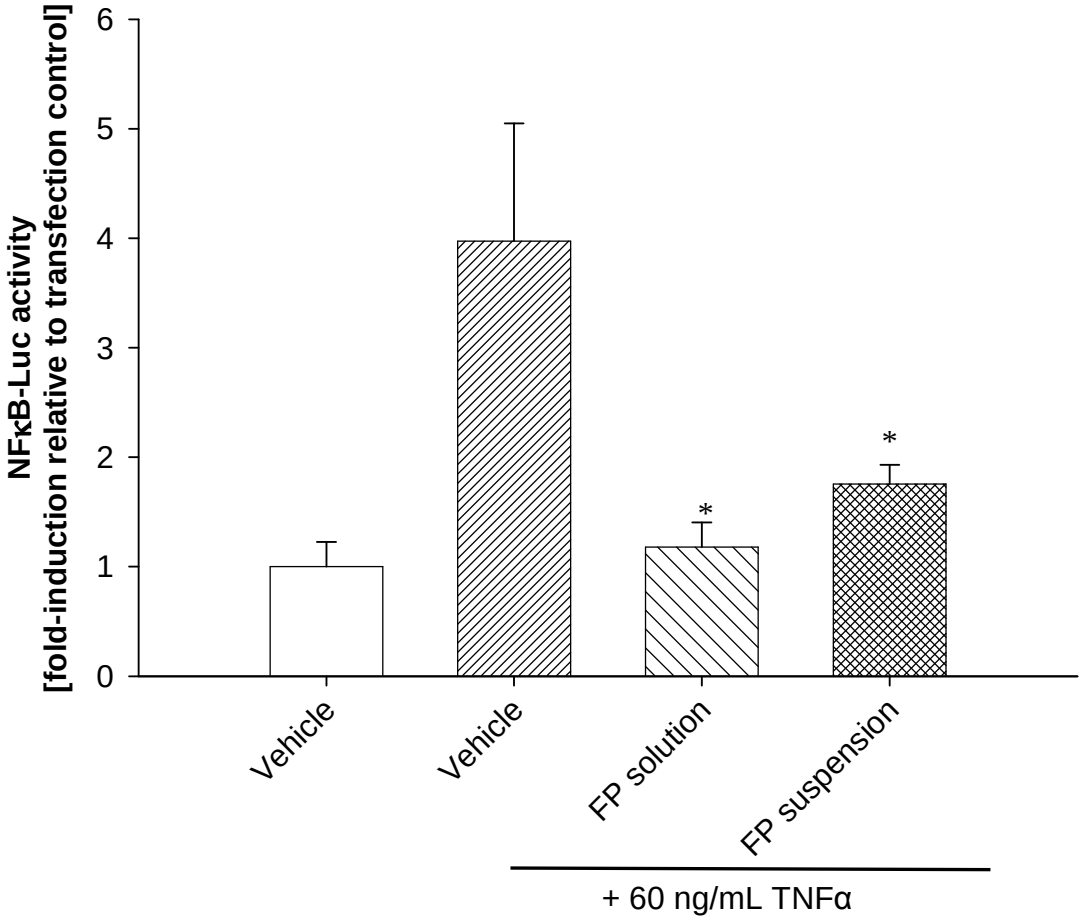

Figure 5.4 Fold-induction of the Luc activity representing the NFκB activity of the transfected Calu-3 monolayers in response to 15 µg/mL FP solution and suspension application, with 6 h stimulation of 60 ng/mL TNFα. Data represent mean±SD from n=10 for the control, n=11 for the TNFα stimulated group and n=4 for the FP tested groups. * indicates the significant decrease in the NFκB-Luc activity by the FP application compared to the TNFα stimulated group ($p<0.05$; ANOVA).

Table 5.4 FP mass and % taken up by the Calu-3 monolayers after 6 h following 15 µg/mL solution or suspension application and incubation, alongside % NFκB activity repression.

Solution/ Suspension	Applied Mass [1] [µg]	Cellular ICS Mass at 6 h [2] [µg]	% Mass taken by the cells [3]	% Repression [4] of NFκB activity
Solution	20.0	8.0 ± 0.7	39.3 ± 2.9	94.0
Suspension	21.7	0.7 ± 0.2	3.4 ± 0.9	74.6

[1] Data: mean: derived by analyzing the applied solution/suspension
[2] (Cellular FP mass) = (Applied Mass) – (FP mass recovered from the Calu-3 cell surface at 6 h). Data: mean ± SD (n=3).
[3] (Cellular FP mass)/ (Applied Mass) x 100. Data: mean ± SD (n=3).
[4] Data: mean: derived from Figure 5.4

5.5 DISCUSSION

The present study has successfully demonstrated that the Andersen cascade impactor (ACI) can be used to deposit ICS aerosol particles generated from commercial inhaler products on the Calu-3 cell monolayers in an accurate and precise manner. The monolayers were tolerant to such a deposition, evidenced by the intactness of the cell barrier and the maintenance of physiological properties. This gave the unique opportunity to deposit ICS aerosol particles on the semi-dry apical surface of these monolayers to study the cascade of events that occur upon aerosol deposition on the lung surface. Classically, such a cascade of events in pulmonary biopharmaceutics has employed only the active pharmaceutical ingredients (APIs) of the inhaler products, applied as solution on the cell surface, rather than the aerosols generated from the inhalers. This was not a true reflection of in vivo or clinical events, such that several attempts have quite recently been made with the Calu-3 monolayers placed inside an

impactor or impinger for direct aerosol deposition [Fiegel *et al*, 2003; Cooney *et al*, 2004]. Even so, these attempts, though being innovative, did not employ the aerosol generated from the inhaler products, and hence, were unable to demonstrate their usefulness for clarifying the cellular disposition and pharmacological events upon aerosol deposition.

The development of confluent Calu-3 monolayers expressing measurable NFκB-dependent luciferase as a biomarker for inflammation was truly challenging due to the resistance of confluent monolayers towards gene construct uptake and its retention. Recently, the efficiency of polyethylinimine in Calu-3 monolayer transfection was tested showing only 10^2 RLU/mg protein of the transfected gene expression without causing a significant cell death [Florea *et al*, 2002]. Such poor transfection efficiency was believed to be caused by the resistance offered by the mucin of the Calu-3 monolayers as well as by the differentiated nature of the monolayers. This resistance is effectively absent in transfection of the non-confluent cells. The resistance to transfection of the monolayers has also been reported for Caco-2 showing inefficient uptake of gene constructs as early as 3 days post-seeding attributed to certain biophysical processes occurring inside the cells [Uduehi *et al*, 1999]. To increase the efficiency of this transfection and hence, gene expression, the pretreatment of the Caco-2 monolayers with a chelating agent such as EGTA was shown to be successful [Artursson and Magnusson, 1990]. Its use was rationalized by providing a greater cellular access for the gene construct entry by creating temporary openings in their Ca^{2+}-dependent intercellular junctions [Artursson and Magnusson, 1990]. The EGTA

exposure appears to be time-dependent at a given concentration and less than 45 min with 2.5 mM EGTA resulted in a temporary Ca^{2+} deficit and thus, a reversible opening of the tight junctions without losing the cell viability. This was shown to increase the transfection efficiency by 5 times in the Caco-2 cell monolayers [Artursson *et al*, 1990]. Accordingly, this project with the Calu-3 monolayers similarly employed pretreatment with 2.5 mM EGTA for 15 min so that successful transfection with ~10^5 RLU/mg protein in the NFκB expression was achieved. Under this condition, 60 ng/mL of TNFα for 6 h further increased the NFκB expression by ~4 times in a relatively reproducible fashion in these transfected cells. It should be noted that this was the first success of the monolayer transfection of a gene construct sufficient enough to study either activation or repression of inflammation.

Using the newly developed dissolution testing system for ICS aerosols, in Chapter 3, the poorly soluble ICS FP showed considerably slow dissolution by 4 % of the aerosol deposits for 6 h. This prompted a question whether FP suffers from this dissolution problem, causing an inefficient anti-inflammatory response. This was now resolved and indeed, the anti-inflammatory response of the FP aerosols was shown to be compromised due to slow dissolution and thus, reduced intracellular uptake. This explained that the “intrinsic” potency of FP towards the NFκB repression reported to be 10-times higher than the readily soluble TA [Jafuel *et al*, 2000] upon a similar mass deposit at ~0.5 µg resulted in comparable anti-inflammatory effects. This effect of dissolution on the apparent anti-inflammatory effects in the Calu-3 monolayers was further substantiated when FP suspension and solution were applied to the transfected

monolayers at equal ICS mass. A compromised response in the NFκB repression was seen for the suspension, compared to that for the solution, attributed to less FP taken by the cells following suspension application.

It becomes clear that % NFκB repression correlated with FP mass taken by the cells. Hence, Figure 5.5 plots such % repression of TNFα-dependent NFκB activity as a function of FP mass taken into the Calu-3 cells following 6 h of incubation in all cases of FP aerosols, suspension and solution. It was clear that, as the FP mass taken by the cells increased, the % repression of the NFκB activity increased. In this context, Roumestan *et al*, 2003 employed non-confluent cultures of human alveolar continuous cell line, A549, and reported 0.1×10^{-12} M (50 ng/mL) of EC_{50} value for the NFκB repression. This data is practically less meaningful, since FP was applied as solution and its cellular uptake did not encounter resistance such as mucin and differentiated nature of confluent cell monolayers. The present study yielded 120 ng FP for 50 % repression of the NFκB activity (Figure 5.5) inside the cells. Therefore, it became apparent that the cell monolayers formed substantial barriers for FP internalization and moreover, its dissolution upon aerosol deposition further reduced the efficiency. By this even the local ICS exposure was considered to be irrelevant to correlate the anti-inflammatory response, but the ICS mass taken by the cells measurable in this monolayer-based assessment.

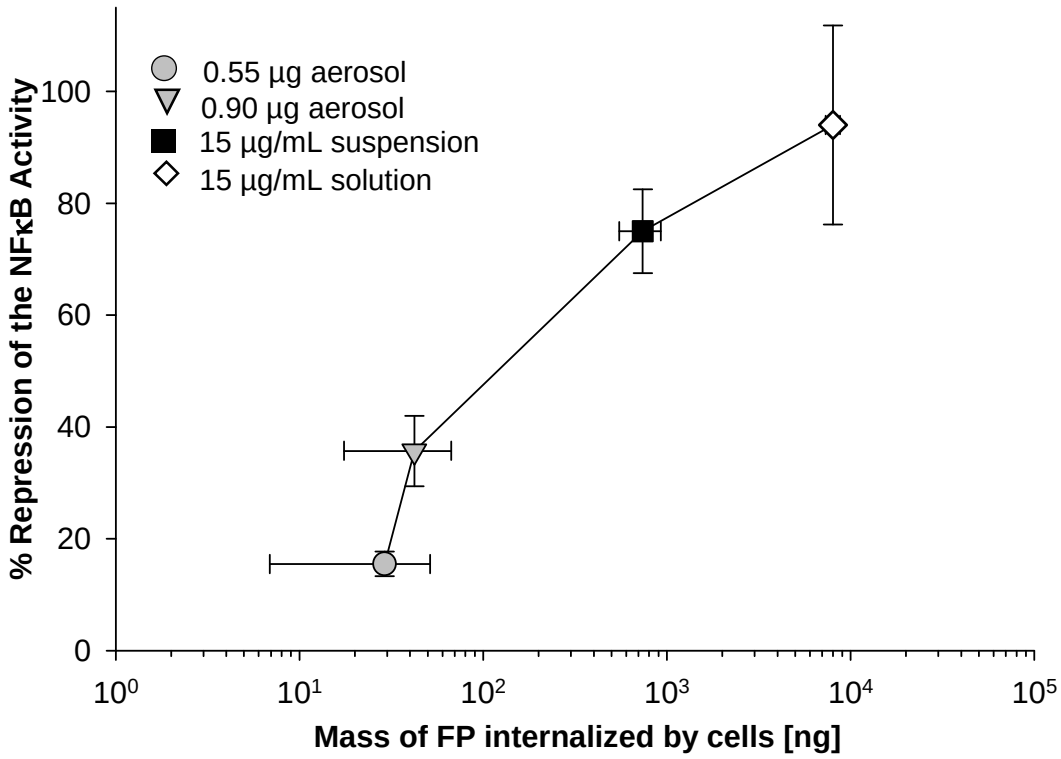

Figure 5.5 % repression of the TNFα-induced NFκB activity as a function of FP mass taken by the Calu-3 cells following 6 h of incubation upon FP aerosol, suspension and solution applications. Mass taken by the cells are taken from Tables 5.3 and 5.4. Data represent mean±SD (n=6 for % repression and n=3 for mass determination).

5.6 SUMMARY AND CONCLUSIONS

The air-interface cultured Calu-3 monolayers were placed inside the Andersen cascade impactor that enabled an accurate and precise deposition of defined-size ICS aerosols generated from commercially available inhaler products. These monolayers were transfected with the plasmid construct of NFκB-dependent luciferase (NFκB-Luc), so that sufficient expression of NFκB could be measured by the Luc activity that was induced by TNFα stimulation. The FP aerosols deposited on the semi-dry surface of the transfected Calu-3 monolayers repressed the NFκB activity in an apparently deposited mass-related fashion. However, despite a 10-times higher potency of FP than TA, their anti-inflammatory activities upon comparable mass deposits in the transfected Calu-3 cell monolayers seemed almost equivalent. This anti-inflammatory response was compromised for the FP aerosols, caused by their poor dissolution on the cell surface and lesser cellular uptake, compared to the more soluble but less potent TA. This finding was further corroborated from FP's near complete repression of the NFκB activity by 94 % upon solution application at 15 µg/mL, as opposed to only 74.6 % following suspension application. These findings suggested that FP's cellular uptake was dissolution rate-limited following aerosol deposition, thereby resulting in an inefficient response of its anti-inflammatory response. Most importantly, it was shown that regardless of dosage form or application the NFκB activity repression was primarily determined by not only the ICS's "intrinsic" molecular potency but also the intracellular mass taken by the cells.

In summary, a novel and innovative confluent “monolayer-based” system of Calu-3 was successfully developed and used to assess the ICS disposition kinetics and pharmacological actions upon aerosol deposition. Such a system will not only facilitate our understanding of pulmonary biopharmaceutics but also serve as a research aid to further study the kinetics and dynamics of inhaled therapeutics, in a setting that more closely resembles in vivo or clinical conditions.

CHAPTER 6

SUMMARY AND GENERAL CONCLUSIONS

In this dissertation, the kinetics of dissolution for aerosol particles of inhaled corticosteroids (ICSs) generated from inhaler products was determined and its importance on their local disposition and anti-inflammatory actions was assessed, using newly developed in vitro models allowing aerosol deposition. A novel in vitro dissolution testing system was developed to enable the determination of the kinetics of dissolution for ICS aerosol particles of defined-size in a limited volume of fluid like that in the lungs. Then, an in vitro lung epithelial cell monolayer system of Calu-3 cells was developed, again enabling defined-size ICS aerosol deposition, such that the importance of the dissolution kinetics on the ICS's cellular uptake and anti-inflammatory actions could be assessed. Using this system, lung cellular disposition of ICSs were systematically studied following a cascade of aerosol deposition, dissolution, cellular uptake and local pharmacological actions.

The novel dissolution profile testing system employed 5 ICSs, i.e., flunisolide (FL), triamcinolone acetonide (TA), budesonide (BD), fluticasone propionate (FP) and beclomethasone dipropionate (BDP) that differed in physicochemical properties (Table 3.1), following their collection from marketed inhalers on membrane filters placed inside the Andersen cascade impactor (ACI). This ACI deposition system enabled 0.7-19.8 µg of ICS aerosol mass to be collected reproducibly in 4.7-5.8 or 2.1-3.3 µm ranges of aerodynamic diameters with a relative standard deviation ≤ 23 % (Table 3.3). The incorporation of this filter with the ICS aerosol particles into a transwell with a limited 40 µL of stationary aqueous fluid on its donor side enabled dissolution and transwell membrane permeation of each drug to be studied. This closely represented ICS dissolution on the lung's mucosal surface in humans upon aerosol deposition from typical inhaled products. When 5 ICSs were compared at the most comparable mass deposit of ~2 (1.6-2.9) µg, the kinetics of dissolution differed substantially between the ICSs while conforming overall to the rank order of their aqueous solubilities (Figure 3.8). However, kinetics of dissolution sometimes differed from those expected based on solubility, as the profiles for the ICSs with similar solubility showed differences. For example, TA and BD with comparable aqueous solubility values of 21 and 16 µg/mL, respectively, showed significantly different dissolution profiles with apparent half-lives of 1.05±0.16 and 3.90±0.87 h, respectively. Similarly, FP and BDP studied with comparable mass deposits of ~2 µg, and despite similar aqueous solubility values of 0.14 and 0.13 µg/mL, respectively, showed substantially different dissolution and permeation in 10 h for <5 % and ~15 %, respectively. Moreover, this profile

interpretation and profile deduction became more complicated, as the profiles were shown to be dependent upon the aerosol size, mass deposit as well as formulation and dosage forms. Hence, it became clear that the ICS aerosol particles from inhalers should be tested for dissolution rather than the ICSs themselves. Of notable interest was the identification of exceptionally slow dissolution for the least soluble ICS, FP compared to the faster kinetics of the readily soluble ICS, TA. When compared at the same 2.4 µg of the deposited aerosol mass, FP showed only 3 % dissolution and permeation in 10 h, which was quite a contrast to 89 % seen in 5 h for TA (Figure 3.8). This finding raised a question whether FP would suffer from compromised local cellular anti-inflammatory activity due to these slow dissolution kinetics, despite reports of its 10-fold greater potency in "intrinsic" molecular activity towards anti-inflammation for FP compared to TA (Jafuel *et al*, 2000).

The air-interface cultured monolayers of a human bronchial epithelial cell line, Calu-3, was then developed to assess the anti-inflammatory activity of the ICS aerosols upon deposition. It was shown that Calu-3 formed well-differentiated monolayers yielding a sufficiently "tight" barrier with restrictive diffusion for a variety of solutes and ~1.5 k $\Omega \cdot cm^2$ of transepithelial electric resistance (TEER, Figure 4.2). Like the airway luminal surface, these monolayers exhibited cilia and intercellular junctions when observed under scanning electron microscope (Figure 4.3), while producing the limited (39.7±12.1 µL) of apical cell lining fluid. A variety of model solutes were tested to characterize their restrictive diffusive barrier nature in accordance with the diffusion

theory (Table 4.4). Notably such restrictive barrier formation was shown to be dependent upon the cell passage and culturing conditions and hence, the study concluded that the Calu-3 monolayers grown under the AIC in the 4.5 cm^2 transwells upon a seeding density of $0.1x10^6$ cells/cm^2 was the most suitable model by virtue of its restrictive diffusive barrier formation and semi-dry mucosal cell surface maintained with about 40 µL of apical lining fluid. This development of the in vitro lung cell monolayer system provided the opportunity to study aerosol particle dissolution, cellular uptake and pharmacological actions together, following drug deposition, a cascade of events that have only been studied previously in whole animals or humans.

The validated AIC Calu-3 monolayers were incorporated into a modified ACI assembly that enabled 0.55±0.02 and 0.90±0.03 µg of FP aerosol deposition and 0.52±0.03 µg of the TA aerosols (Table 5.1), generated from the respective inhaler products to be deposited. The monolayers tolerated the deposition conditions well, as evidenced by insignificant changes in TEER. For FP, deposition of 0.55 and 0.90 µg far exceeded the drug's solubility (0.14 µg/mL) assuming entire dissolution in ~40 µL of the Calu-3's cell lining fluid (13.8-22.5 µg/mL). In contrast, 0.52 µg of the TA aerosols could possibly be dissolved, given TA's solubility of 21 µg/mL. Accordingly, the significance of dissolution kinetics for these aerosol particles on cellular uptake and anti-inflammatory actions was assessed under the TNFα-induced inflammation in Calu-3 monolayers transfected with NFκB (a pro-inflammatory transcription factor) -dependent reporter plasmid of luciferase. Following exhaustive optimization of the

transfection protocol, the Calu-3 monolayers were shown to produce 3.97±1.07-fold induced NFκB activity (Table 5.2), representing cellular inflammation. FP and TA aerosol deposition in the modified ACI assembly on these transfected monolayers showed anti-inflammatory effects in varying magnitudes following 6 h incubation. Notably, a similar mass deposit of ~0.5 µg of both FP and TA aerosol particles resulted in 15.5 % and 10.4 % repression of the TNFα-induced NFκB activity despite FP's reported "intrinsic" molecular potency for anti-inflammation being 10 times greater than TA (Winkler *et al*, 2004). This apparently compromised anti-inflammatory response of FP aerosols corresponded well with only 4.7±2.7 % (29.1 ng) cellular uptake of the FP aerosols as opposed to 32.6±7.8 % (170 ng) for TA. This showed that the greater TA mass taken up by the cells compensated for its reported 10-fold lower intrinsic potency of the NFκB activity, compared to FP. Even so, the increased FP aerosols at 0.90 µg successfully repressed the NFκB activity by 35.7 %, which resulted from FP's slightly higher cellular uptake of 42.2 ng (Table 5.3). Taken together, the FP aerosols exerted the compromised anti-inflammatory activity, presumably due to exceptionally slow dissolution. This was further supported, when FP directly applied as solution at 15 µg/mL was shown to yield much higher 94 % repression of the NFκB activity, compared to 74.6 % for the suspension application at 15 µg/mL (Table 5.4). The cellular uptake after 6 h was 39 % and 3.4 % of the total mass applied, respectively, corresponding well to the increased response for this drug observed for the FP solution. Consequently, this also corroborated the notion that slow dissolution of FP aerosols and suspension reduced the cellular uptake and thus, compromised anti-inflammatory

response. In this context, the literature in this area has over-rated the local anti-inflammatory actions of ICSs due to the use of simple non-confluent cell-based assay systems, disregarding the cascade of events that occur upon aerosol deposition. Finally it was well-correlated that regardless of aerosol deposition or solution or suspension application, intracellular FP masses defined the magnitude of the anti-inflammation, e.g., NFκB repression seen with transfected Calu-3 monolayers. Through this project, it was emphasized that exposure of the drugs in the lung was still not sufficient to deduce clinical potencies of many ICSs. This lung “cell monolayer”-based assessment system coupled with aerosol deposition was shown to be an excellent research tool for systematically studying lung biopharmaceutics and pharmacology for inhaled therapeutics.

REFERENCES

REFERENCES

Adler KB, Holden-Stauffer, Repine JE. Oxygen metabolites stimulate release of high-molecular weight glycol-conjugates by cell and organ cultures of rodent-respiratory epithelium via an arachidonic acid-dependent mechanism. *J Clin Invest* 1990: 85:75-85

Amidon GL, Lennernas H, Shah VP, Crison JR. A theoretical basis for a biopharmaceutics drug classification system: the correlation of *in vitro* drug product dissolution and in vivo bioavailability. *Pharm Res* 1995; 12: 413-420.

Artursson P, Magnusson C. Epithelial transport of drugs in cell culture. II: effect of extracellular calcium concentration on the paracellular transport of drugs of different lipophilicities across monolayers of intestinal epithelial (Caco-2) cells. *J Pharm Sci* 1990; 79: 595-600.

Arya V, Coowanitwong I, Brugos B, Kim WS, Singh R, Hochhaus G. Pulmonary targeting of sustained release formulation of budesonide in neonatal rats. *J Drug Target* 2006; 14: 680-686.

Baldwin AS. The NF-kB and IkB proteins: new discoveries and insights. *Annu Rev Immunol* 1996; 14: 649-681.

Behrens I, Kissel T. Do cell culture condition influence the carrier-mediated transport of peptides in Caco-2 cell monolayers? *Eur J Pharm* Sci 2003; 19: 433-442.

Borchard G, Cassara ML, Roemele PEH, Florea BI, Junginger HE. Transport and local metabolism of budesonide and fluticasone propionate in a human bronchial epithelial cell line (Calu-3). *J Pharm Sci* 2002; 91:1561-1567.

Briske-Anderson MJ, Finley JW, Newman Sm. The influence of culture time and passage number on the morphological and physiological development of Caco-2 cells. *Proc Soc Exp Biol Med* 1997; 214: 248-257.

Byron PR, Katayama H, Sun Z, Rypacek F. Opportunities for protein delivery by aerosol. *Pol Prep* 1990; 31:167-168.

Byron PR, Phillips EM. Absorption, clearance and dissolution in the lung. In: Byron PR (Ed.), *Respiratory Drug Delivery*, CRC Press, Inc., Florida, 1990; 107-142.

Byron PR, Patton JS. Drug delivery via the respiratory tract. *J Aerosol Med* 1994; 71: 49-75.

Chowhan ZT, Amaro AA. Pulmonary absorption studies utilizing in situ rat lung model: designing dosage regimen for bronchial delivery of new drug entities. *J Pharm Sci* 1976; 65: 1669-1672.

Daley-Yates PT, Stone S, Allen A, Lambert J. Nasal absorption of fluticasone propionate: influence of formulation, dissolution and breath holding. *Respiratory Drug Delivery Europe 2007*, Davies Healthcare International Publishing, IL, 2007: 271-274.

Cheek JM, Evans MJ, Crandall ED. Type I cell-like morphology in tight alveolar epithelial monolayers. *Exp Cell Res* 1989; 184: 3753-3787.

Cooney D, Kazantseva M, Hickey AJ. Development of a size-dependent aerosol deposition model utilizing human airway epithelial cells for evaluating aerosol drug delivery. *ATLA* 2004; 32: 581-590.

Dalby RN, Byron PR. Formulations for delivery of beclomethasone diproprionate by metered dose inhalers containing no chlorofluorocarbon propellants. US Patent 5202110, April 1993.

Davies NM, Feddah MR. A novel method for assessing dissolution of aerosol inhaler products. *Int J Pharm* 2003; 255: 175-187.

Derendorf H, Nave R, Drollmann A, Cerasoli F, Wurst W. Relevance of pharmacokinetics and pharmacodynamics of inhaled corticosteroids to asthma**.** *Eur Respir J* 2006; 28:1042-50.

Dhand R. Aerosol delivery during mechanical ventilation: from basic techniques to new devices. *J Aerosol Med Pulm Drug Deliv* 2008; 21:45-60.

Gonda I. Aerosols for delivery of therapeutic and diagnostic agents to the respiratory tract. *Crit Rev Ther Drug Carrier Syst* 1990; 6:273-313.

Dobbs LG. Isolation and culture of alveolar Type II cells. Am J Physiol 1990; 258: L134-L147.

Düchler M, Pengg M, Brunner S, Müller M, Brem G, Wagner E. Transfection of epithelial cells is enhanced by combined treatment with mannitol and polyethyleneglycol. *J Gene Med.* 2001; 2:115-24.

Edsbäcker S, Johansson CJ. Airway selectivity: an update of pharmacokinetic factors affecting local and systemic disposition of inhaled corticosteroids. *Basic Clin Pharmacol Toxicol* 2006; 98: 523-536.

Edsbäcker S, Wollmer P, Selroos O, Borgström L, Olsson B, Ingelf J. Do airway clearance mechanisms influence the local and systemic effects of inhaled corticosteroids?*Pulm Pharmacol Ther* 2008; 21:247-58.

Effectene® Transfection Reagent Handbook. Qiagen, May 2002. Available for download at www.qiagen.com.

Ehrhardt C, Fiegel J, Hanes J, Lehr CM. Drug Absorption by the Respiratory Mucosa: Cell Culture Models and Particulate Drug Carriers. *J Aerosol Med* 2002; 15: 131-139.

Ehrhardt C, Kneuer C, Fiegel J, Lehr CM. Influence of apical fluid volume on the development of functional intercellular junctions in the human epithelial cell line 16HBE14o-: implications for the use of this cell line as an *in vitro* model for bronchial drug absorption studies. *Cell Tissue Res* 2002; 308: 391-400. .

Eight stage non-viable impactor, series 20-800, instructions manual, Thermo Electron Corporation, MA. Available for download at www.thermo.com.

Eissa NT, Huston DP. Therapeutic targets in airway inflammation. Marcel Dekker Inc., New York, NY, 2003.

Elbert KJ, Schafer UF, Schafers HJ, Lehr CM. Monolayers of human alveolar epithelial cells in primary culture for pulmonary absorption studies. *Pharm Res* 1999; 16: 601-608.

Electronic Orange Book, Approved Drug Products with Therapeutic Equivalence Evaluations. http://www.fda.gov/cder/ob/default.htm.

Fang X, Song Y, Zemans R, Matthay MA. Fluid transport across cultured rat alveolar epithelial cells: a novel *in vitro* system. *Am J Physiol Lung Cell Mol Physiol* 2004; 27: L104-L110.

Food and Drug Administration. Guidance for industry: waiver of in vivo bioavailability and bioequivalence studies for immediate-release solid oral dosage forms based on a

biopharmaceutics classification system. Food and Drug Administration, Rockville, MD, 2000, Available at http://www.fda.gov/cder/guidance/index.htm.

Food and Drug Administration. Guidance for industry: Metered dose inhaler (MDI) and dry powder inhaler (DPI) drug products chemistry, manufacturing, and controls documentation. Food and Drug Administration, Rockville, MD, 1998, Available at http://www.fda.gov/cder/guidance/2180dft.htm.

Forbes B. Human airway epithelial cells for in vitro drug transport and metabolism studies. *Pharm Sci Technol Today* 2000. 3:18-27

Fiegel J, Ehrhardt C, Schaefer UF, Lehr CM, Hanes J. Large porous particle impingement on lung epithelial cell monolayers – toward improved particle characterization in the lung. *Pharm Res* 2003; 20:788-796.

Florea BI, Meaney C, Junginger HE, Borchard G. Transfection efficiency and toxicity of polyethylenimine in differentiated Calu-3 and nondifferentiated COS-1 cell cultures. *AAPS PharmSci* 2002; 4:E12.

Forbes B, Ehrhardt C. Human respiratory epithelial cell culture for drug delivery applications. *Eur J Pharm Biopharm* 2004; 60: 193-205.

Forbes B. Human airway epithelial cell lines for *in vitro* drug transport and metabolism studies. *Pharm Sci Techno Today* 2000; 3: 18-27.

Freiwald M, Valotis A, Kirschbaum A, McClellan M, Mürdter T, Fritz P, Friedel G, Thomas M, Högger P. Monitoring the initial pulmonary absorption of two different beclomethasone dipropionate aerosols employing a human lung reperfusion model. *Respir Res* 2005; 6: 21.

Fylstra D, Lasdon L, Watson J, Warren A. Design and use of Microsoft Excel Solver. *Interface* 1998; 28: 29-55.

Geys J, Nemery B, Hoet PH. Optimization of culture conditions to develop an in vitro pulmonary permeability model. *Toxicol In Vitro* 2007; 21:1215-1219.

Gonzåles-Mariscal L. Biosynthesis of the tight junctions. In: Cereijido M. (Ed.), *Tight Junctions,* CRC Press, Inc., Florida, 1992, 243-255.

Gonzalez-Rothi RJ, Suarez S, Hochhaus G, Schreier H, Lukyanov A, Deredorf H, Costa TD. Pulmonary targeting of liposomal triamcinolone acetonide phosphate. *Pharm Res* 1996; 13: 1699-1703.

Grainger CI, Greenwell LL, Forbes B. Culture of Calu-3 cells at the air interface provides a representative model of the airway epithelial barrier. *Pharm Res* 2006; 23: 1482-90.

Grainger CI, Greenwell LL, Lockley DJ, Forbes B. The evaluation of an *in vitro* depositional system using airway epithelial cells for the permeability of inertially impacted aerosols. *Respiratory Drug Delivery X*, Davies Healthcare International Publishing, IL, 2006: 647-649.

Gray VA, Hickey AJ, Balmer P, Davies NM, Dunbar C, Foster TS, Olsson BL, Sakagami M, Shah VP, Smurtwaite MJ, Veranth JM, Zaidi K. The inhalation ad hoc advisory panel for the USP performance tests of inhalation dosage forms. *Pharmacop Forum* 2008; 34: 1068-1074.

Guidance for Industry, Waiver of In Vivo Bioavailability and Bioequivalence studies for Immediate Release Solid Oral Dosage Forms based on a Biopharmaceutics Classification System, Food and Drug Administration, Rockville, MD, 2000, Available at http://www.fda.gov/cder/guidance/index.htm.

Guidance for Industry, Dissolution Testing of Immediate Release Solid Oral Dosage Forms, August 1997, FDA/CDER.

Hastings RH, Grady M, Sakuma T, Matthay MA. Clearance of different-sized proteins from the alveolar space in humans and rabbits. *J Appl Physiol* 1992; 73: 1310-1316.

Hickey AJ. Inhalation aerosols: physical and biological basis for therapy. Marcel Dekker, Inc., New York, NY, 1996.

Hochhaus G, Möllmann H, Derendorf H, Gonzales-Rothi RJ. Pharmacokinetic/pharmacodynamic aspects of aerosol therapy using glucocorticoids as a model. *J Clin Pharmacol* 1997; 37: 881-892.

Hochhaus G. New developments in corticosteroids. *Proc Am Thorac Soc* 2004; 1: 269-274.

Hogger P, Rohdewald P. Dissolution, tissue binding and kinetics of receptor binding of inhaled glucocorticoids. *Glucocorticoid Therapy Eur Respir J* 1993; 6 (Suppl 17): 584 s.

Hosoya O, Chono S, Saso K, Juni K, Morimoto K, Seki T. Determination of diffusion coefficients of peptides and prediction of permeability through a porous membrane. *J Pharm Pharmacol* 2004; 56: 1501-1507.

Jafuel D, Demoly P, Bousquet J, Mathieu M. Transcriptional potencies of inhaled glucocorticoids. *Am J Respir Crit Care Med* 2000; 162: 57-63.

Johnson LG, Dickman KG, Moore KL, Mandel LJ, Boucher RC. Enhance Na^+ transport in an air-interface culture system. *Am J Physiol* 1993; 264: L560-L565.

Kibbe M. Pharmaceutical excipients, 3rd Edition, 2000. American Pharmcaeutical Association and Pharmaceutical Press.

Knowles M, Marray G, Shallal J, Askin F, Ranga V, Gatzy J, Boucher R. Bioelectric properties and ion flow across excised human bronchi. *J App Physiol* 1984; 56: 868-877.

Krishnaswamy S, Möllmann H, Derendorf H, Hochhaus G. A sensitive LC-MS/MS method for the quantification of fluticasone propionate in human plasma. *J Pharm Biomen Anal* 2000; 22: 123-129.

Kumar VV, Singh RS, Chaudhuri A. Cationic transfection lipids in gene therapy: successes, set-backs, challenges and promises. *Curr Med Chem* 2003; 10: 1297-1306.

Leach CL, Davidson PJ, Hasselquist BE, Boudreau RJ.Lung deposition of hydrofluoroalkane-134a beclomethasone is greater than that of chlorofluorocarbon fluticasone and chlorofluorocarbon beclomethasone : a cross-over study in healthy volunteers. *Chest* 2002; 122:510-6.

Lee YJ, Chung SJ, Shim CK. Limited role of P-glycoprotein in the intestinal absorption of cyclosporine A. *Biol Pharm Bull* 2005; 28: 760-763.

Li L, Mathias NR, Heran CL, Moench P, Wall DA, Smith RL. Carbopol-mediated paracellular transport enhancement in Calu-3 cell layers. *J Pharm Sci* 2006; 95: 326-335.

Martin A, Bustamante P (Ed.). Physical Pharmacy. Lippincot Williams and Wilkins, Maryland, 4th Edition, 1993; 330-334.

Martin A, Bustamante P (Ed.). Physical Pharmacy. Lippincot Williams and Wilkins, Maryland, 4th Edition, 1993; 400-401.

Mathias NR, Timoszyk J, Smith RL, Wall DA. Permeability characteristics of Calu-3 human bronchial epithelial cells: *in vitro- in vivo* correlation to predict lung absorption in rats. *J Drug Target* 2002; 10:31-40.

Meaney C, Florea BI, Ehrhardt C, Schaefer UF, Lehr CM, Junginger HE, Borchard G. Bronchial epithelial cell cultures, in: Lehr CM (Ed.), Cell Culture Models of Biological Barriers, Taylor and Francis, London, 2002, 211-227.

Mercer RR, Russel ML, Roggli VL, Crapo JD. Cell number and distribution in human and rat airways. *Am J Respir Cell Mol Bio* 1994; 10:613-624.

Pang Y. Kinetics and mechanisms of insulin disposition in the isolated perfused rat lung. Ph.D. dissertation, Virginia Commonwealth University, 2004.

Patton JS, Byron PR. Inhaling medicines: delivering drugs to the body through the lungs. *Nat Rev Drug Discov* 2007; 6:67-74.

Patton JS. Mechanisms of macromolecular absorption by the lungs. *Adv Drug Deliv Rev* 1996; 19: 3-36.

Product Information Sheet for ATCC Catalog Number HTB-55. Available for download at www.atcc.org .

Renkin ME. Filtration, diffusion, and molecular sieving through porous cellulose membranes. *J Gen Phys* 1954; 38: 225-43.

Rennard SI, Basset G Lecossier D, O'Donnell KM, Pinkston P, Martin PG, Crystal RG. Estimation of volume of epithelial lining fluid recovered by lavage using urea as marker of dilution. *J Appl Physiol* 1986; 60: 532-538.

Roumestan C, Henriquet C, Mathieu M. Fluticasone propionate and mometasone furoate have equivalent transcriptional potencies. *Clin Exp Allergy* 2003; 33: 895-901.

Sakagami M. Kinetics and mechanisms of macromolecular disposition in the rat lung. Ph.D. dissertation, Virginia Commonwealth University, 2000.

Sakagami M, Kinoshita W, Sakon K, Makino Y. Mucoadhesive beclomethasone microspheres for powder inhalation; their pharmacokinetics and pharmacodynamics evaluation. *J Control Release* 2002; 80: 207-218.

Sakagami M, Byron PR. Respirable microspheres for inhalation: the potential of manipulating pulmonary disposition for improved therapeutic efficacy. *Clin Pharmacokinet* 2005; 44: 263-267.

Sakagami M. In vivo, *in vitro* and ex vivo models to assess pulmonary absorption and disposition of inhaled therapeutics for systemic delivery. *Adv Drug Deliv Rev* 2006; 58: 1030-1060.

Sambuy Y, Angelis ID, Ranaldi G, Scarino ML, Stammati A, Zucco F. The Caco-2 cell line as a model of the intestinal barrier: influence of cell and culture-related factors on Caco-2 cell functional characteristics. *Cell Bio and Toxicol* 2005; 21:1-26.

Schleimer RP, O'Byrne PM, Szefler SJ, Brattsand R. Inhaled steroids in asthma: optimizing effects in the airways. Marcel Dekker, Inc., New York, NY, 2002.

Seki T, Mochida J, Okamota M, Morimoto K. Measurement of diffusion coefficients of parabens and steroids in water and 1-octanol. *Chem Pharm Bull* 2003a; 51: 34-736.

Smith BT. Cell line A549: a model system for the study of alveolar type II cell function. *Am Rev Respir Di* 1977; 115: 285-93.

Sun JZ. Pulmonary absorption of fluorophore-labeled polyaspartamides from the airways of the isolated perfused rat lung. Ph.D. dissertation, Virginia Commonwealth University, 1995.

Tanguay FJ, Sun J, Adjei A. A reproducible, sensitive, single spray quantitation method for triamcinolone acetonide pressurized metered dose inhaler (pMDI) using the breath coordinated inhaler (BCI). *Respiratory Drug Delivery VII*, Davies Healthcare International Publishing, IL, 2000: 319-322.

Taylor MK, Hickey AJ, Van Oort M. Manufacture, characterization and pharmacodynamic evaluation of engineered ipratropium bromide particles. *Pharm Dev Technol* 2006; 11: 321-336.

Trehin R, Krauss U, Beck-Sickinger AG, Merkle HP, Nielsen HM. Cellular uptake but low permeation of human calcitonin-derived cell penetrating peptides and Tat(47-57) through well-differentiated epithelial models. *Pharm Res* 2004; 21: 1248-1256.

Uduehi AN, Moss SH, Nuttall J, Pouton CW. Cationic lipid-mediated transfection of differentiated Caco-2 cells: a filter culture model of gene delivery to a polarized epithelium. *Pharm Res* 1999; 16: 1805-11.

United States Pharmacopoeia, USP 26, NF 21. Chapter <601> Aerosols, metered dose inhalers, and dry powder inhalers. USP Convention Inc., Rockville, MD; 2003: 2105-2123.

United States Pharmacopoeia, USP 26, NF 21. Chapter <711> Dissolution. USP Convention Inc., Rockville, MD; 2003: 2155-2165.

Usmani OS, Ito K, Maneechotesuwan K, Ito M, Johnson M, Barnes PJ, Adcock IM. Glucocorticoid receptor nuclear translocation in airway cells after inhaled combination therapy. *Am J Respir Crit Care Med* 2005; 172:704-12.

Wang Z, Zhang Q. Transport of proteins and peptides across human cultured alveolar A549 cell monolayer. *Int J Pharm* 2004; 269: 451-6.

Widdicombe JG. Airway liquid: a barrier to drug diffusion? *Eur Respir J* 1997; 10: 2194-2197.

Winkler J, Hochhaus G, Derendorf H. How the lung handles drugs: pharmacokinetics and pharmacodynamics of inhaled corticosteroids. *Proc Am Thorac Soc* 2004; 1: 356-363.

Wurster DE, Taylor PW Jr. Dissolution kinetics of certain crystalline forms of prednisolone. *J Pharm Sci* 1965; 54: 670-676.

Yang TZ, Mustafa F, Bai SH, Ahsan F. Pulmonary delivery of low molecular weight heparins. *Pharm Res* 2004; 21: 2009-2016.

Yazdanian M, Briggs K, Hawi A. The High Solubility Definition of the Current FDA Guidance on the Biopharmaceutical Classification System may be too Strict for Acidic Drugs. *Pharm Res* 2004; 21: 293-299.

Yu H, Cook TJ, Sinko PJ**.** Evidence for diminished functional expression of intestinal transporters in Caco-2 cell monolayers at high passages. *Pharm Res* 1997; 14: 757-762.

APPENDIX A1

CALU-3 CELL CULTURE: STANDARD OPERATING PROCEDURES

This Calu-3 cell culture was established and validated by our laboratory to ensure a continuous supply of the cells for the use as an air-interface cultured Calu-3 monolayer system. The confluent Calu-3 cell monolayers grown under this air-interface culture formed a tight barrier to diffusion, while their apical (mucosal) surface remained semi-dry with a limited ~40 µL of lining fluid; as shown in Chapter 4.

Accordingly, this dissertation project employed the air-interface cultured Calu-3 monolayers to study the importance of dissolution for certain inhaled corticosteroid (ICSs) aerosols on their surfaces on their cellular uptake and local pharmacological actions. Overall, operating procedure of the Calu-3 cell culture has been of this adapted from the recommendations by the American Type Culture Collection (ATCC, Rockville, MD).

A.1.1 CALU-3 CELL PROPAGATION

Calu-3 cells (Passage 29-36) were received as frozen cells from ATCC. These were slowly defrosted to 37 °C. The cell suspension (e.g., 1 x 10^6 cells in 1 mL) was transferred into a 50 mL centrifuge tube, and 8 mL of the culture media, Eagles Minimum Essential Medium (EMEM; ATCC, Rockville, MD; Table A.1) supplemented with 10% (v/v) fetal bovine serum (FBS; Invitrogen, Carlsbad, CA) and 1% (v/v) penicillin-streptomycin (PS; Sigma-Aldrich; St. Louis, MO) was added in a drop-wise fashion; this was to avoid cell damage due to drastic temperature and osmotic pressure alterations. The cell suspension (i.e., 9 mL) was centrifuged at 120 x g for 6 min at room temperature (25 ºC) and the supernatant containing the cryo-preservative agents was discarded. The cells were re-suspended with the pipetter with 10 mL of the culture media and seeded into 25 cm^2 culture flask (Corning Costar; Cambridge, MA). The flasks were maintained under the humidified 95% (v/v) air and 5% (v/v) CO_2 at 37 °C in the incubator (Model 5410, NAPCO; Milliville, NJ) connected to a CO_2 gas cylinder (National Welders; Richmond, VA). The culture media was changed every other day, during which the cell growth was monitored under the microscope (Nikon-TMS phase contrast microscope, Image Systems Inc.; Columbia, MD). Typically, the cells reached the confluence by 5-7 days, such that they were passaged or frozen for the cell bank storage following trypsin-EDTA (Sigma-Aldrich) treatment, as described below.

Table A.1.1 Composition of Eagles Minimum Essential Medium used for Calu-3 cell culture.

Organic Salts	Concentration (g/L)
$CaCl_2$ (anhydrous)	0.20000
$MgSO_4$ (anhydrous)	0.09767
KCl	0.40000
$NaHCO_3$	1.50000
NaCl	6.80000
$NaH_2PO_4 \cdot H_2O$	0.14000

Amino Acids	Concentration (g/L)
L-Alanine	0.00890
L-Arginine·HCl	0.12640
L-Asparagine·H_2O	0.01500
L-Aspartic Acid	0.01330
L-Cystine·2HCl	0.03120
L-Glutamic Acid	0.01470
Glycine	0.00750
L-Histidine·HCl·H_2O	0.04190
L-Isolecine	0.05250
L-Leucine	0.05250
L-Lysine·HCl	0.07250
L-Methionine	0.01500
L-Phenylalanine	0.03250
L-Proline	0.01150
L-Serine	0.01050
L-Threonine	0.04760
L-Tryptophan	0.01000
L-Tyrosine·2Na·2H_2O	0.05190
L-Valine	0.04680

Vitamins	Concentration (g/L)
Choline Chloride	0.00100
Folic Acid	0.00100
myo-Inositol	0.00200
Nicotinamide	0.00100
D-Pantothenic Acid (hemicalcium)	0.00100
Pyridoxine·HCl	0.00100
Riboflavin	0.00010
Thiamine·HCl	0.00100

Others	Concentration (g/L)
D-Glucose	1.00000
Phenol Red, Na salt	0.01000
Sodium Pyruvate	0.11000

The culture flasks were subcultured every 5-7 days following visual confirmation of 70-80 % confluence. The culture medium was removed from the flask, and the cells were washed with pre-warmed phosphate-buffered saline (37 °C). Subsequently, 2 mL of pre-warmed (37 °C) trypsin-EDTA (Sigma, St. Louis, MO) was applied to the cells for the 25 cm^2 flask, and the flask was gently rocked for 30 s. The cells were incubated with trypsin-EDTA solution in the incubator for 5-10 min at 37 °C. Progress of trypsinization was periodically checked under the microscope, while the anchored cells were dislodged by banging the flask. Once the cells were detached from the flask, 5 mL of the EMEM containing 10 % FBS and 1 % PS was added for trypsin neutralization. At this point, the cells were homogeneously suspended and therefore, 20 μL sample was taken for cell counting using the Neubauer hemocytometer (Fisher Scientific, Atlanta, GA). The rest of the cell suspension was centrifuged at 120 x g for 6 min at room temperature. Following the cell yield determination, the cells were seeded at a density of $1x10^5$ cells/cm^2 into a new 25 or 75 cm^2 along with 8 or 24 mL of the culture media as a newly passaged culture flask. Typically, the cells were split into 1:2 to 1:3 at each passage.

A.1.2 CALU-3 CELL BANKING

Periodically, the cells were transferred into a frozen stock to avoid wasteful passage and to ensure a constant supply of cells in the laboratory. For this, two types of the media were prepared; a freezing media was EMEM supplemented with 10 % (v/v)

FBS and 5 % (v/v) dimethyl sulfoxide (DMSO, ATCC) while the process media was EMEM supplemented with 10 % FBS (v/v) only. Cryotubes (Fisher-Scientific) were appropriately labeled with cell line name, passage, concentration, date and operator. The Calu-3 cells were trypsinized, as described above, however, recovered in the freezing media. For cell banking, 1 mL of the cell suspension at $1x10^6$ cells/mL was aliquoted to each cryotube (Fisher-Scientific). The cryotubes were then embedded in cotton wool and placed in a polystyrene freezing box (Fisher-Scientific). The freezing box was sealed with tape and placed at -80 °C for 2-4 h; this allowed the cells to cool down slowly and gradually. The cryotubes were then transferred in the liquid nitrogen storage.

APPENDIX A2

ORIGINAL DATASHEETS

TABLE OF CONTENTS:

- Table A.2.5: Cumulative mass and mass fraction dissolved and permeated into the receptor compartment as a function of time for FL aerosols collected on Stage 4 following 5 shots of Aerobid® MDI.
- Table A.2.6: Cumulative mass and mass fraction dissolved and permeated into the receptor compartment as a function of time for FL aerosols collected on Stage 4 following 10 shots of Aerobid® MDI.
- Table A.2.7: Cumulative mass and mass fraction dissolved and permeated into the receptor compartment as a function of time for TA aerosols collected on Stage 2 following single shot of Azmacort® MDI.
- Table A.2.8: Cumulative mass and mass fraction dissolved and permeated into the receptor compartment as a function of time for TA aerosols collected on Stage 2 following 5 shots of Azmacort ® MDI.
- Table A.2.9: Cumulative mass and mass fraction dissolved and permeated into the receptor compartment as a function of time for TA aerosols collected on Stage 2 following 10 shots of Azmacort ® MDI.
- Table A.2.10: Cumulative mass and mass fraction dissolved and permeated into the receptor compartment as a function of time for TA aerosols collected on Stage 4 following single shot of Azmacort ® MDI.
- Table A.2.11: Cumulative mass and mass fraction dissolved and permeated into the receptor compartment as a function of time for TA aerosols collected on Stage 4 following 5 shots of Azmacort ® MDI.

- Table A.2.24: Cumulative mass and mass fraction dissolved and permeated into the receptor compartment as a function of time for BDP aerosols collected on Stage 2 following 14 shots of Qvar ® MDI.
- Table A.2.25: Cumulative mass and mass fraction dissolved and permeated into the receptor compartment as a function of time for BDP aerosols collected on Stage 4 following 14 shots of Qvar ® MDI.
- Table A.2.26: Cumulative mass and mass fraction dissolved and permeated into the receptor compartment as a function of time for BDP aerosols collected on Stage 2 following 7 shots of Vanceril ® MDI.
- Table A.2.27: Cumulative mass and mass fraction dissolved and permeated into the receptor compartment as a function of time for BDP aerosols collected on Stage 4 following 7 shots of Vanceril ® MDI.

- **Chapter 4**
  - Table A.2.28: Cumulative FNa mass permeated across air-interface cultured Calu-3 monolayers grown in 1.13 cm^2 transwells at a seeding density of $0.1x10^6$ cells/cm^2.
  - Table A.2.29: Cumulative FNa mass permeated across air-interface cultured Calu-3 monolayers grown in 1.13 cm^2 transwells at a seeding density of $0.5x10^6$ cells/cm^2.
  - Table A.2.30: Cumulative FNa mass permeated across air-interface cultured Calu-3 monolayers grown in 4.5 cm^2 transwells at a seeding density of $0.1x10^6$ cells/cm^2.

- Table A.2.31: Cumulative FD-10 mass permeated across air-interface cultured Calu-3 monolayers grown in 4.5 cm^2 transwells at a seeding density of $0.1x10^6$ cells/cm^2.
- Table A.2.32: Cumulative FD-70 mass permeated across air-interface cultured Calu-3 monolayers grown in 4.5 cm^2 transwells at a seeding density of $0.1x10^6$ cells/cm^2.
- Table A.2.33: Cumulative FD-150 mass permeated across air-interface cultured Calu-3 monolayers grown in 4.5 cm^2 transwells at a seeding density of $0.1x10^6$ cells/cm^2.

- **Chapter 5**
  - Table A.2.34: Data sheets to obtain fold-induction of NFκB-activity with or without 60 ng/mLTNFα incubation for 6 h.
  - Table A.2.35: Data sheets to obtain fold-induction of NFκB-activity with 60 ng/mLTNFα and various ICS treatment (aerosol, solution or suspension) incubation for 6 h.
  - Table A.2.36: Mass balance to calculate the cellular uptake of ICSs by Calu-3 cells following various treatment incubations at the start (t=0 h) and at the end (t=6 h) of the experiment.

Table A.2.1 Cumulative mass and mass fraction dissolved and permeated into the receptor compartment as a function of time for FL aerosols collected on Stage 2 following single shot of Aerobid® MDI.

Inhaler	Aerobid					
Shots/Actuations	1					
Stage	2					
ICS	Flunisolide (FL)					
FL mass permeated (µg)	#1	#2	#3			
Time (min)						
15	0.18	0.13	0.15			
30	0.22	0.27	0.28			
45	0.27	0.35	0.35			
60	0.32	0.38	0.41			
90	0.39	0.49	0.52			
120	0.45	0.51	0.55			
150	0.48	0.57	0.57			
180	0.51	0.61	0.60			
240	0.53	0.64	0.64			
300	0.57	0.66	0.66			
Mass remaining on filter (R)	0.04	0.05	0.04	Mean ± SD	RSD	
Sum (P+R)	0.61	0.71	0.70	0.68 ± 0.05	7.35	
Fraction FL permeated	#1	#2	#3	Mean	SD	SE
Time (min)						
15	0.29	0.18	0.22	0.23	0.06	0.03
30	0.36	0.37	0.40	0.38	0.02	0.01
45	0.44	0.49	0.51	0.48	0.03	0.02
60	0.51	0.53	0.59	0.55	0.04	0.02
90	0.63	0.68	0.74	0.69	0.06	0.03
120	0.73	0.71	0.79	0.74	0.04	0.03
150	0.78	0.80	0.82	0.80	0.02	0.01
180	0.83	0.85	0.86	0.85	0.02	0.01
240	0.86	0.90	0.92	0.89	0.03	0.02
300	0.93	0.93	0.94	0.94	0.01	0.00

Table A.2.2 Cumulative mass and mass fraction dissolved and permeated into the receptor compartment as a function of time for FL aerosols collected on Stage 2 following 5 shots of Aerobid® MDI.

Inhaler	Aerobid					
Shots/Actuations	5					
Stage	2					
ICS	Flunisolide (FL)					
FL mass permeated (µg)	#1	#2	#3			
Time (min)						
15	1.91	1.30	1.17			
30	3.47	2.25	2.40			
45	4.11	3.03	2.75			
60	5.31	3.24	3.18			
90	5.80	4.13	4.16			
120	6.31	4.49	4.31			
150	6.60	4.79	4.85			
180	6.61	4.92	5.04			
240	6.92	5.24	5.23			
300	7.06	5.26	5.33			
Mass remaining on filter (R)	0.37	0.35	0.36	Mean ± SD	RSD	
Sum (P+R)	7.43	5.61	5.69	6.24 ± 1.03	16.51	
Fraction FL permeated	#1	#2	#3	Mean	SD	SE
Time (min)						
15	0.26	0.23	0.20	0.23	0.03	0.02
30	0.47	0.40	0.42	0.43	0.03	0.02
45	0.55	0.54	0.48	0.53	0.04	0.02
60	0.71	0.58	0.56	0.62	0.08	0.05
90	0.78	0.74	0.73	0.75	0.03	0.02
120	0.85	0.80	0.76	0.80	0.05	0.03
150	0.89	0.85	0.85	0.86	0.02	0.01
180	0.89	0.88	0.89	0.88	0.01	0.00
240	0.93	0.93	0.92	0.93	0.01	0.00
300	0.95	0.94	0.94	0.94	0.01	0.00

Table A.2.3 Cumulative mass and mass fraction dissolved and permeated into the receptor compartment as a function of time for FL aerosols collected on Stage 2 following 10 shots of Aerobid® MDI.

Inhaler	Aerobid					
Shots/Actuations	10					
Stage	2					
ICS	Flunisolide (FL)					
FL mass permeated (µg)	#1	#2	#3			
Time (min)						
15	1.32	3.29	0.99			
30	3.82	4.56	2.20			
45	5.04	5.28	3.26			
60	6.99	5.88	3.50			
90	8.00	7.22	4.75			
120	8.80	7.56	5.48			
150	9.16	7.81	5.90			
180	9.63	7.86	6.13			
240	10.06	8.18	6.73			
300	10.24	8.25	6.94			
Mass remaining on filter (R)	0.76	0.41	0.68	Mean ± SD		
Sum (P+R)	11.00	8.66	7.62	9.09 ± 1.73	19.03	
Fraction FL permeated	#1	#2	#3	Mean	SD	SE
Time (min)						
15	0.12	0.38	0.13	0.21	0.15	0.08
30	0.35	0.53	0.29	0.39	0.12	0.07
45	0.46	0.61	0.43	0.50	0.10	0.06
60	0.64	0.68	0.46	0.59	0.12	0.07
90	0.73	0.83	0.62	0.73	0.11	0.06
120	0.80	0.87	0.72	0.80	0.08	0.04
150	0.83	0.90	0.77	0.84	0.06	0.04
180	0.88	0.91	0.81	0.86	0.05	0.03
240	0.91	0.94	0.88	0.91	0.03	0.02
300	0.93	0.95	0.91	0.93	0.02	0.01

Table A.2.4 Cumulative mass and mass fraction dissolved and permeated into the receptor compartment as a function of time for FL aerosols collected on Stage 4 following single shot of Aerobid® MDI.

Inhaler	Aerobid					
Shots/Actuations	1					
Stage	4					
ICS	Flunisolide (FL)					
FL mass permeated (µg)	#1	#2	#3			
Time (min)						
15	0.41	0.44	0.36			
30	0.78	0.96	0.90			
45	1.26	1.49	1.18			
60	1.45	1.60	1.30			
90	1.89	1.90	1.55			
120	2.03	2.06	1.73			
150	2.06	2.11	1.80			
180	2.13	2.21	1.92			
240	2.24	2.25	2.03			
300	2.29	2.30	2.09			
Mass remaining on filter (R)	0.13	0.09	0.13	Mean ± SD	RSD	
Sum (P+R)	2.42	2.39	2.22	2.34 ± 0.11	4.70	
Fraction FL permeated	#1	#2	#3	Mean	SD	SE
Time (min)						
15	0.17	0.19	0.16	0.17	0.01	0.01
30	0.32	0.40	0.41	0.38	0.05	0.03
45	0.52	0.62	0.53	0.56	0.06	0.03
60	0.60	0.67	0.58	0.62	0.05	0.03
90	0.78	0.79	0.70	0.76	0.05	0.03
120	0.84	0.86	0.78	0.83	0.04	0.02
150	0.85	0.88	0.81	0.85	0.03	0.02
180	0.88	0.92	0.87	0.89	0.03	0.02
240	0.93	0.94	0.92	0.93	0.01	0.01
300	0.95	0.96	0.94	0.95	0.01	0.01

Table A.2.5 Cumulative mass and mass fraction dissolved and permeated into the receptor compartment as a function of time for FL aerosols collected on Stage 4 following 5 shots of Aerobid® MDI.

Inhaler	Aerobid					
Shots/Actuations	5					
Stage	4					
ICS	Flunisolide (FL)					
FL mass permeated (µg)	#1	#2	#3			
Time (min)						
15	1.62	0.70	0.74			
30	3.11	2.51	3.00			
45	4.18	3.32	4.19			
60	5.50	4.33	5.01			
90	7.72	6.69	6.93			
120	8.79	7.56	8.14			
150	9.46	8.17	9.10			
180	9.97	8.90	9.77			
240	10.47	9.59	10.37			
300	10.64	9.76	10.51			
Mass remaining on filter (R)	0.65	0.65	0.60	Mean ± SD	RSD	
Sum (P+R)	11.29	10.41	11.11	10.93 ± 0.47	4.30	
Fraction FL permeated	#1	#2	#3	Mean	SD	SE
Time (min)						
15	0.14	0.07	0.07	0.09	0.04	0.03
30	0.28	0.24	0.27	0.26	0.02	0.01
45	0.37	0.32	0.38	0.36	0.03	0.02
60	0.49	0.42	0.45	0.45	0.04	0.02
90	0.68	0.64	0.62	0.65	0.03	0.02
120	0.78	0.73	0.73	0.75	0.03	0.02
150	0.84	0.79	0.82	0.81	0.03	0.02
180	0.88	0.86	0.88	0.87	0.01	0.01
240	0.93	0.92	0.93	0.93	0.01	0.00
300	0.94	0.94	0.95	0.94	0.00	0.00

Table A.2.6 Cumulative mass and mass fraction dissolved and permeated into the receptor compartment as a function of time for FL aerosols collected on Stage 4 following 10 shots of Aerobid® MDI.

Inhaler	Aerobid					
Shots/Actuations	10					
Stage	4					
ICS	Flunisolide (FL)					
FL mass permeated (µg)	#1	#2	#3			
Time (min)						
15	1.90	0.91	1.14			
30	5.05	2.56	3.48			
45	6.14	4.27	6.34			
60	10.03	5.69	7.02			
90	13.47	10.53	11.18			
120	15.83	11.24	13.36			
150	16.59	14.31	13.81			
180	17.68	14.95	15.46			
240	18.50	16.12	16.35			
300	18.77	16.40	17.47			
Mass remaining on filter (R)	1.09	1.21	1.40	Mean ± SD	RSD	
Sum (P+R)	19.86	17.61	18.87	18.78 ± 1.13	6.02	
Fraction FL permeated	#1	#2	#3	Mean	SD	SE
Time (min)						
15	0.10	0.05	0.06	0.07	0.02	0.01
30	0.25	0.15	0.18	0.19	0.06	0.03
45	0.31	0.24	0.34	0.30	0.05	0.03
60	0.51	0.32	0.37	0.40	0.09	0.05
90	0.68	0.60	0.59	0.62	0.05	0.03
120	0.80	0.64	0.71	0.71	0.08	0.05
150	0.84	0.81	0.73	0.79	0.05	0.03
180	0.89	0.85	0.82	0.85	0.04	0.02
240	0.93	0.92	0.87	0.90	0.03	0.02
300	0.95	0.93	0.93	0.93	0.01	0.01

Table A.2.7 Cumulative mass and mass fraction dissolved and permeated into the receptor compartment as a function of time for TA aerosols collected on Stage 2 following single shot of Azmacort® MDI.

Inhaler	Azmacort					
Shots/Actuations	1					
Stage	2					
ICS	Triamcinolone Acetonide (TA)					
TA mass permeated (µg)	#1	#2	#3			
Time (min)						
15	0.20	0.23	0.09			
30	0.44	0.36	0.41			
45	0.52	0.47	0.45			
60	0.59	0.59	0.56			
90	0.79	0.70	0.65			
120	0.89	0.78	0.76			
150	0.96	0.86	0.80			
180	1.01	0.90	0.86			
240	1.07	0.94	0.90			
300	1.09	0.98	0.10			
Mass remaining on filter (R)	0.12	0.10	1.00	Mean ± SD	RSD	
Sum (P+R)	1.21	1.08	1.00	1.09 ± 0.11	10.09	
Fraction TA permeated	#1	#2	#3	Mean	SD	SE
Time (min)						
15	0.16	0.22	0.09	0.16	0.07	0.04
30	0.36	0.33	0.33	0.34	0.02	0.01
45	0.43	0.43	0.41	0.43	0.01	0.01
60	0.49	0.55	0.45	0.50	0.05	0.03
90	0.65	0.65	0.56	0.62	0.05	0.03
120	0.73	0.73	0.66	0.71	0.04	0.03
150	0.79	0.79	0.76	0.78	0.02	0.01
180	0.83	0.83	0.81	0.82	0.01	0.01
240	0.89	0.87	0.87	0.88	0.01	0.01
300	0.90	0.91	0.90	0.90	0.00	0.00

Table A.2.8 Cumulative mass and mass fraction dissolved and permeated into the receptor compartment as a function of time for TA aerosols collected on Stage 2 following 5 shots of Azmacort® MDI.

Inhaler	Azmacort					
Shots/Actuations	5					
Stage	2					
ICS	Triamcinolone Acetonide (TA)					
TA mass permeated (µg)	#1	#2	#3			
Time (min)						
15	0.73	0.84	0.65			
30	1.55	1.37	1.36			
45	2.34	2.12	2.04			
60	3.14	2.50	2.33			
90	4.32	3.70	3.27			
120	5.65	3.99	4.08			
150	5.88	4.57	4.65			
180	6.48	4.98	5.13			
240	7.48	5.35	5.82			
300	7.92	5.65	6.01			
Mass remaining on filter (R)	1.38	1.13	0.96	Mean ± SD	RSD	
Sum (P+R)	9.30	6.78	6.97	7.68 ± 1.40	18.23	
Fraction TA permeated	#1	#2	#3	Mean	SD	SE
Time (min)						
15	0.08	0.12	0.09	0.10	0.02	0.01
30	0.17	0.20	0.19	0.19	0.02	0.01
45	0.25	0.31	0.29	0.29	0.03	0.02
60	0.34	0.37	0.33	0.35	0.02	0.01
90	0.46	0.55	0.47	0.49	0.05	0.03
120	0.61	0.59	0.59	0.59	0.01	0.01
150	0.63	0.67	0.67	0.66	0.02	0.01
180	0.70	0.73	0.74	0.72	0.02	0.01
240	0.80	0.79	0.83	0.81	0.02	0.01
300	0.85	0.83	0.86	0.85	0.01	0.01

Table A.2.9 Cumulative mass and mass fraction dissolved and permeated into the receptor compartment as a function of time for TA aerosols collected on Stage 2 following 10 shots of Azmacort® MDI.

Inhaler	Azmacort					
Shots/Actuations	10					
Stage	2					
ICS	Triamcinolone Acetonide (TA)					
TA mass permeated (µg)	#1	#2	#3			
Time (min)						
15	0.88	0.89	0.91			
30	1.95	1.94	2.17			
45	3.31	3.11	2.85			
60	3.95	4.07	3.65			
90	5.26	5.91	5.44			
120	6.89	6.87	6.49			
150	7.77	7.57	7.34			
180	8.53	8.78	8.15			
240	9.75	9.39	9.07			
300	10.91	10.15	10.18			
Mass remaining on filter (R)	4.12	3.72	2.83	Mean ± SD	RSD	
Sum (P+R)	15.03	13.87	13.01	13.97 ± 1.02	7.30	
Fraction TA permeated	#1	#2	#3	Mean	SD	SE
Time (min)						
15	0.06	0.06	0.07	0.06	0.01	0.00
30	0.13	0.14	0.17	0.15	0.02	0.01
45	0.22	0.22	0.22	0.22	0.00	0.00
60	0.26	0.29	0.28	0.28	0.02	0.01
90	0.35	0.43	0.42	0.40	0.04	0.02
120	0.46	0.50	0.50	0.48	0.02	0.01
150	0.52	0.55	0.56	0.54	0.02	0.01
180	0.57	0.63	0.63	0.61	0.04	0.02
240	0.65	0.68	0.70	0.67	0.02	0.01
300	0.73	0.73	0.78	0.75	0.03	0.02

Table A.2.10 Cumulative mass and mass fraction dissolved and permeated into the receptor compartment as a function of time for TA aerosols collected on Stage 4 following single shot of Azmacort ® MDI.

Inhaler	Azmacort					
Shots/Actuations	1					
Stage	4					
ICS	Triamcinolone Acetonide (TA)					
TA mass permeated (µg)	#1	#2	#3			
Time (min)						
15	0.08	0.06	0.06			
30	0.15	0.10	0.10			
45	0.20	0.15	0.13			
60	0.24	0.18	0.15			
90	0.28	0.21	0.20			
120	0.31	0.24	0.23			
150	0.28	0.26	0.26			
180	0.33	0.28	0.28			
240	0.35	0.30	0.29			
300	0.37	0.32	0.32			
Mass remaining on filter (R)	0.04	0.04	0.04	Mean ± SD	RSD	
Sum (P+R)	0.41	0.36	0.36	0.37 ± 0.03	8.11	
Fraction TA permeated	#1	#2	#3	Mean	SD	SE
Time (min)						
15	0.20	0.17	0.18	0.18	0.02	0.01
30	0.37	0.29	0.28	0.31	0.05	0.03
45	0.50	0.41	0.36	0.42	0.07	0.04
60	0.59	0.49	0.43	0.50	0.08	0.05
90	0.68	0.59	0.55	0.61	0.07	0.04
120	0.76	0.66	0.63	0.68	0.06	0.04
150	0.69	0.73	0.72	0.71	0.02	0.01
180	0.81	0.77	0.79	0.79	0.02	0.01
240	0.86	0.84	0.80	0.83	0.03	0.02
300	0.90	0.89	0.89	0.89	0.01	0.00

Table A.2.11 Cumulative mass and mass fraction dissolved and permeated into the receptor compartment as a function of time for TA aerosols collected on Stage 4 following 5 shots of Azmacort® MDI.

Inhaler	Azmacort					
Shots/Actuations	5					
Stage	4					
ICS	Triamcinolone Acetonide (TA)					
TA mass permeated (µg)	#1	#2	#3			
Time (min)						
15	0.19	0.24	0.21			
30	0.51	0.48	0.54			
45	0.80	0.69	0.97			
60	1.12	0.88	1.05			
90	1.47	1.21	1.45			
120	1.78	1.42	1.61			
150	1.95	1.63	1.74			
180	2.06	1.78	1.88			
240	2.27	1.97	2.04			
300	2.40	2.08	2.07			
Mass remaining on filter (R)	0.36	0.28	0.21	Mean ± SD	RSD	
Sum (P+R)	2.76	2.36	2.28	2.47 ± 0.26	10.53	
Fraction TA permeated	#1	#2	#3	Mean	SD	SE
Time (min)						
15	0.07	0.10	0.09	0.09	0.02	0.01
30	0.19	0.20	0.24	0.21	0.03	0.02
45	0.29	0.29	0.43	0.34	0.08	0.05
60	0.41	0.37	0.46	0.41	0.04	0.02
90	0.53	0.51	0.63	0.56	0.07	0.04
120	0.64	0.60	0.70	0.65	0.05	0.03
150	0.71	0.69	0.76	0.72	0.04	0.02
180	0.75	0.75	0.82	0.77	0.04	0.02
240	0.82	0.83	0.89	0.85	0.04	0.02
300	0.87	0.88	0.91	0.89	0.02	0.01

Table A.2.12 Cumulative mass and mass fraction dissolved and permeated into the receptor compartment as a function of time for TA aerosols collected on Stage 4 following 10 shots of Azmacort® MDI.

Inhaler	Azmacort					
Shots/Actuations	10					
Stage	4					
ICS	Triamcinolone Acetonide (TA)					
TA mass permeated (µg)	#1	#2	#3			
Time (min)						
15	0.24	0.45	0.45			
30	0.75	0.99	0.84			
45	1.11	1.13	1.20			
60	1.60	1.46	1.61			
90	2.48	2.05	2.06			
120	2.53	2.33	2.59			
150	2.95	2.80	2.93			
180	3.29	3.02	3.41			
240	3.71	3.55	3.64			
300	3.88	3.80	3.98			
Mass remaining on filter (R)	0.58	0.97	0.73	Mean ± SD	RSD	
Sum (P+R)	4.46	4.77	4.71	4.67 ± 0.17	3.64	
Fraction TA permeated	#1	#2	#3	Mean	SD	SE
Time (min)						
15	0.05	0.09	0.10	0.08	0.02	0.01
30	0.17	0.21	0.18	0.18	0.02	0.01
45	0.25	0.24	0.26	0.25	0.01	0.01
60	0.36	0.31	0.34	0.34	0.03	0.02
90	0.56	0.43	0.44	0.47	0.07	0.04
120	0.57	0.49	0.55	0.53	0.04	0.02
150	0.66	0.59	0.62	0.62	0.04	0.02
180	0.74	0.63	0.72	0.70	0.06	0.03
240	0.83	0.74	0.77	0.78	0.04	0.03
300	0.87	0.80	0.85	0.84	0.04	0.02

Table A.2.13 Cumulative mass and mass fraction dissolved and permeated into the receptor compartment as a function of time for BD aerosols collected on Stage 2 following 5 shots of Pulmicort® DPI.

Inhaler	Pulmicort					
Shots/Actuations	5					
Stage	2					
ICS	Budesonide (BUD)					
BUD mass permeated (µg)	#1	#2	#3			
Time (min)						
15	0.19	0.15	0.17			
30	0.25	0.28	0.19			
45	0.30	0.33	0.24			
60	0.38	0.41	0.30			
90	0.49	0.52	0.49			
120	0.52	0.57	0.59			
150	0.57	0.59	0.64			
180	0.59	0.62	0.70			
240	0.64	0.66	0.75			
300	0.66	0.68	0.80			
360	0.68	0.71				
420	0.78	0.73				
Mass remaining on filter (R)	0.29	0.38	0.58	Mean ± SD	RSD	
Sum (P+R)	1.32	1.40	1.75	1.49 ± 0.23	15.44	
Fraction BUD permeated	#1	#2	#3	Mean	SD	SE
Time (min)						
15	0.19	0.15	0.21	0.18	0.03	0.02
30	0.25	0.28	0.22	0.25	0.03	0.02
45	0.30	0.33	0.26	0.30	0.03	0.02
60	0.38	0.41	0.30	0.36	0.05	0.03
90	0.49	0.52	0.34	0.45	0.10	0.06
120	0.52	0.57	0.36	0.49	0.11	0.06
150	0.57	0.59	0.51	0.56	0.04	0.02
180	0.59	0.62	0.54	0.58	0.04	0.02
240	0.64	0.66	0.60	0.63	0.03	0.02
300	0.66	0.68	0.67	0.67	0.01	0.01
360	0.68	0.71		0.70	0.02	0.01
420	0.78	0.73		0.75	0.04	0.02

Table A.2.14 Cumulative mass and mass fraction dissolved and permeated into the receptor compartment as a function of time for BD aerosols collected on Stage 2 following 10 shots of Pulmicort® DPI.

Inhaler	Pulmicort					
Shots/Actuations	10					
Stage	2					
ICS	Budesonide (BUD)					
BUD mass permeated (µg)	#1	#2	#3			
Time (min)						
15	0.18	0.19	0.21			
30	0.29	0.36	0.26			
45	0.41	0.41	0.38			
60	0.49	0.58	0.49			
90	0.63	0.76	0.60			
120	0.75	0.83	0.66			
150	0.81	0.90	0.72			
180	0.88	0.97	0.78			
240	0.94	1.04	0.85			
300	1.03	1.10	1.04			
360	1.07	1.15	1.08			
420	1.13	1.18	1.12			
Mass remaining on filter (R)	0.82	0.73	0.73	Mean ± SD	RSD	
Sum (P+R)	1.95	1.91	1.85	1.90 ± 0.05	2.63	
Fraction BUD permeated	#1	#2	#3	Mean	SD	SE
Time (min)						
15	0.09	0.10	0.11	0.10	0.01	0.01
30	0.15	0.19	0.14	0.16	0.03	0.01
45	0.21	0.21	0.20	0.21	0.01	0.00
60	0.25	0.30	0.26	0.27	0.03	0.02
90	0.32	0.40	0.33	0.35	0.04	0.02
120	0.38	0.44	0.35	0.39	0.04	0.02
150	0.42	0.47	0.39	0.43	0.04	0.02
180	0.45	0.51	0.42	0.46	0.04	0.03
240	0.48	0.54	0.46	0.50	0.04	0.02
300	0.52	0.58	0.56	0.56	0.03	0.02
360	0.55	0.60	0.59	0.58	0.03	0.02
420	0.58	0.62	0.61	0.60	0.02	0.01

Table A.2.15 Cumulative mass and mass fraction dissolved and permeated into the receptor compartment as a function of time for BD aerosols collected on Stage 4 following single shot of Pulmicort ® DPI.

Inhaler	Pulmicort					
Shots/Actuations	1					
Stage	4					
ICS	Budesonide (BUD)					
BUD mass permeated (µg)	#1	#2	#3			
Time (min)						
15	0.14	0.12	0.08			
30	0.18	0.20	0.22			
45	0.28	0.30	0.28			
60	0.32	0.34	0.35			
90	0.39	0.41	0.45			
120	0.44	0.46	0.50			
150	0.46	0.51	0.51			
180	0.50	0.54	0.54			
240	0.53	0.58	0.57			
300	0.55	0.60	0.59			
Mass remaining on filter (R)	0.22	0.23	0.16	Mean ± SD	RSD	
Sum (P+R)	0.77	0.83	0.75	0.78 ± 0.04	5.13	
Fraction BUD permeated	#1	#2	#3	Mean	SD	SE
Time (min)						
15	0.18	0.14	0.11	0.14	0.04	0.02
30	0.24	0.24	0.29	0.26	0.03	0.02
45	0.36	0.36	0.37	0.36	0.01	0.00
60	0.42	0.41	0.47	0.43	0.03	0.02
90	0.51	0.49	0.60	0.53	0.06	0.03
120	0.57	0.55	0.66	0.60	0.06	0.03
150	0.60	0.61	0.68	0.63	0.04	0.03
180	0.65	0.65	0.72	0.67	0.04	0.02
240	0.69	0.69	0.76	0.72	0.04	0.02
300	0.71	0.72	0.79	0.74	0.04	0.02

Table A.2.16 Cumulative mass and mass fraction dissolved and permeated into the receptor compartment as a function of time for BD aerosols collected on Stage 4 following 5 shots of Pulmicort® DPI.

Inhaler	Pulmicort					
Shots/Actuations	5					
Stage	4					
ICS	Budesonide (BUD)					
BUD mass permeated (µg)	#1	#2	#3			
Time (min)						
15	0.20	0.20	0.17			
30	0.32	0.34	0.35			
45	0.46	0.42	0.47			
60	0.57	0.46	0.57			
90	0.71	0.67	0.80			
120	0.85	0.76	0.92			
150	0.94	0.89	1.02			
180	0.99	0.97	1.07			
240	1.08	1.07	1.13			
300	1.13	1.14	1.21			
360	1.17	1.18	1.25			
420	1.22	1.22	1.43			
Mass remaining on filter (R)	0.31	0.45	0.32	Mean ± SD	RSD	
Sum (P+R)	1.53	1.67	1.75	1.65 ± 0.11	6.67	
Fraction BUD permeated	#1	#2	#3	Mean	SD	SE
Time (min)						
15	0.13	0.12	0.10	0.12	0.02	0.01
30	0.21	0.20	0.20	0.21	0.00	0.00
45	0.30	0.25	0.27	0.27	0.02	0.01
60	0.37	0.27	0.33	0.33	0.05	0.03
90	0.47	0.40	0.45	0.44	0.04	0.02
120	0.56	0.45	0.53	0.51	0.05	0.03
150	0.61	0.53	0.58	0.58	0.04	0.02
180	0.65	0.58	0.61	0.61	0.03	0.02
240	0.71	0.64	0.65	0.66	0.04	0.02
300	0.74	0.68	0.69	0.70	0.03	0.02
360	0.77	0.70	0.71	0.73	0.04	0.02
420	0.80	0.73	0.82	0.78	0.04	0.03

Table A.2.17 Cumulative mass and mass fraction dissolved and permeated into the receptor compartment as a function of time for BD aerosols collected on Stage 4 following 10 shots of Pulmicort® DPI.

Inhaler	Pulmicort					
Shots/Actuations	10					
Stage	4					
ICS	Budesonide (BUD)					
BUD mass permeated (µg)	#1	#2	#3			
Time (min)						
15	0.27	0.31	0.20			
30	0.43	0.43	0.32			
45	0.57	0.60	0.47			
60	0.66	0.78	0.65			
90	0.96	0.97	0.89			
120	1.07	1.21	1.01			
150	1.27	1.38	1.25			
180	1.37	1.49	1.36			
240	1.55	1.71	1.64			
300	1.70	1.86	1.74			
360	1.79	1.98	1.87			
420	1.87	2.04	1.99			
Mass remaining on filter (R)	0.87	0.72	1.05	Mean ± SD	RSD	
Sum (P+R)	2.74	2.76	3.04	2.85 ± 0.16	5.61	
Fraction BUD permeated	#1	#2	#3	Mean	SD	SE
Time (min)						
15	0.10	0.11	0.07	0.09	0.02	0.01
30	0.16	0.15	0.11	0.14	0.03	0.02
45	0.21	0.22	0.15	0.19	0.04	0.02
60	0.24	0.28	0.21	0.24	0.03	0.02
90	0.35	0.35	0.29	0.33	0.03	0.02
120	0.39	0.44	0.33	0.39	0.05	0.03
150	0.46	0.50	0.41	0.46	0.04	0.03
180	0.50	0.54	0.45	0.50	0.05	0.03
240	0.56	0.62	0.54	0.57	0.04	0.02
300	0.62	0.67	0.57	0.62	0.05	0.03
360	0.65	0.72	0.62	0.66	0.05	0.03
420	0.68	0.74	0.65	0.69	0.04	0.02

Table A.2.18 Cumulative mass and mass fraction dissolved and permeated into the receptor compartment as a function of time for FP aerosols collected on Stage 2 following 5 shots of Flovent HFA ® (44 µg) MDI.

Inhaler	Flovent HFA 44 µg					
Shots/Actuations	5					
Stage	2					
ICS	Fluticasone Propionate (FP)					
FP mass permeated (ng)	#1	#2	#3			
Time (min)						
30	3.92	3.92	3.92			
60	14.73	7.46	7.57			
90	27.88	14.64	12.43			
120	35.53	20.64	22.33			
150	44.48	27.17	26.16			
180	54.07	32.52	28.03			
240	73.38	37.76	39.96			
300	84.62	49.82	46.39			
360	99.41	61.84	51.17			
420	107.62	69.66	55.50			
480	120.05	72.67	67.53			
540	129.60	79.88	72.01			
600	138.18	90.95	82.89			
Mass remaining on filter (R)	1552.00	1764.79	1608.05	Mean ± SD	RSD	
Sum (P+R)	1690.18	1855.74	1690.94	1745.62 ± 95.37	5.46	
Fraction FP permeated	#1	#2	#3	Mean	SD	SE
Time (min)						
30	0.00	0.00	0.00	0.00	0.00	0.00
60	0.01	0.00	0.00	0.01	0.00	0.00
90	0.02	0.01	0.01	0.01	0.01	0.00
120	0.02	0.01	0.01	0.02	0.01	0.00
150	0.03	0.01	0.02	0.02	0.01	0.00
180	0.03	0.02	0.02	0.02	0.01	0.00
240	0.04	0.02	0.02	0.03	0.01	0.01
300	0.05	0.03	0.03	0.03	0.01	0.01
360	0.06	0.03	0.03	0.04	0.02	0.01
420	0.06	0.04	0.03	0.04	0.02	0.01
480	0.07	0.04	0.04	0.05	0.02	0.01
540	0.08	0.04	0.04	0.05	0.02	0.01
600	0.08	0.05	0.05	0.06	0.02	0.01

Table A.2.19 Cumulative mass and mass fraction dissolved and permeated into the receptor compartment as a function of time for FP aerosols collected on Stage 2 following 5 shots of Flovent HFA ® (220 µg) MDI.

Inhaler	Flovent HFA 220 µg					
Shots/Actuations	5					
Stage	2					
ICS	Fluticasone Propionate (FP)					
FP mass permeated (ng)	#1	#2	#3			
Time (min)						
30	9.03	12.57	13.91			
60	25.69	28.66	27.80			
90	35.30	37.91	37.66			
120	44.99	50.55	51.44			
150	57.15	60.02	62.60			
180	72.64	73.26	77.53			
240	87.73	90.00	92.72			
300	102.69	109.73	114.20			
360	119.65	117.27	122.49			
420	138.11	137.25	140.40			
480	153.07	153.86	151.00			
540	165.03	163.74	163.46			
600	182.72	176.78	183.51			
Mass remaining on filter (R)	12888.96	15500.58	20106.48	Mean ± SD	RSD	
Sum (P+R)	13071.68	15677.36	20289.99	16346.34 ± 3655.36	22.36	
Fraction FP permeated	#1	#2	#3	Mean	SD	SE
Time (min)						
30	6.9E-04	8.0E-04	6.9E-04	0.00	0.00	0.00
60	2.0E-03	1.8E-03	1.4E-03	0.00	0.00	0.00
90	2.7E-03	2.4E-03	1.9E-03	0.00	0.00	0.00
120	3.4E-03	3.2E-03	2.5E-03	0.00	0.00	0.00
150	4.4E-03	3.8E-03	3.1E-03	0.00	0.00	0.00
180	5.6E-03	4.7E-03	3.8E-03	0.00	0.00	0.00
240	6.7E-03	5.7E-03	4.6E-03	0.01	0.00	0.00
300	7.9E-03	7.0E-03	5.6E-03	0.01	0.00	0.00
360	9.2E-03	7.5E-03	6.0E-03	0.01	0.00	0.00
420	1.1E-02	8.8E-03	6.9E-03	0.01	0.00	0.00
480	1.2E-02	9.8E-03	7.4E-03	0.01	0.00	0.00
540	1.3E-02	1.0E-02	8.1E-03	0.01	0.00	0.00
600	1.4E-02	1.1E-02	9.0E-03	0.01	0.00	0.00

Table A.2.20 Cumulative mass and mass fraction dissolved and permeated into the receptor compartment as a function of time for FP aerosols collected on Stage 4 following 5 shots of Flovent HFA ® (44 µg) MDI.

Inhaler	Flovent HFA 44 µg					
Shots/Actuations	5					
Stage	4					
ICS	Fluticasone Propionate (FP)					
FP mass permeated (ng)	#1	#2	#3			
Time (min)						
30	0.23	0.54	0.54			
60	8.60	5.85	7.49			
90	15.33	12.47	8.76			
120	22.14	15.22	12.83			
150	24.72	19.47	21.69			
180	30.23	26.92	22.17			
240	43.34	32.76	33.32			
300	49.22	44.30	36.60			
360	60.27	50.00	43.67			
420	70.19	61.89	44.89			
480	75.20	71.38	57.04			
540	85.02	73.79	65.60			
600	96.16	86.66	73.69			
Mass remaining on filter (R)	3679.00	5408.02	5105.24	Mean ± SD	RSD	
Sum (P+R)	3775.16	5494.68	5178.93	4816.26 ± 915.33	19.00	
Fraction FP permeated	#1	#2	#3	Mean	SD	SE
Time (min)						
30	0.00	0.00	0.00	0.00	0.00	0.00
60	0.00	0.00	0.00	0.00	0.00	0.00
90	0.00	0.00	0.00	0.00	0.00	0.00
120	0.01	0.00	0.00	0.00	0.00	0.00
150	0.01	0.00	0.00	0.00	0.00	0.00
180	0.01	0.00	0.00	0.01	0.00	0.00
240	0.01	0.01	0.01	0.01	0.00	0.00
300	0.01	0.01	0.01	0.01	0.00	0.00
360	0.02	0.01	0.01	0.01	0.00	0.00
420	0.02	0.01	0.01	0.01	0.01	0.00
480	0.02	0.01	0.01	0.01	0.00	0.00
540	0.02	0.01	0.01	0.02	0.01	0.00
600	0.03	0.02	0.01	0.02	0.01	0.00

Table A.2.21 Cumulative mass and mass fraction dissolved and permeated into the receptor compartment as a function of time for FP aerosols collected on Stage 4 following 5 shots of Flovent HFA ® (220 µg) MDI.

Inhaler	Flovent HFA 220 µg					
Shots/Actuations	5					
Stage	4					
ICS	Fluticasone Propionate (FP)					
FP mass permeated (ng)	#1	#2	#3			
Time (min)						
30	8.90	11.84	8.78			
60	16.85	25.84	18.03			
90	23.93	35.02	29.33			
120	35.95	40.94	35.93			
150	43.64	56.66	44.06			
180	59.43	67.28	57.55			
240	72.07	87.16	70.12			
300	80.15	104.65	85.32			
360	93.29	114.65	92.37			
420	103.44	129.42	106.33			
480	113.69	149.48	122.05			
540	124.46	157.71	129.80			
600	135.14	171.34	138.69			
Mass remaining on filter (R)	19000.34	19439.62	20548.10	Mean ± SD	RSD	
Sum (P+R)	19135.48	19610.96	20686.79	19811.08 ± 794.78	4.01	
Fraction FP permeated	#1	#2	#3	Mean	SD	SE
Time (min)						
30	4.7E-04	6.0E-04	4.2E-04	0.00	0.00	0.00
60	8.8E-04	1.3E-03	8.7E-04	0.00	0.00	0.00
90	1.3E-03	1.8E-03	1.4E-03	0.00	0.00	0.00
120	1.9E-03	2.1E-03	1.7E-03	0.00	0.00	0.00
150	2.3E-03	2.9E-03	2.1E-03	0.00	0.00	0.00
180	3.1E-03	3.4E-03	2.8E-03	0.00	0.00	0.00
240	3.8E-03	4.4E-03	3.4E-03	0.00	0.00	0.00
300	4.2E-03	5.3E-03	4.1E-03	0.00	0.00	0.00
360	4.9E-03	5.8E-03	4.5E-03	0.01	0.00	0.00
420	5.4E-03	6.6E-03	5.1E-03	0.01	0.00	0.00
480	5.9E-03	7.6E-03	5.9E-03	0.01	0.00	0.00
540	6.5E-03	8.0E-03	6.3E-03	0.01	0.00	0.00
600	7.1E-03	8.7E-03	6.7E-03	0.01	0.00	0.00

Table A.2.22 Cumulative mass and mass fraction dissolved and permeated into the receptor compartment as a function of time for FP aerosols collected on Stage 2 following 22 shots of Flovent Diskus ® DPI.

Inhaler	Flovent Diskus 50 µg					
Shots/Actuations	22					
Stage	2					
ICS	Fluticasone Propionate (FP)					
FP mass permeated (ng)	#1	#2	#3			
Time (min)						
30	15.57	8.47	10.32			
60	27.24	15.12	13.08			
90	37.19	21.07	22.75			
120	45.22	25.76	28.15			
150	55.06	32.36	34.68			
180	61.25	36.47	41.64			
240	75.27	44.93	46.42			
300	80.90	51.86	52.09			
360	89.83	57.62	60.64			
420	95.93	63.06	64.95			
480	99.70	68.08	72.81			
540	106.37	75.40	77.32			
600	111.33	79.84	82.45			
Mass remaining on filter (R)	1909.44	2427.05	1946.10	Mean ± SD	RSD	
Sum (P+R)	2020.767	2506.894	2028.558	2185.41 ± 278.44	12.74	
Fraction FP permeated	#1	#2	#3	Mean	SD	SE
Time (min)						
30	0.01	0.00	0.01	0.01	0.00	0.00
60	0.01	0.01	0.01	0.01	0.00	0.00
90	0.02	0.01	0.01	0.01	0.01	0.00
120	0.02	0.01	0.01	0.02	0.01	0.00
150	0.03	0.01	0.02	0.02	0.01	0.00
180	0.03	0.01	0.02	0.02	0.01	0.00
240	0.04	0.02	0.02	0.03	0.01	0.01
300	0.04	0.02	0.03	0.03	0.01	0.01
360	0.04	0.02	0.03	0.03	0.01	0.01
420	0.05	0.03	0.03	0.03	0.01	0.01
480	0.05	0.03	0.04	0.04	0.01	0.01
540	0.05	0.03	0.04	0.04	0.01	0.01
600	0.06	0.03	0.04	0.04	0.01	0.01

Table A.2.23 Cumulative mass and mass fraction dissolved and permeated into the receptor compartment as a function of time for FP aerosols collected on Stage 4 following 22 shots of Flovent Diskus ® DPI.

Inhaler	Flovent Diskus 50 μg					
Shots/Actuations	22					
Stage	4					
ICS	Fluticasone Propionate (FP)					
FP mass permeated (ng)	#1	#2	#3			
Time (min)						
30	5.13	6.55	9.89			
60	9.59	11.16	17.68			
90	13.85	16.16	24.80			
120	19.00	16.99	27.60			
150	22.61	23.15	33.82			
180	26.59	24.41	41.06			
240	29.84	32.52	48.81			
300	34.28	37.21	55.12			
360	39.85	39.35	62.55			
420	45.29	45.89	70.09			
480	49.01	51.19	76.25			
540	53.38	55.03	80.87			
600	56.10	59.39	87.71			
Mass remaining on filter (R)	2063.86	2839.62	2183.18	Mean ± SD	RSD	
Sum (P+R)	2119.962	2899.007	2270.897	2429.96 ± 413.16	17.00	
Fraction FP permeated	#1	#2	#3	Mean	SD	SE
Time (min)						
30	0.00	0.00	0.00	0.00	0.00	0.00
60	0.00	0.00	0.01	0.01	0.00	0.00
90	0.01	0.01	0.01	0.01	0.00	0.00
120	0.01	0.01	0.01	0.01	0.00	0.00
150	0.01	0.01	0.01	0.01	0.00	0.00
180	0.01	0.01	0.02	0.01	0.00	0.00
240	0.01	0.01	0.02	0.02	0.01	0.00
300	0.02	0.01	0.02	0.02	0.01	0.00
360	0.02	0.01	0.03	0.02	0.01	0.00
420	0.02	0.02	0.03	0.02	0.01	0.00
480	0.02	0.02	0.03	0.02	0.01	0.00
540	0.03	0.02	0.04	0.03	0.01	0.00
600	0.03	0.02	0.04	0.03	0.01	0.01

Table A.2.24 Cumulative mass and mass fraction dissolved and permeated into the receptor compartment as a function of time for BDP aerosols collected on Stage 2 following 14 shots of Qvar® MDI.

Inhaler	Qvar					
Shots/Actuations	14					
Stage	2					
ICS	Beclomethasone Dipropionate (BDP)					
BDP mass permeated (ng)	#1	#2	#3			
Time (min)						
30	3.23	11.83	5.63			
60	6.63	18.36	7.80			
120	7.48	20.98	8.45			
150	9.28	25.07	10.01			
180	9.00	26.51	11.51			
240	11.75	29.09	13.11			
300	13.08	34.26	15.66			
360	15.17	36.85	17.66			
420	16.56	43.80	19.22			
480	17.66	48.13	22.22			
540	18.93	51.07	24.46			
600	20.42	53.72	25.80			
Mass remaining on filter (R)	452.99	599.98	516.82	Mean ± SD	RSD	
Sum (P+R)	473.41	653.70	542.6143	556.58 ± 90.95	16.34	
Fraction BDP permeated	#1	#2	#3	Mean	SD	SE
Time (min)						
30	0.01	0.02	0.01	0.01	0.01	0.00
60	0.01	0.03	0.01	0.02	0.01	0.00
120	0.02	0.03	0.02	0.02	0.01	0.01
150	0.02	0.04	0.02	0.03	0.01	0.01
180	0.02	0.04	0.02	0.03	0.01	0.01
240	0.02	0.04	0.02	0.03	0.01	0.01
300	0.03	0.05	0.03	0.04	0.01	0.01
360	0.03	0.06	0.03	0.04	0.01	0.01
420	0.03	0.07	0.04	0.05	0.02	0.01
480	0.04	0.07	0.04	0.05	0.02	0.01
540	0.04	0.08	0.05	0.05	0.02	0.01
600	0.04	0.08	0.05	0.06	0.02	0.01

Table A.2.25 Cumulative mass and mass fraction dissolved and permeated into the receptor compartment as a function of time for BDP aerosols collected on Stage 4 following 14 shots of Qvar® MDI.

Inhaler	Qvar µg					
Shots/Actuations	14					
Stage	4					
ICS	Beclomethasone Dipropionate (BDP)					
BDP mass permeated (ng)	#1	#2	#3			
Time (min)						
30	66.70	39.36	45.12			
60	90.52	70.92	75.71			
120	123.91	106.93	106.83			
150	123.20	128.58	117.68			
180	130.39	133.56	133.15			
240	154.43	157.07	153.35			
300	177.56	175.52	175.05			
360	183.47	188.59	189.83			
420	201.33	209.14	209.82			
480	212.33	226.71	221.15			
540	228.05	240.88	237.92			
600	241.57	258.98	258.67			
Mass remaining on filter (R)	1275.10	1290.32	1434.51	Mean ± SD	RSD	
Sum (P+R)	1516.668	1549.295	1693.179	1586.38 ± 93.92	5.92	
Fraction BDP permeated	#1	#2	#3	Mean	SD	SE
Time (min)						
30	0.04	0.03	0.03	0.03	0.01	0.01
60	0.06	0.05	0.04	0.05	0.01	0.00
120	0.08	0.07	0.06	0.07	0.01	0.01
150	0.08	0.08	0.07	0.08	0.01	0.00
180	0.09	0.09	0.08	0.08	0.00	0.00
240	0.10	0.10	0.09	0.10	0.01	0.00
300	0.12	0.11	0.10	0.11	0.01	0.00
360	0.12	0.12	0.11	0.12	0.01	0.00
420	0.13	0.13	0.12	0.13	0.01	0.00
480	0.14	0.15	0.13	0.14	0.01	0.00
540	0.15	0.16	0.14	0.15	0.01	0.00
600	0.16	0.17	0.15	0.16	0.01	0.00

Table A.2.26 Cumulative mass and mass fraction dissolved and permeated into the receptor compartment as a function of time for BDP aerosols collected on Stage 2 following 7 shots of Vanceril ® MDI.

Inhaler	Vanceril					
Shots/Actuations	7					
Stage	2					
ICS	Beclomethasone Dipropionate (BDP)					
BDP mass permeated (ng)	#1	#2	#3			
Time (min)						
30	48.86	41.65	29.15			
60	91.70	67.36	68.47			
90	94.25	77.77	73.57			
120	117.18	88.73	89.61			
150	130.60	93.66	102.74			
180	143.03	104.90	107.39			
240	160.40	115.73	119.81			
300	181.94	131.23	140.50			
360	209.01	144.95	158.55			
420	224.36	160.37	169.18			
480	242.77	167.51	180.98			
540	264.62	188.57	198.79			
600	294.76	203.13	215.71			
Mass remaining on filter (R)	1029.38	1009.70	1095.96	Mean ± SD	RSD	
Sum (P+R)	1324.138	1212.828	1311.671	1282.88 ± 60.99	4.75	
Fraction BDP permeated	#1	#2	#3	Mean	SD	SE
Time (min)						
30	0.04	0.03	0.02	0.03	0.01	0.00
60	0.07	0.06	0.05	0.06	0.01	0.01
90	0.07	0.06	0.06	0.06	0.01	0.00
120	0.09	0.07	0.07	0.08	0.01	0.01
150	0.10	0.08	0.08	0.08	0.01	0.01
180	0.11	0.09	0.08	0.09	0.01	0.01
240	0.12	0.10	0.09	0.10	0.02	0.01
300	0.14	0.11	0.11	0.12	0.02	0.01
360	0.16	0.12	0.12	0.13	0.02	0.01
420	0.17	0.13	0.13	0.14	0.02	0.01
480	0.18	0.14	0.14	0.15	0.03	0.02
540	0.20	0.16	0.15	0.17	0.03	0.02
600	0.22	0.17	0.16	0.18	0.03	0.02

Table A.2.27 Cumulative mass and mass fraction dissolved and permeated into the receptor compartment as a function of time for BDP aerosols collected on Stage 4 following 7 shots of Vanceril ® MDI.

Inhaler	Vanceril					
Shots/Actuations	7					
Stage	4					
ICS	Beclomethasone Dipropionate (BDP)					
BDP mass permeated (ng)	#1	#2	#3			
Time (min)						
30	19.23	21.78	13.55			
60	38.77	44.93	24.57			
90	48.86	55.21	33.00			
120	63.40	62.70	40.09			
150	80.28	75.84	51.07			
180	82.28	80.15	52.98			
240	91.05	90.79	66.21			
300	113.68	102.10	79.11			
360	137.11	132.78	99.46			
420	159.53	135.18	105.16			
480	172.24	153.38	123.16			
540	199.47	191.23	149.55			
600	219.60	200.98	158.19			
Mass remaining on filter (R)	1507.47	1387.03	1226.21	Mean ± SD	RSD	
Sum (P+R)	1727.071	1588.014	1384.397	1566.49 ± 172.35	11.00	
Fraction BDP permeated	#1	#2	#3	Mean	SD	SE
Time (min)						
30	0.01	0.01	0.01	0.01	0.00	0.00
60	0.02	0.03	0.02	0.02	0.01	0.00
90	0.03	0.03	0.02	0.03	0.01	0.00
120	0.04	0.04	0.03	0.04	0.01	0.00
150	0.05	0.05	0.04	0.04	0.01	0.00
180	0.05	0.05	0.04	0.05	0.01	0.00
240	0.05	0.06	0.05	0.05	0.00	0.00
300	0.07	0.06	0.06	0.06	0.00	0.00
360	0.08	0.08	0.07	0.08	0.01	0.00
420	0.09	0.09	0.08	0.08	0.01	0.00
480	0.10	0.10	0.09	0.10	0.01	0.00
540	0.12	0.12	0.11	0.11	0.01	0.00
600	0.13	0.13	0.11	0.12	0.01	0.00

Table A.2.28 Cumulative FNa mass permeated across air-interface cultured Calu-3 monolayers grown in 1.13 cm^2 transwells at a seeding density of $0.1x10^6$ cells/cm^2.

Transwell: 12 mm diameter, 0.4 um poresize, PE membrane, PS plate,12 wells/ plate								
Area	1.13 cm^2							
Seeding density	$0.1x10^6/cm^2$							
Apical	0.5 mL							
Basolateral	1.5 mL							
Solute								
Apical	40 µg/mL Na-F in KRB							
Basolateral	KRB							
Time(min)	#1 CumFNa [µg]	#2 CumFNa [µg]	#3 CumFNa [µg]	#4 CumFNa [µg]	#5 CumFNa [µg]	#6 CumFNa [µg]	Mean [µg]	SD
0	0.00	0.00	0.00	0.00	0.00	0.00	0.00	0.00
10	0.03	0.01	0.00	0.02	0.00	0.00	0.01	0.01
30	0.04	0.03	0.02	0.04	0.02	0.02	0.03	0.01
60	0.08	0.07	0.04	0.07	0.04	0.04	0.06	0.02
90	0.14	0.10	0.07	0.10	0.07	0.08	0.09	0.03
120	0.17	0.14	0.10	0.14	0.11	0.11	0.13	0.03
150	0.21	0.17	0.14	0.18	0.15	0.14	0.17	0.03
180	0.23	0.20	0.16	0.21	0.18	0.17	0.19	0.03

Table A.2.29 Cumulative FNa mass permeated across air-interface cultured Calu-3 monolayers grown in 1.13 cm^2 transwells at a seeding density of $0.5x10^6$ cells/cm^2.

Transwell: 12 mm diameter, 0.4 um poresize, PE membrane, PS plate,12 wells/ plate								
Area	1.13 cm^2							
Seeding density	$0.5x10^6/cm^2$							
Volume								
Apical	0.5 mL							
Basolateral	1.5 mL							
Solute								
Apical	40 µg/mL Na-F in KRB							
Basolateral	KRB							
Time(min)	#1 CumFNa [µg]	#2 CumFNa [µg]	#3 CumFNa [µg]	#4 CumFNa [µg]	#5 CumFNa [µg]	Mean [µg]	SD	
0	0.00	0.00	0.00	0.00	0.00	0.00	0.00	
10	0.00	0.00	0.00	0.00	0.00	0.00	0.00	
30	0.01	0.01	0.01	0.01	0.00	0.01	0.00	
60	0.02	0.02	0.01	0.02	0.02	0.02	0.00	
90	0.02	0.03	0.02	0.03	0.04	0.03	0.01	
120	0.03	0.03	0.02	0.04	0.06	0.04	0.02	
150	0.04	0.04	0.03	0.05	0.09	0.05	0.02	
180	0.05	0.04	0.04	0.06	0.10	0.06	0.03	

Table A.2.30 Cumulative FNa mass permeated across air-interface cultured Calu-3 monolayers grown in 4.5 cm^2 transwells at a seeding density of $0.1x10^6$ cells/cm^2.

Transwell: 24 mm diameter, 0.4 um poresize, PE membrane, PS plate,12 wells/ plate							
Area	4.5 cm^2						
Seeding density	$0.1x10^6$/cm^2						
Volume							
Apical	1.5 mL						
Basolateral	2.6 mL						
Solute							
Apical	10 µg/mL Na-F in KRB						
Basolateral	KRB						
Time(min)	#1 CumFNa [µg]	#2 CumFNa [µg]	#3 CumFNa [µg]	#4 CumFNa [µg]	#5 CumFNa [µg]	Mean [µg]	SD
0	0.00	0.00	0.00	0.00	0.00	0.00	0.00
10	0.00	0.00	0.00	0.00	0.00	0.00	0.00
30	0.00	0.00	0.00	0.01	0.00	0.00	0.00
60	0.01	0.00	0.00	0.02	0.01	0.01	0.01
90	0.01	0.01	0.01	0.03	0.02	0.02	0.01
120	0.03	0.02	0.02	0.04	0.03	0.03	0.01
150	0.04	0.03	0.03	0.05	0.04	0.04	0.01
180	0.06	0.04	0.05	0.06	0.06	0.05	0.01

Table A.2.31 Cumulative FD-10 mass permeated across air-interface cultured Calu-3 monolayers grown in 4.5 cm^2 transwells at a seeding density of $0.1x10^6$ cells/cm^2.

Transwell: 24 mm diameter, 0.4 um poresize, PE membrane, PS plate,12 wells/ plate					
Area	4.5 cm^2				
Seeding density	$0.1x10^6/cm^2$				
Volume					
Apical	1.5 mL				
Basolateral	2.6 mL				
Solute					
Apical	500 µg/mL FD-10 in KRB				
Basolateral	KRB				
Time(min)	#1 CumFD [µg]	#2 CumFD [µg]	#3 CumFD [µg]	Mean [µg]	SD
0	0.00	0.00	0.00	0.00	0.00
30	0.23	0.07	0.28	0.19	0.11
60	0.41	0.28	0.75	0.48	0.24
90	0.66	0.48	0.85	0.66	0.19
120	0.84	0.68	1.42	0.98	0.39
150	1.14	0.90	1.61	1.22	0.36
180	1.31	1.08	2.11	1.50	0.54

Table A.2.32 Cumulative FD-70 mass permeated across air-interface cultured Calu-3 monolayers grown in 4.5 cm^2 transwells at a seeding density of $0.1x10^6$ cells/cm^2.

Transwell: 24 mm diameter, 0.4 um poresize, PE membrane, PS plate,12 wells/ plate						
Area	4.5 cm^2					
Seeding density	$0.1x10^6/cm^2$					
Volume						
Apical	1.5 mL					
Basolateral	2.6 mL					
Solute						
Apical	1 mg/mL FD-70 in KRB					
Basolateral	KRB					
Time(min)	#1 CumFD [µg]	#2 CumFD [µg]	#3 CumFD [µg]	#4 CumFD [µg]	Mean [µg]	SD
0	0.00	0.00	0.00	0.00	0.00	0.00
30	0.07	0.02	0.11	0.00	0.05	0.05
60	0.13	0.13	0.29	0.14	0.17	0.08
90	0.34	0.25	0.32	0.28	0.30	0.04
120	0.41	0.47	0.36	0.48	0.43	0.05
150	0.57	0.75	0.43	0.57	0.58	0.13
180	0.74	0.87	0.55	0.73	0.72	0.13

Table A.2.33 Cumulative FD-150 mass permeated across air-interface cultured Calu-3 monolayers grown in 4.5 cm^2 transwells at a seeding density of $0.1x10^6$ cells/cm^2.

Transwell: 24 mm diameter, 0.4 um poresize, PE membrane, PS plate,12 wells/ plate						
Area	4.5 cm^2					
Seeding density	$0.1x10^6/cm^2$					
Volume						
Apical	1.5 mL					
Basolateral	2.6 mL					
Solute						
Apical	2 mg/mL FD-150 in KRB					
Basolateral	KRB					
Time(min)	#1 CumFD [µg]	#2 CumFD [µg]	#3 CumFD [µg]	#4 CumFD [µg]	Mean [µg]	SD
0	0.00	0.00	0.00	0.00	0.00	0.00
30	0.00	0.00	0.01	0.01	0.01	0.00
60	0.04	0.01	0.04	0.08	0.04	0.03
90	0.07	0.02	0.22	0.09	0.10	0.08
120	0.10	0.04	0.33	0.16	0.16	0.13
150	0.14	0.07	0.57	0.21	0.25	0.23
180	0.20	0.08	0.81	0.22	0.33	0.33

Table A.2.34 Data sheets to obtain fold-induction of NFκB-activity with or without 60 ng/mLTNFα incubation for 6 h. The concentration of protein in cell samples was calculated using the standard curve for albumin in the BCA.

	Corrected Average Abs* after BCA	Conc** of protein by BCA (µg/mL)	Dilution Factor	Actual Conc of protein (µg/mL)	RLU per 20 µL cell sample	Protein in 20 µL of sample (µg)	RLU per mg of protein	Fold Induction
Control	0.43	1148.25	6.00	6889.50	44571	137.79	323470.50	1.30
	0.50	1310.75	6.00	7864.50	27156	157.29	172649.25	0.70
	0.47	1346.00	6.00	8076.00	49210	161.52	304668.15	1.29
	0.59	1658.50	6.00	9951.00	42445	199.02	213270.02	0.90
	0.55	1549.75	6.00	9298.50	35477	185.97	190767.33	0.81
	0.52	1082.80	6.00	6496.80	17770	129.94	136759.64	0.87
	0.52	1079.80	6.00	6478.80	23016	129.58	177625.49	1.13
	0.58	991.00	6.00	5946.00	62198	118.92	523023.88	0.86
	0.64	1091.83	6.00	6551.00	69477	131.02	530277.82	0.87
	0.53	906.83	6.00	5441.00	83715	108.82	769297.92	1.27
TNFα	0.50	1324.50	6.00	7947.00	98851	158.94	621939.10	3.30
	0.40	1073.25	6.00	6439.50	105538	128.79	819458.03	3.30
	0.54	1528.50	6.00	9171.00	197242	183.42	1075357.10	4.55
	0.53	1486.00	6.00	8916.00	172766	178.32	968853.75	4.10
	0.51	1453.50	6.00	8721.00	141671	174.42	812240.57	3.44
	0.66	1375.80	6.00	8254.80	78379	165.10	474748.03	3.02
	0.54	1121.80	6.00	6730.80	58456	134.62	434242.59	2.76
	0.52	1086.80	6.00	6520.80	79451	130.42	609212.06	3.88
	0.64	1099.33	6.00	6596.00	387622	131.92	2938311.10	4.84
	0.57	974.33	6.00	5846.00	278702	116.92	2383698.26	3.92
	0.56	957.67	6.00	5746.00	460240	114.92	4004872.96	6.59

* Abs: Absorbance obtained at 262 nm.
** Conc: Concentration.

Table A.2.35 Data sheets to obtain fold-induction of NFκB-activity with 60 ng/mLTNFα and various ICS treatment (aerosol, solution or suspension) incubation for 6 h. The concentration of protein in cell samples was calculated using the standard curve for albumin in the BCA.

Corrected Average Abs* after BCA	Conc** of protein by BCA (µg/mL)	Dilution Factor	Actual Conc of protein (µg/mL)	RLU per 20 µL cell sample	Protein in 20 µL of sample (µg)	RLU per mg of protein	Fold Induction
FP 0.55 µg (Flovent HFA 10 shots)							
0.52	1481.00	6.00	8886.00	172492	177.72	970582.94	4.11
0.50	1423.50	6.00	8541.00	134321	170.82	786330.64	3.33
0.54	1526.00	6.00	9156.00	166023	183.12	906634.99	3.84
0.45	1194.50	6.00	7167.00	100853	143.34	703592.86	2.84
0.47	1237.00	6.00	7422.00	125850	148.44	847817.30	3.42
FP 0.90 µg (Flovent HFA 20 shots)							
0.59	1642.25	6.00	9853.50	156411	197.07	793682.45	3.36
0.58	1634.75	6.00	9808.50	167022	196.17	851414.59	3.60
0.61	1697.25	6.00	10183.50	142748	203.67	700878.87	2.97
0.51	1068.80	6.00	6412.80	45002	128.26	350876.37	2.23
0.54	1133.80	6.00	6802.80	53325	136.06	391934.20	2.49
0.48	1001.80	6.00	6010.80	53129	120.22	441946.16	2.81
TA 0.52 µg (Azmacort 25 shots)							
0.51	1065.80	6.00	6394.80	60782	127.90	475245.51	3.02
0.58	1205.80	6.00	7234.80	63479	144.70	438705.98	2.79
0.51	1061.80	6.00	6370.80	54458	127.42	427403.15	2.72
0.53	918.50	6.00	5511.00	305237	110.22	2769343.13	4.56
0.59	1017.67	6.00	6106.00	319673	122.12	2617695.71	4.31
0.62	1062.67	6.00	6376.00	353347	127.52	2770914.37	4.56
FP Solution							
0.53	1402.00	6.00	8412.00	40424	168.24	240275.80	0.97
0.41	1092.00	6.00	6552.00	45955	131.04	350694.44	1.41
0.61	1958.33	6.00	11750.00	121649	235.00	517655.32	1.33
0.55	1750.00	6.00	10500.00	82674	210.00	393685.71	1.01
FP Suspension							
0.44	1164.50	6.00	6987.00	69426	139.74	496822.67	2.00
0.42	1124.50	6.00	6747.00	53893	134.94	399384.91	1.61
0.53	1673.33	6.00	10040.00	129530	200.80	645069.72	1.65
0.54	1713.33	6.00	10280.00	140899	205.60	685306.42	1.75

* Abs: Absorbance obtained at 262 nm.

** Conc: Concentration.

Table A.2.36 Mass balance to calculate the cellular uptake of ICSs by Calu-3 cells following various treatment incubations at the start (t=0 h) and at the end (t=6 h) of the experiment. The mass was determined by washing the surface of cells with 60/40 CH_3CN/H_2O and these samples were analyzed using validated HPLC methods for FP and TA.

Sample	Time-point (h)	Mass (μg)
TA aerosol following 25 shots of Azmacort		
	0	0.52
	6	0.34
	6	0.32
	6	0.40
FP aerosol following 10 shots of Flovent HFA		
	0	0.52
	6	0.50
	6	0.51
	6	0.47
FP aerosol following 20 shots of Flovent HFA		
	0	0.91
	6	0.87
	6	0.88
	6	0.84

VITA

Deepika Arora was born on November 5, 1981 in New Delhi, India and is an Indian citizen. She received Bachelor degree in Pharmacy from Delhi Institute of Pharmaceutical Sciences and Research (DIPSAR), New Delhi, India in 2003. In 2004, she joined School of Pharmacy, Virginia Commonwealth University (VCU) upon acceptance into the Ph.D. program in Pharmaceutics, with full scholarship and teaching assistantship. She has co-authored seven abstracts and currently three research papers are in preparation. During her Ph.D. study at VCU, she gave three presentations at the Annual Daniel Watts Student Research Symposium in 2005, 2006 and 2007, presented twice at the VCU School of Pharmacy Research and Career Day in 2006 and 2007 and was awarded the Best Poster in 2007. At VCU, she served as a teaching assistant at Department of Pharmaceutics for three years, as the Chair of the Graduate Student Association (GSA) Research Symposium organized by VCU's Graduate School and as the Vice-President of the GSA at Department of Pharmaceutics. In 2005, she presented a podium at the annual meeting of Graduate Research Association for Students in Pharmacy, Boston, MA, for which she was awarded the best podium presentation. In 2006, Schering Plough Research Institute awarded her with a travel grant to present her research at the Annual Association of Pharmaceutical Scientists (AAPS), San Antonio, Texas. In 2007, Deepika was selected as a fellowship recipient from the International Foundation for Ethical Research (IFER), Chicago, IL. In 2008, she was awarded at the Graduate Student Symposium in Pharmaceutics and Drug Delivery at AAPS, Atlanta, GA. Her dissertation research contributed towards the luminometer equipment award by Turner Biosystems. She is a member of AAPS. Upon completion of her Ph.D. study, Deepika will be working at Food and Drug Administration, Silver Spring, MD.